Deposition of metal nanoparticles on magnetic nanobeads and evaluation of their catalytic activity

Doctoral Thesis presented by

Francesca Besostri

For the degree of

Doctor of Sciences by Universität Regensburg

and

Doctor of Chemical Science and Technology by Universitat Rovira i Virgili

Regensburg 2016

This work was supervised by:	Prof. Dr. Oliver Reiser
	Prof. Dr. Miquel A. Pericas Brondo
Graduation request filled on:	17. May 2016
Oral examination done on:	27. June 2016

This thesis was performed inside the **EU-ITN Network Mag(net)icFun** in accordance to the cotutelle agreement between the University of Regensburg and the Universitat Rovira i Virgili for a joint PhD degree programme.

The experimental work from February 2013 to March 2015 was done under the supervision of Prof. Dr. Oliver Reiser, at the *Institut für Organische Chemie der Universität Regensburg*. From April 2015 to January 2016 the experimental work was done under the supervision of Prof. Dr. Miquel A. Pericas at *the Institut Català d'Investigació Química* (ICIQ, Tarragona).

Prof. Dr. OLIVER REISER and Prof. Dr. MIQUEL A. PERICÀS BRONDO,

STATE, that the present Doctoral Thesis entitled: "**Deposition of metal nanoparticles on magnetic nanobeads and evaluation of their catalytic activity**", presented by Francesca Besostri to recieve the degree of Doctor, has been carried out under their supervision between the University of Regensburg (UR) and the Institute of Chemical Research of Catalonia (ICIQ).

Regensburg, 4th May 2016

Tarragona, 5th May 2016

Prof. Dr. Oliver Reiser

Prof. Dr. Miquel Àngel Pericàs Brondo

Table of contents

Thesis abstract

The present dissertation presents the scientific work developed in the last three years at the University of Regensburg (UR, Regensburg, Germany) and at the Institut Català d'Investigació Química (ICIQ, Tarragona, Spain). The work was focused on the development of nanocatalysts composed of metal nanoparticles deposited on the surface of magnetic nanobeads and the evaluation of their catalytic activity.

The first chapter describes the two types of magnetic supports employed in this work. On one hand, cobalt magnetic nanobeads with an average diameter of 50 nm were used. These nanobeads are composed of a metallic core surrounded by a graphene-like shell, which protects the core from oxidation and ensures thermal and chemical stability. On the other hand, iron oxide nanobeads with an average diameter of 6 nm, synthesised by thermal decomposition of $Fe(acac)_3$ in the presence of oleic acid and oleylamine as surfactant agents, were employed as magnetic support.

The second chapter deals with the evaluation of the activity for the Suzuki-Miyaura cross-coupling reaction of a catalyst composed by palladium nanoparticles deposited on the surface of the carbon-coated Co nanobeads. High catalytic activity was found for the coupling of phenylboronic acid with aryl iodides and bromides. The use of microwave irradiation was proven to be particularly advantageous for this transformation, allowing significantly shorter reaction times. In fact, full conversions of the aryl iodides and bromides were obtained after only 5 and 15 minutes respectively, when the reaction mixture was heated to 100 and 120 °C by microwave irradiation. Moreover, low metal loading of 0.1 and 0.5 mol% were required and no further chromatographic purification was needed to isolate the products. The recyclability and metal leaching in the final products were also evaluated. The nanocatalyst could be easily recovered from the reaction mixture by applying an external magnetic field and directly reused for subsequent reactions, being active for at least six runs. However, the detected metals leaching (Co and Pd) was above the allowed limits. Thus, a functionalisation consisting on a silica coating over the carbon shell and incorporation of a palladium complex was studied in order to minimize the leaching of metals. The resulting catalyst showed high catalytic activity for the Suzuki-Miyaura cross-coupling of phenylboronic acid with aryl iodides and bromides, proving its recyclability for four consecutive runs. The silica coating was found to minimize the metals leaching, being the palladium amount found in the final products below the required limits whereas the cobalt still exceeding them.

The third chapter describes the deposition of noble metals (Au and Pt), on the carbon coating of the cobalt nanobeads and the assessment of their catalytic activity. Aiming to obtain small (~ 5 nm) catalytically active metals nanoparticles, different synthetic pathways were studied. The synthesis of an active gold catalyst was achieved proving its potential for the hydrogenation of *para*-nitrophenol.

Contrarily, synthesising an active supported platinum catalyst was more difficult. High metal loading were achieved but the Pt was forming big clusters, without a catalytic activity, on the surface of the magnetic support.

The fourth chapter deals with the deposition of nickel nanoparticles on the surface of two different magnetic nanobeads and the evaluation of their catalytic activity for a broad range of reactions. On one hand, the carbon coated cobalt nanobeads were employed as support, taking in consideration the tendency of carbonaceous materials to incorporate metal nanoparticles. On the other hand, the ability of nickel to link to C-C double bonds present on the surface of iron oxide nanobeads was investigated. Unfortunately, in no case, an active catalysts was obtained due to the formation of nickel oxide nanoparticles and agglomeration of the metal on the surface of the magnetic supports.

Zusammenfassung

Die vorliegende Dissertation zeigt die wissenschaftliche Arbeit, die in den letzten drei Jahren an der Universität Regensburg (UR, Regensburg, Deutschland) und am Institut Català d'Investigació Química (ICIQ, Tarragona, Spanien) entwickelt wurde. Die Arbeit konzentrierte sich auf die Entwicklung von Nanokatalysatoren bestehenden aus Metallnanopartikeln auf der Oberfläche von magnetischen Nanobeads und auf die weitere Auswertung ihrer katalytischen Aktivität.

Das erste Kapitel beschreibt die zwei Arten von magnetischen Trägern, die in dieser Arbeit verwendet wurden. Einerseits wurden magnetische Nanobeads mit einem durchschnittlichen Durchmesser von 50 nm bestehend aus einem Cobaltkern umgeben mit einer graphenähnlichen Schicht verwendet, die den Kern vor Oxidation schützt und thermische und chemische Stabilität sichert. Andererseits wurden Eisenoxidnanobeads als mögliche magnetische Träger mit einem durchschnittlichen Durchmesser von 6 nm verwendet, die durch thermische Zersetzung von $Fe(acac)_3$ in Anwesenheit von Ölsäure und Oleylamin als oberflächenaktive Substanz synthetisiert wurden.

Das zweite Kapitel beschäftigt sich mit der Auswertung der Aktivität für die Suzuki-Miyaura Kreuzkupplungsreaktion eines Katalysators bestehend aus Palladiumnanopartikel abgeschieden auf der Oberfläche kohlenstoffbeschichteter Cobaltnanobeads. Es konnte eine hohe katalytische Aktivität für die Kupplung von Phenylborsäure mit Aryliodid und Arylbromid gezeigt werden. Die Verwendung von Mikrowellenbestrahlung erwies sich durch Minimierung der Reaktionszeit in der Praxis als vorteilhaft für die Transformation. In der Tat wurde kompletter Umsatz der Ausgangsmaterialien nach nur jeweils 5 und 15 Minuten für Aryliodid und Arylbromid beim Erhitzen der Reaktionsmischung auf 100 und 120 °C mit Mikrowellenbestrahlung erhalten. Darüber hinaus wurde eine niedrige Metallbeladung von 0.1 und 0.5 mol% benötigt und keine weitere chromatographische Aufreinigung war nötig. Ebenfalls wurde die Recycelbarkeit und das Leaching der Produkte untersucht. Der Nanokatalysator konnte von der Reaktionsmischung einfach mit Hilfe eines externen magnetischen Feldes wiedergewonnen werden und direkt für weitere Reaktion wiederverwendet werden mit Aktivität für mindestens sechs weitere Läufe. Jedoch war das detektierte Metallleaching (Co und Pd) über den erlaubten Grenzwerten. Daher wurde eine Funktionalisierung bestehend aus einer Silicaschicht über der Kohlenstoffhülle und Aufnahmen eines Palladiumkomplexes untersucht um das Metallleaching zu minimieren. Der entstandene Katalysator zeigte hohe katalytische Aktivität für Suzuki-Miyaura Kreuzkupplung von Phenylborsäure mit Aryliodid und Arylbromid mit Recycelbarkeit für vier aufeinanderfolgende Läufe. Die Silicaschicht reduzierte das Metallleaching des Palladiums im Endprodukt unter den benötigten Grenzwert, wobei der Cobaltwert immer noch darüber liegt.

Das dritte Kapitel beschreibt die Ablagerung von Edelmetallen (Au und Pt) auf die Kohlenstoffhülle der Cobaltnanobeads und die Bewertung der katalytischen Aktivität.

Hierbei war das Ziel kleine (~ 5 nm) katalytisch aktive Metallnanopartikel zu erhalten, es wurden verschiedene synthetische Weg erforscht. Die Synthese eines aktiven Goldkatalysators wurde erreicht und dessen Potential für dir Hydrierung von *para*-Nitrophenol gezeigt. Im Gegensatz dazu war die Synthese eines aktiven Platinkatalysators schwieriger. Hohe Metallbeladungen konnten erreicht werden, aber Pt bildete große Cluster ohne jegliche katalytische Aktivität auf der Oberfläche der magnetischen Träger.

Das vierte Kapitel beschäftigt sich mit der Abscheidung von Nickelnanopartikeln auf den Oberflächen von zwei verschiedenen magnetischen Nanobeads und der Bewertung ihrer katalytischen Aktivität für eine breite Auswahl an Reaktionen. Einerseits wurde die kohlenstoffumhüllten Cobaltnanobeads als Träger verwendet, mit der Überlegung dass kohlenstoffhaltige Materialien eine Tendenz zur Aufnahme von Metallnanopartikeln aufweisen. Andererseits wurde die Fähigkeit von Nickel zum Binden an C-C Doppelbindungen, die auf der Oberfläche der Eisenoxidnanobeads vorhanden sind, untersucht. Unglücklicherweise wurde in keinem Fällen ein aktiver Katalysator erhalten, wegen der Bildung von Nickeloxidnanopartikeln und Agglomeration des Metalls auf den magnetischen Trägern.

Resumen

La presente tesis doctoral expone el trabajo doctoral realizado durante los últimos tres años en la Universidad de Regensburg (UR, Regensburg, Alemania) y el Institut Català d'Investigació Química (ICIQ, Tarragona, España). El trabajo se enfocó en el desarrollo de nanocatalizadores compuestos de nanopartículas metálicas depositadas en la superficie de nanoperlas magnéticas y su consecuente evaluación catalítica.

El primer capítulo describe los dos tipos de soportes magnéticos utilizados en este trabajo. Por un lado, se emplearon nanoperlas magnéticas de cobalto con un diámetro promedio de 50 nm. Dichas nanoperlas están compuestas por un núcleo de Co^0 rodeado por una capa de tipo grafeno la cual brinda protección al núcleo metálico, evitando su oxidación y garantizando su estabilidad química y térmica. Por otro lado, nanoperlas de óxido de hierro con un diámetro promedio de 6 nm fueron usadas como posible soporte magnético. Estas perlas fueron sintetizadas por medio de la descomposición térmica de $Fe(acac)_3$ en presencia de ácido oleico y oleilamina como surfactantes.

El segundo capítulo trata la evaluación catalítica en la reacción de acoplamiento Suzuki-Miyaura de un catalizador compuesto por nanopartículas de paladio depositadas en la superficie de nanoperlas de cobalto envueltas en carbono. Una alta actividad catalítica fue encontrada para el acoplamiento de ácido fenilborónico con yoduros y bromuros de arilo. El uso de irradiación con microondas fue de particular utilidad para esta transformación ya que permitió reducir apreciablemente los tiempos de reacción. Conversiones completas de yoduros y bromuros de arilo fueron obtenidas en 5 y 15 minutos respectivamente, cuando la mezcla de reacción fue calentada a 100 y 120 º C usando irradiación de microondas. Adicionalmente, bajas cargas de catalizador (0.1 y 0.5 mol %) pudieron ser usadas y no se requirió purificación por cromatografía para el aislamiento de los productos. La reciclabilidad del catalizador y la contaminación de los productos por lixiviación metálica fueron evaluadas. El nanocatalizador pudo ser fácilmente separado de la mezcla de reacción mediante la aplicación de un campo magnético externo mostrando actividad catalítica en al menos 6 ensayos catalíticos, sin embargo, el contenido metálico (Co y Pd) en los productos se encontró por encima de los límites permisibles. Con el objetivo de contrarrestar este efecto se exploró el uso de un recubrimiento de sílica sobre la capa de carbono en la cual se incorporó un complejo de paladio. El catalizador resultante mostró alta actividad catalítica para el acoplamiento Suzuki-Miyaura de ácido fenilborónico con yoduros y bromuros de arilo pudiendo ser también reutilizado en al menos 4 reacciones consecutivas. El recubrimiento de sílica redujo efectivamente la pérdida de metales del catalizador, encontrándose los niveles de paladio por debajo de los límites requeridos aunque la contaminación por cobalto aún los supera.

El tercer capítulo describe la deposición de los metales nobles (Au y Pt) en la cubierta de carbono de las nanoperlas de cobalto y su evaluación catalítica.

Con el objetivo de obtener nanopartículas pequeñas (~ 5 nm) que fuesen catalíticamente activas se estudiaron diversas metodologías de síntesis. Nanopartículas de oro catalíticamente activas pudieron ser sintetizadas y su potencial en la hidrogenación de *para*-nitrofenol fue estudiado. Por otro lado, la síntesis de un catalizador activo de platino soportado presentó dificultades. Altas incorporaciones de Pt fueron observadas, sin embargo, la formación de clústeres de gran tamaño, sin actividad catalítica, fue predominante en la superficie del soporte magnético.

El cuarto capítulo trata la deposición de nanopartículas de níquel en la superficie de dos diferentes nanoperlas y la evaluación de su actividad catalítica en una gran variedad de reacciones. Por un lado se utilizaron nanoperlas de cobalto recubiertas con carbono, teniendo en cuenta la tendencia de los materiales carbonaceos a la incorporación de nanopartículas metálicas. Del otro lado, nanoperlas de óxido de hierro fueron empleadas. La alta afinidad del níquel por los dobles enlaces C-C presentes en la superficie de las nanoperlas fue usada para unir el catalizador al soporte. Desafortunadamente en ningún caso se obtuvieron catalizadores activos, principalmente por causa de la formación de nanopartículas de óxido de níquel y aglomeración del metal en la superficie de ambos soportes magnéticos.

Introduction

Metal nanoparticles on solid supports: synthesis and applications

Nanoscience, the emerging science of objects with dimensions in the range of few to 100 nm,[1] (Figure 1) has received in the last decade great attention from different disciplines (*i.e.* physics, medicine, chemistry, biology and engineering) and still plays a main role in the technological progress for the development of efficient approaches for the synthesis of chemicals, materials and energy generation.[2,3] It mostly focuses on a) the development of methods and tools for the synthesis of nanostructures, b) the evaluation of the physical and chemical properties of the obtained nanomaterials and c) their final application in different fields.[4]

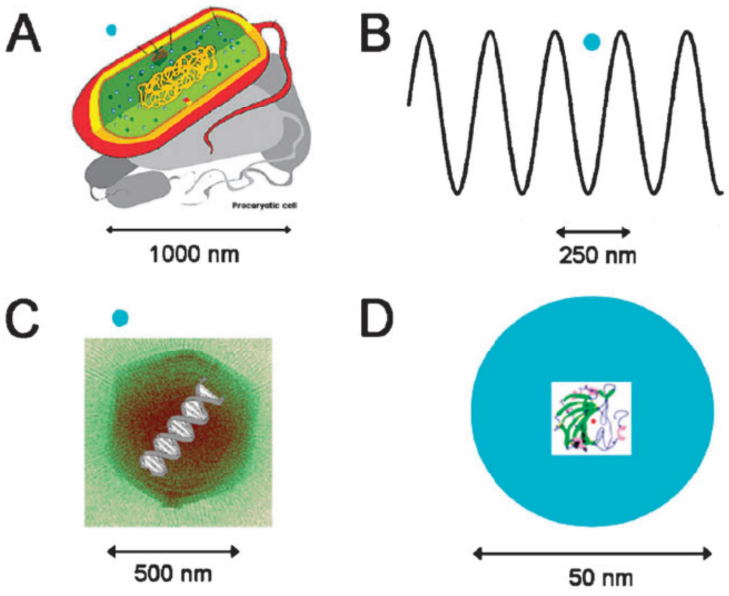

Figure 1 Depiction of the size regime of nanoparticles related to common "nano" scale objects. (A) prokaryotic cell, (B) ultraviolet wave, (C) virus and (D) enzyme. Blue sphere represents a 50 nm metal nanoparticle. Reproduced from Reference [9], with permission from The Royal Society of Chemistry.

Nanomaterials (*i.e.* carbon-based and inorganic materials) have been widely investigated due to their application as building blocks for the assembly of nanoscale machines and heterogeneous catalysis, in particular, significant interest has been placed on metallic nanoparticles (MNPs). These, display different properties compared to the related bulk materials, such as large surface-to-volume ratio, degenerated density of energy states, higher catalytic activity and optical, mechanical and chemical properties that can be tuned by modifying their size and composition (Figure 2).[4]

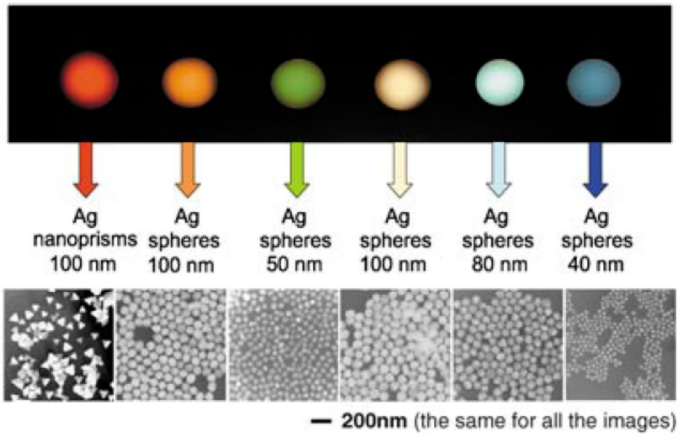

Figure 2 Size, shape and composition matters. This statement is illustrated here by considering the Rayleigh light-scattering properties of various nanoparticles (quoted nanoparticles sizes are all approximated). Reprinted from Reference [4]. Copyright © 2005 Wiley-VCH Verlag GmbH & Co. KGaA, D-69451 Weinheim.

Due to their size, metal nanoparticles are thermodynamically unstable because of the high surface energies.[5] Thus, their synthesis and growth must be performed under controlled conditions. Two different methods can be applied to obtain stable metal nanoparticles. On the one hand, organic ligands, capping materials or polymers can be employed to form protected core-shell nanocomposites.[6] An alternative and widely investigated procedure, is their immobilization on solid supports.[7] The latter method minimizes some of the disadvantages encountered employing bare metal nanoparticles, such as aggregation, poisoning and deactivation.[8] The properties of supported metal nanoparticles are strongly related to their morphology (size and shape), dispersion and interaction with the support material, rendering them suitable for a broad spectrum of applications.[9]
In the following sections an overview of the most widely employed supports, common deposition methods and applications of the corresponding nanocomposites is presented.

1.1 Supports

A variety of materials is employed as support for metal nanoparticles, each of them possessing specific advantages and influencing the final characteristics of the nanohybrids.[9,10] Among these, carbon based materials, metal oxides, polymers and magnetic nanobeads are the most widely applied families in the synthesis of supported metal nanoparticles.

Carbon-based materials

Carbon nanotubes (CNTs) are an important class of materials frequently investigated in the last years because of their intrinsic and specific characteristics such as high mechanical strength, high surface area and high electrical and thermal conductivity, which make them attractive for different applications.[11] Carbon nanotubes are one-dimensional tube-like materials with the carbon layer rolled up into a long, thin cylinder with diameters in the nanoscale range. They exist in two forms: single-walled carbon nanotubes (SWCNTs) have a diameter between 1 and 10 nm and are usually capped at the end while the multi-walled ones (MWCNTs), consisting in concentric cylinders held together by Van der Waals forces, are consequently larger with diameters between 5 to a few hundred nm (Figure 3).[12,13]

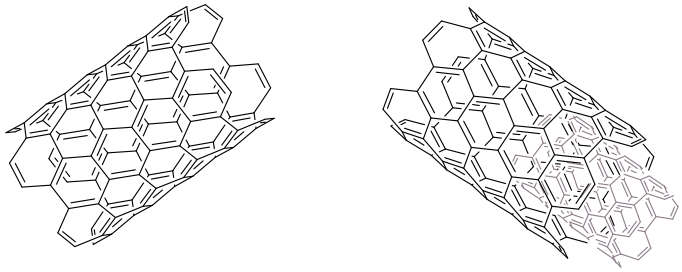

Figure 3 Schematic representation of single-walled (left) and multi-walled carbon nanotubes (right).

Moreover, the surface of CNTs can be tailored by covalent and non-covalent functionalisation strategies. These modifications involve the incorporation of new elements (*e.g.* oxygen and nitrogen), the anchoring of organic functionalities (*e.g.* biological macromolecules, polymers or surfactants) and also the deposition of metal nanoparticles.[11,13] In 2010, Bi *et al.* successfully deposited RuO_2 nanoparticles on the surface of MWCNTs by a solution-based method. The structure of the MWCNTs with a diameter of 60-100 nm was retained after the treatment and scanning electron microscopy (SEM) showed a rougher surface indicating the presence of RuO_2 nanoparticles. Transmission electron microscopy (TEM) and high resolution transmission electron microscopy (HRTEM) revealed carbon nanotubes coated with very small (< 2 nm) and well-dispersed RuO_2 nanoparticles (Figure 4).[14] Similarly, Choi *et al*. selectively deposited small Pt and Au nanoparticles on the sidewall of MWCNTs.[15]

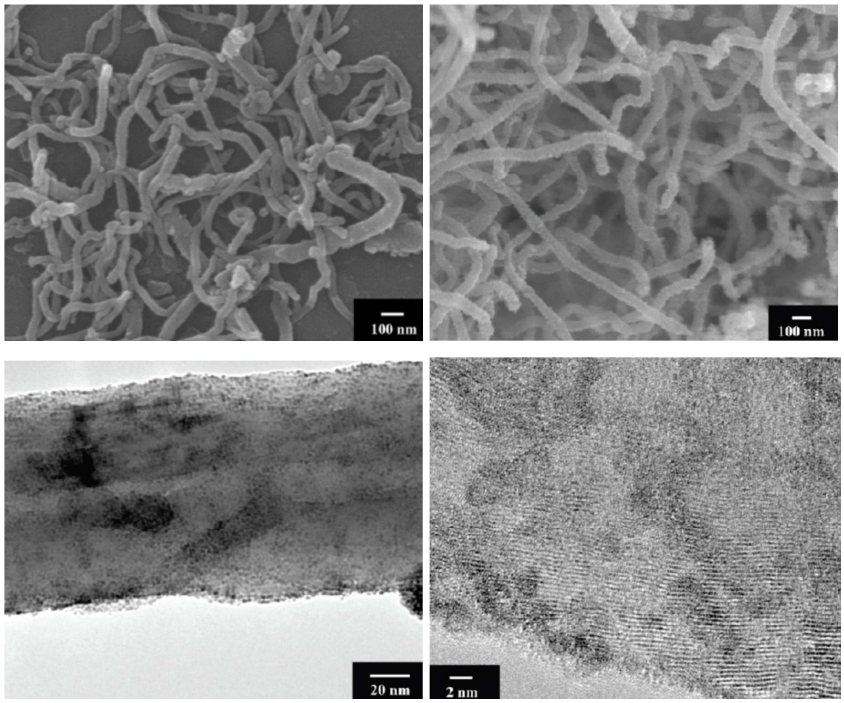

Figure 4 Upper panel: SEM picture of the multi-walled CNTs used (left) and the as prepared RuO_2/CNT nanocomposites (RuO_2/CNT = 6:7 in wt %) (right). Bottom panel: TEM (left) and HRTEM (right) images of the as prepared RuO_2/CNT nanocomposites (RuO_2/CNT = 6:7 in wt %). Images adapted with permission from Reference [14]. Copyright © 2010 American Chemical Society.

Graphene is another carbon-based material commonly used as a support for metal nanoparticles.[16,17] It is a two-dimensional single-layer sp^2 carbon atom network that is densely packed in a honeycomb structure.[16,18] As in the case of CNTs, graphene possesses several interesting properties as large surface area, high adsorption capacity, excellent electrical and thermal conductivity and high mechanical strength that render it attractive for a number of applications.[19] Functionalisation of the surface of graphene sheets allows to obtain versatile hybrid materials with use in different fields (*i.e.* solar cells, fuel cells, water treatment and catalysis).[16] A common modification is the introduction of defects on their surface to improve the electronic transport properties.

In fact, intrinsic graphene is a zero bandgap material with small on/off ratios that lead to a limitation for the electronic applications.[20] Disadvantages that can be encountered working with graphene are connected to the possible agglomeration caused by the high π-π stacking between the nanosheets, leading to a decrease in activity as the catalytic sites are blocked.[21]

Nevertheless, several examples of well-dispersed ultrafine metal nanoparticles on graphene are reported in literature. A uniform coating of FePt nanoparticles with an average diameter of 7 nm was obtained by Guo *et al*. applying a solution-phase-assembly strategy.[18]

Similarly, Shang *et al*. deposited Pt nanoparticles on reduced graphene oxide sheet,[21] obtained by oxidation of graphite and composed of exfoliated sheets.[19] A uniform distribution of ultrafine Pt nanoparticles with an average diameter of 1.6 nm was achieved and the nanohybrid was successfully applied in catalysis.[21]

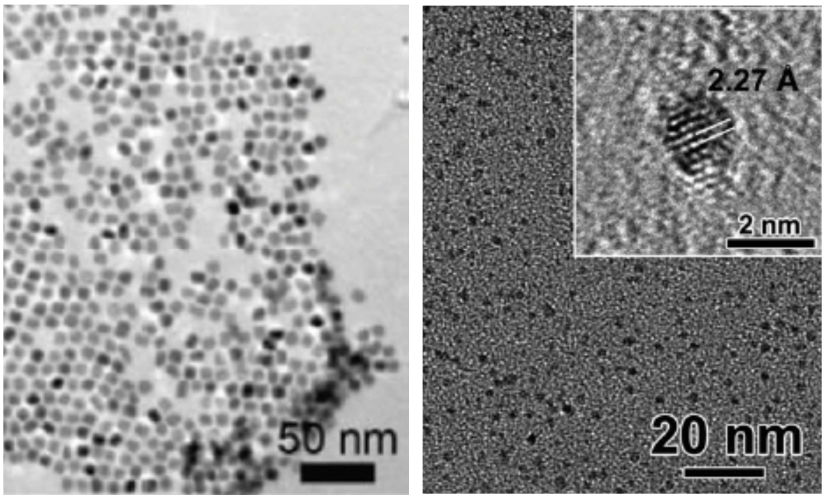

Figure 5 Left: TEM image of the G/$Fe_{18}Pt_{82}$ NCs. Adapted with permission from Reference [18]. Copyright © 2012 American Chemical Society. Right: TEM image of Pt-rGO (etched). Reprinted from Reference [21]. Copyright © 2014 Wiley-VCH Verlag GmbH & Co. KGaA, Weinheim.

(Bio)polymers

Biopolymers are a class of organic materials characterized by their robustness, chemical stability and easy chemical modification. They have been widely investigated as supports for metal and metal oxide nanoparticles leading to the synthesis of hybrid materials with unique properties and applications. The dispersion of the metal nanoparticles inside the polymer network takes place through a combination of different mechanisms (*i.e*. complexation and electrostatic interactions) and strongly depends on the morphology, porosity and surface area of the support.[22]

Chitosan is a polysaccharide biopolymer derived by deacetylation of natural chitin that displays unique characteristics as film-forming and chelating properties due to the presence of amino and hydroxyl functional groups. Moreover, it can be easily separated from the reaction mixture and is nontoxic, biocompatible and biodegradable, making its use feasible for pharmaceutical and biomedical applications.[23] In 2010, Wei *et al*. achieved the synthesis of Au and Ag-chitosan bio-conjugates, where the chitosan was able to directly reduce the metal source to metal nanoparticles (Figure 6). Similarly, homogeneously distributed Pd nanoparticles with an average diameter of 5 nm were described by Sarkar *et al*. showing a different nanoparticles size depending on the metal loading, which indicates the presence of agglomerates when the loading was too high (Figure 6).[22]

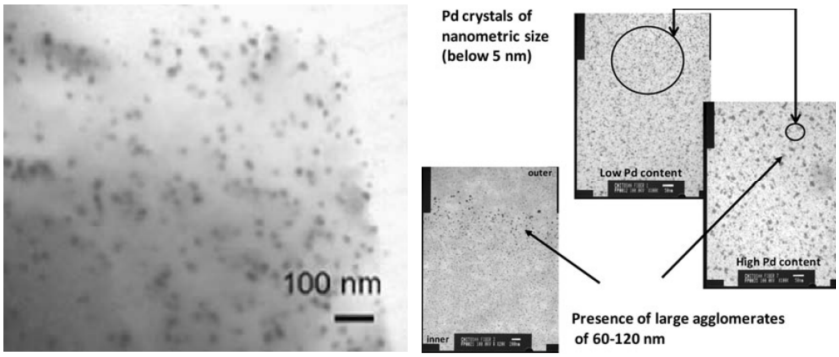

Figure 6 Left: Image of metal NPs-chitosan bio-conjugates by exposure of 30 mg chitosan flakes to 6.0 mM $AgNO_3$ at 95 °C. Reprinted from Reference [23]. Copyright © 2009 Elsevier Ltd. Right: TEM analysis of chitosan-Pd catalyst. Adapted with permission of Springer from Reference [22]. Copyright © 2012 Springer Science+Business Media B.V.

Nanocelluloses are another class of biopolymer obtained from vegetal cellulose. They are characterized by a rod-like or ribbon-like shape with length between 50-1000 nm and width in the range of 3-50 nm. The final structure depends on the preparation conditions and the starting cellulose that can be derived from several different sources (*i.e.* wood, cotton, bacteria, bamboo). Nevertheless, nanocelluloses have high surface area, high aspect ratio, high crystalline order and chirality, good mechanical strength and feasible surface modification due to the presence of hydroxy and sulphate ester groups. Because of these unique characteristics, together with the ability to form stable suspensions in water, nanocelluloses have been widely investigated as support for metal nanoparticles and organometallic species for catalytic applications.

Metal oxides

Another family of widely used supports for metal nanoparticles are metal oxides, which in turn can be classified as inert (SiO_2) and active (TiO_2, CeO_2, ZrO_2, Al_2O_3). In general, they possess high thermal and chemical stability together with a well-developed porous structure and high surface area.[2] Their use enhances the stability of the metal nanoparticles and allows their application in different fields as optics, analytic chemistry and catalysis.[24]

Moreover, active metal oxide supports participate in catalytic reactions through interactions with the metal nanoparticles. An example is the application of Pt@CeO_2 catalyst in water/gas shift reactions.[25] In this case, on one hand, the ceria drives the activated oxygen to the Pt and, on the other hand, the Pt nanoparticles enhance light absorption and charge-carrier separation in the metal oxide semiconductor. Jin *et al*. achieved the synthesis of nanohybrids where metal nanoparticles were uniformly distributed on the surface of different metal oxides (Figure 7).[25] An additional example comes from the application of precious metals supported on TiO_2 nanospheres for photocatalytic water-splitting

reactions. It has been demonstrated that metal nanoparticles induce a shift in the Fermi level to more negative potentials, leading to the formation of nanohybrids with improved energetics and efficiency in the interfacial charge-transfer process.[26]

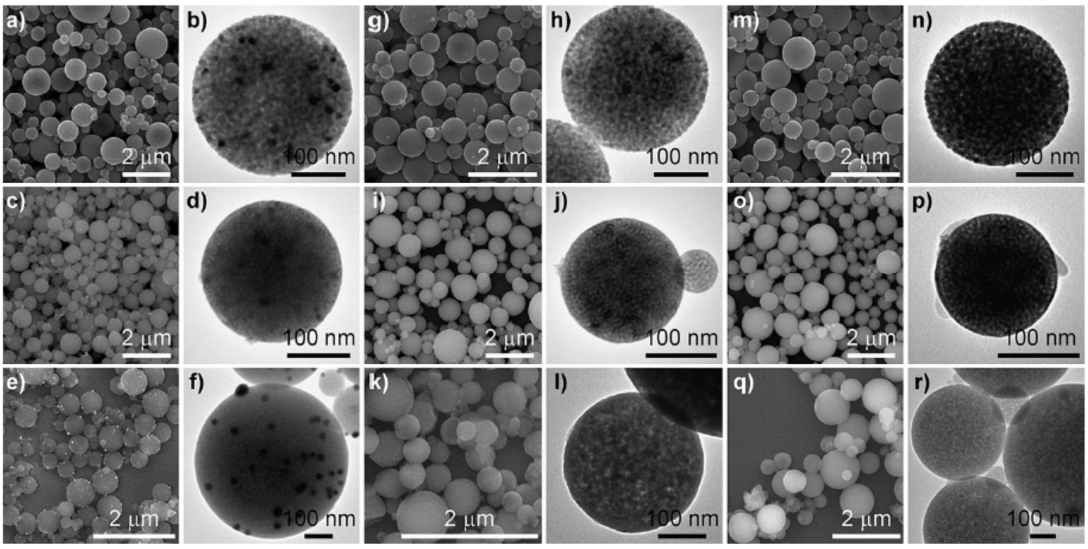

Figure 7 SEM (first, third and fifth column) and TEM (second, fourth and sixth column) images of the mesoporous metal oxides microspheres loaded with metal nanoparticles. a, b) Au@TiO_2. c, d) Au@ZrO_2. e, f) Au@Al_2O_3. g, h) Pd@TiO_2. i, j) Pd@ZrO_2. k, l) Pd@Al_2O_3. m, n) Pt@TiO_2. o, p) Pt@ZrO_2. q, r) Pt@Al_2O_3. Reprinted from Reference [25]. Copyright © 2012 Wiley-VCH Verlag GmbH & Co. KGaA, Weinheim.

Magnetic nanobeads

The use of magnetic nanobeads as support has also been widely investigated in the recent years because of their properties as high surface area to volume ratio, chemical inertness and thermal stability. Moreover, they can be easily recovered from the reaction mixture by applying an external magnetic field, which greatly facilitates the reaction work-up.[27] In fact, time-consuming and tedious protocols as filtration and centrifugation can be avoided and the catalyst can be reused.[28] Furthermore, the surface of the magnetic nanobeads can be functionalised in different ways such as silica/carbon coating or by the addition of surfactants and polymers.

This leads to a stabilization of the nanoparticles themselves and also introduce the possibility to anchor different molecules or deposit metal nanoparticles on the surface.[27]

1.2 Deposition Methods

Different preparation routes, physical or chemical, can be applied to achieve the deposition of metal nanoparticles onto solid supports.[9] Today's focus on sustainable chemistry drives the development of synthetic pathways that employ less toxic precursors, environmentally friendly solvents, ambient reaction temperatures and few synthetic steps. Moreover, minimum quantities of by-products and waste should be generated.[29]

Atomic layer deposition

Atomic layer deposition (ALD) is a technique employed for the deposition of thin films[30] on different supports such as nanoparticles, nanowires, nanotubes, soft and biological materials.[31,32] This technique is extensively used as a consequence of the reproducibility of the obtained films together with the large range of applications of the synthesised hybrid structures (*i.e*. catalysis, microelectronics, energy storage and sensing). ALD is based on the reaction of precursors that are separated into successive surface reactions. In this way, the reactants are kept separated and react with the surface in a self-limiting process. Every surface reaction is separated by a purge step, where unreacted precursor and by-products are removed. In each cycle, a film with a defined thickness is deposited and the cycles are continued until the final desired film is obtained (Figure 9).[32] Nevertheless, sometimes nanoparticles can be deposited instead of films, being particularly convenient for catalysis applications due to the higher surface area. In 2009, Liu *et al*. achieved the deposition of uniform and well-dispersed Pt nanoparticles on carbon nanotubes as it is possible to observe in Figure 8 where the Pt nanoparticles appear as white dots.[31]

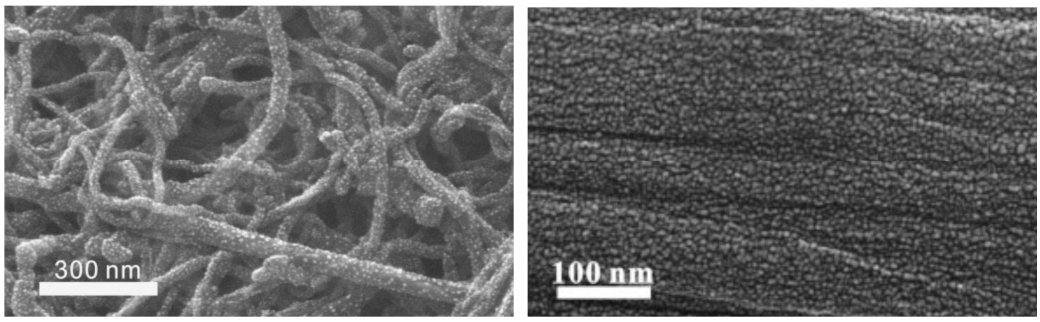

Figure 8 Left: SEM cross-section of the carbon nanotubes on Si wafer after ALD of Pt for 100 cycles. The carbon nanotubes were acid treated for 6 h. Right: SEM images of carbon cloth, with acid treatment for 6 h, after ALD of Pt. Reprinted from Reference [31]. Copyright © 2009 Wiley-VCH Verlag GmbH & Co. KGaA, Weinheim.

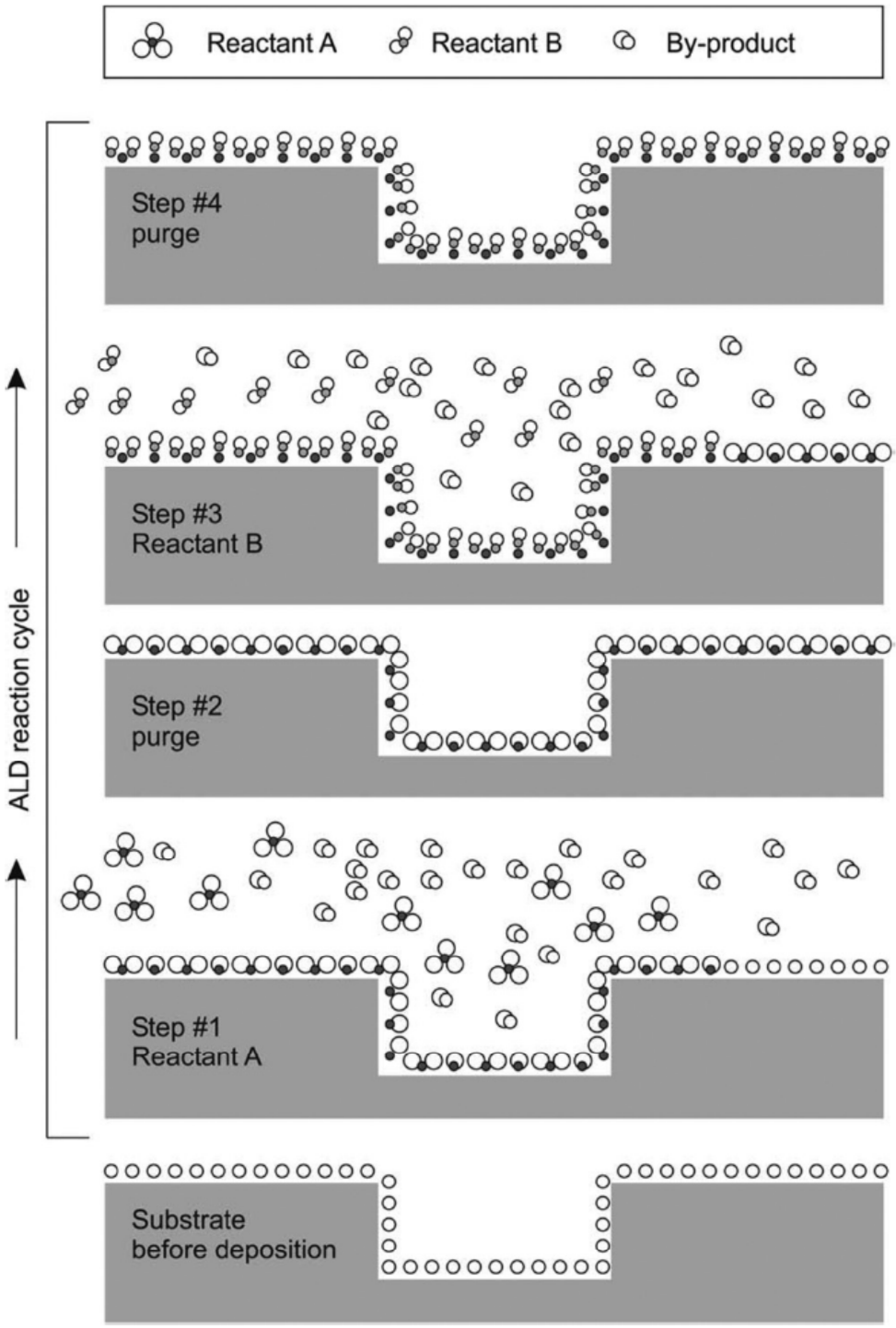

Figure 9 Schematic illustration of one ALD reaction cycle. Reprinted from Reference [30], with the permission of AIP Publishing. Step 1: pulse of the reactant A leading to its absorption on the surface. Step 2: purge of the unreacted precursor A and of the by-products. Step 3: pulse of the reactant B, which reacts with the surface species created by precursor A. Step 4: purge of the unreacted precursor B and of by-products.

Microwave irradiation

Microwave (MW) heating found in the recent years large application in different fields such as synthesis of nanomaterials, solid-state chemistry, nanotechnology and organic synthesis.[33] MW application in the synthesis of organic, inorganic and hybrid materials allows to obtain nanoparticles with uniform size/shape because of the fast and uniform heating of the reaction mixture. Moreover, it often allowed a fine dispersion of the metals on the supports, a generally difficult goal with methods as co-precipitation and impregnation.[34] In 2008, Campelo *et al*. developed an easy and fast procedure to deposit metal nanoparticles on polysaccharide-derived mesoporous materials by microwave irradiation and avoiding the use of reducing agents. The synthesis required microwave heating for 2 min at 100-140 °C (300–450 W) of an ethanol/acetone or ethanol/water solution of the desired metal salt. They demonstrated how microwave irradiation was critical for the synthesis of nanoparticles with uniform size, shape and distribution. Moreover, the controlled temperature allowed the deposition of only reduced metal nanoparticles. A comparison with nanohybrids obtained by conventional heating was also made. In this case, low metal loading was achieved together with an irregular nanoparticle shape, size and distribution.[35] Similarly, Guo *et al*. employed microwave irradiation for the deposition of platinum nanoparticles on graphene sheets with a one-step protocol. High loading of Pt nanoparticles with a uniform distribution and small size (2.6 nm) was achieved. The nanohybrids were then successfully applied for electroanalytical applications.[36]

Sonochemistry

Sonochemistry is an additional deposition methodology that can be applied to the synthesis of supported metal nanoparticles. The advantages related to this procedure such as controllable size distribution, environmentally friendly protocol and ambient temperature reaction conditions, are due to the acoustic cavitation phenomena involving the formation, growth and collapse of bubbles in a liquid.[37] During the sonochemical process, three different regions are formed in the liquid medium: 1) the gas phase of the collapsing bubbles, where high temperatures (> 5000 °C) and pressures (> 20 MPa) are reached, causing water to pyrolyse into H and OH radicals; 2) interfacial region with temperatures high enough (few hundred °C) to induce reactions and 3) the bulk solution at ambient temperature.[38] Pol *et al*. demonstrated how sonochemical processes lead to the deposition of small (~ 5 nm) Ag and Au nanoparticles on silica nanospheres with a uniform distribution. Furthermore, no reducing agents were added to the reaction mixture, being the high temperature and pressure reached during the sonochemical process, responsible for the reduction of the metal ions to the amorphous form.[37,39]

Chemical vapour deposition

Hybrid materials such as microelectronic devices, optics and membrane reactors synthesised by chemical vapour deposition (CDV) of thin films on solid supports can be used in a variety of applications. Moreover, CDV allows a conformal and selective deposition of metals. The process involves the thermally induced reaction of a metal precursor on a heated surface. In particular, a volatile metal precursor (inorganic, metal-organic or organometallic) is transported in the reactor and to the support where it adsorbs and reacts to liberate the ligand that is subsequently desorbed and transported out of the reactor. The metal atoms then diffuse to form stable nucleus and the film coating (Figure 10).[40] This methodology was employed by Okumara *et al*. to deposit small (2-3 nm) and well-dispersed gold nanoparticles on different metal oxide supports, Al_2O_3, SiO_2 and TiO_2. The same good results could not be achieved applying liquid phase preparation methods.[41]

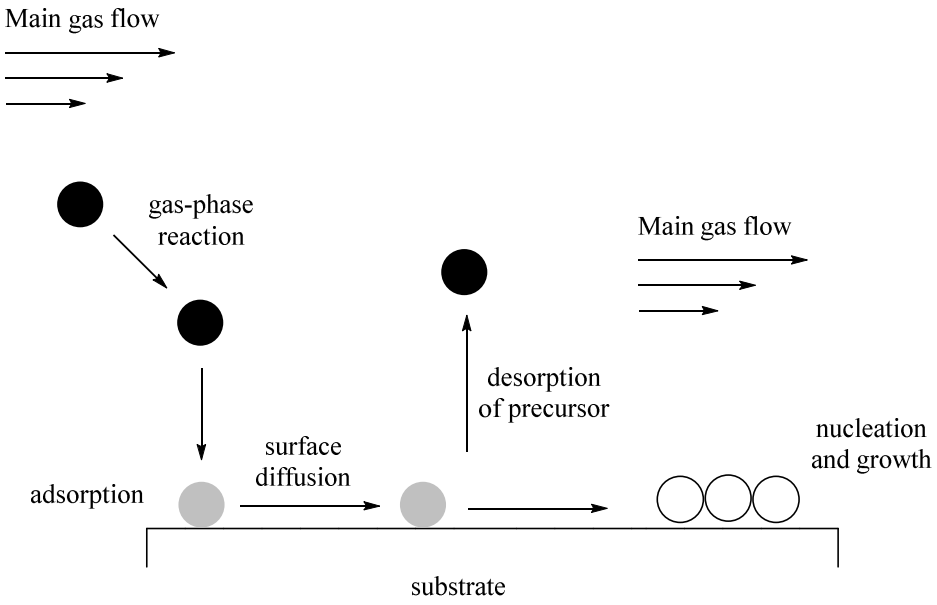

Figure 10 Schematic representation of the key steps involved in the chemical vapour deposition process.

Pulsed laser deposition

Pulsed laser deposition (PLD) is a clean and low-cost physical technique employed for the deposition of thin metal films on solid supports.[42] In PLD, a high power pulsed laser is focused on the target surface. Applying a sufficiently high laser fluence (~1 J/cm^2), each laser pulse is able to vaporise or ablate a small amount of material which expands rapidly from the surface in vacuum and provides the deposition flux of thin film growth.[43] The dimension and morphology of the nanoparticles are usually controlled by the number of laser pulses, leading to spherical small nanoparticles (1 nm) with a narrow size dispersion for low metal loading.[44] In 2012, Dai *et al*. deposited CdSe quantum dots on ternary metal oxide nanoparticles Zn_2SnO_4 for photovoltaic application by pulsed laser deposition.

This methodology allowed to use non-toxic chemicals and to obtain a uniform monolayer of small quantum dots varying laser parameters.[42]

Deposition-precipitation method

Currently, this methodology is particularly employed for the deposition of metal nanoparticles on functionalised/coated magnetic nanobeads. It consists in the sonication of the support in the desired metal salt solution followed by addition of a reducing agent. Zhu *et al*. applied this method to incorporate Pd nanoparticles on the surface of iron oxide (Fe_3O_4) nanobeads coated with a carbon layer derived from glucose carbonization.[45] Similarly, Liu *et al*. deposited Ag, Pd and Au on the polymer coating of magnetic nanospheres (Fe_3O_4@P(MBAAm-*co*-MAA). The loading of the metal nanoparticles was achieved by exchange of sodium cations present in the ionized microsphere, leading to the formation of uniform and well-dispersed Ag and Pd nanoparticles on the shell layer of the microspheres. In the case of Au, nanoparticles with irregular shape and distribution were formed, probably because of the weak interaction between the Au and the polymer coating (Figure 11).[46]

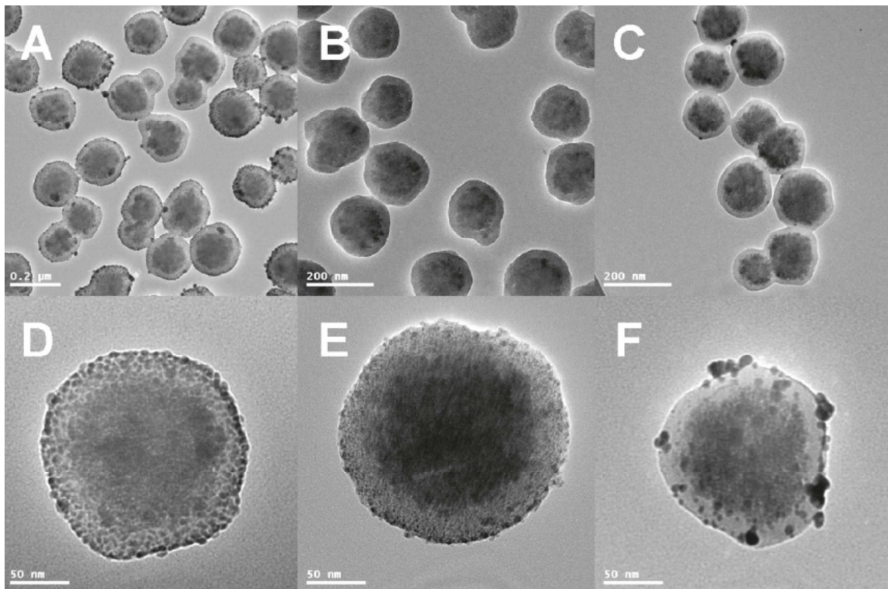

Figure 11 TEM images of (A, D) Fe_3O_4@P(MBAAm-*co*-MAA)/Ag microspheres, (B, E) Fe_3O_4@P(MBAAm-*co*-MAA)/Ag microspheres and (C, F) Fe_3O_4@P(MBAAm-*co*-MAA)/Au microspheres. Adapted with permission from Reference [46]. Copyright © 2011 American Chemical Society.

Microemulsion

Water-in-oil microemulsion is a well-known procedure to synthesise supported metal nanoparticles. In fact, the interaction between the microemulsion itself and the support is believed to enhance the hydrophobicity of the latter rendering it more chemically-compatible.[9]

Yoon *et al*. employed this method to synthesise a catalyst composed of Pd and Rh nanoparticles uniformly distributed on carbon nanotubes, of average size between 2 and 10 nm. Hexane was added to an aqueous solution of the desired metal containing a surfactant agent, obtaining a two-phase system. The solution was purged with nitrogen and hydrogen, leading to the formation of the nanoparticles within the microemulsion. The nanoparticles were anchored on the support by stirring the carbon nanotubes into the microemulsion. It has been moreover demonstrated that, with a direct deposition of metal nanoparticles on the carbon nanotubes, not employing the microemulsion method, large Pd and Rh clusters (1 order of magnitude larger) were obtained (Figure 12).[47]

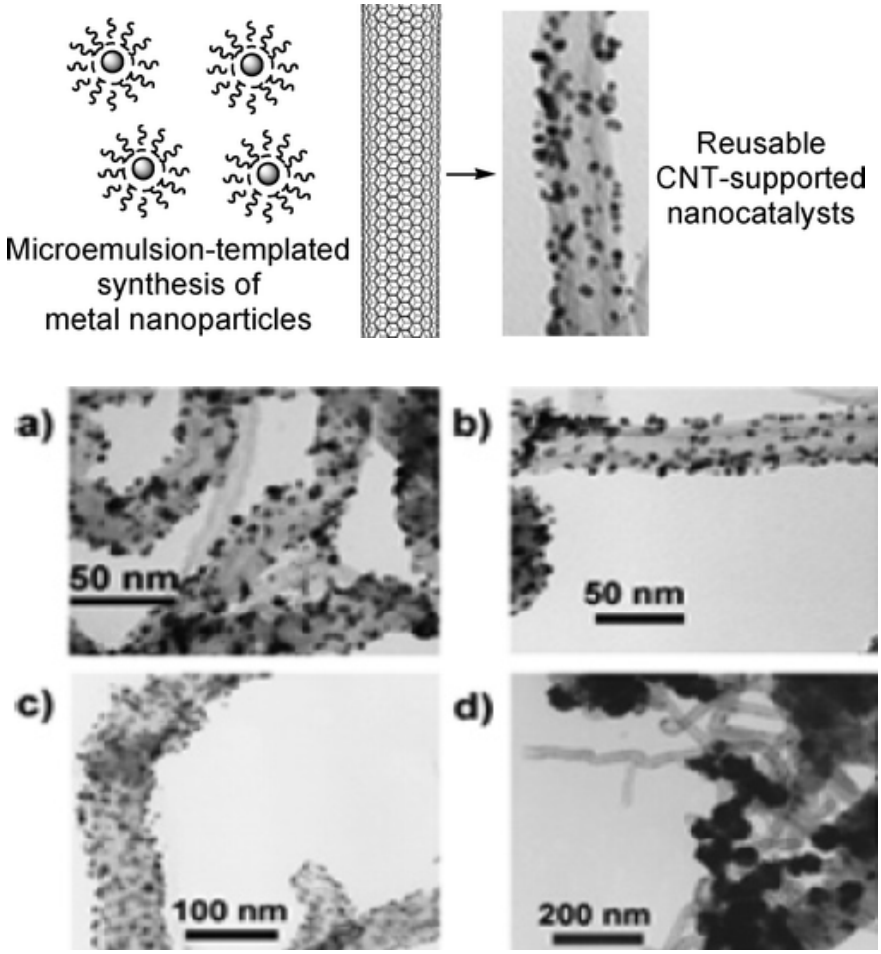

Figure 12 Upper panel: Schematic representation of the microemulsion-based method for the deposition of metal nanoparticles on carbon nanotubes. Bottom panel: TEM images of the microemulsion-templated synthesis of CNTs-supported metal nanoparticles: a) Pd/CNTs, b) Rh/CNTs, c) Pd/Rh bimetallic nanoparticles from the microemulsion methods and d) Pd/CNTs from an aqueous Na_2PdCl_4 solution. Adapted with permission from Reference [47]. Copyright © 2005 American Chemical Society.

Impregnation

This approach, also known as wetness impregnation, consists in the "wetting" of a solid support with a solution containing the desired metal. Usually, nanoparticles with a broad distribution of sizes is observed.[9] In 2011, Choi *et al*. developed graphene-supported metal nanoparticles employing impregnation method obtaining materials composed of small nanoparticles (Pt = 1.9 nm; Pd = 2.0 nm; Rh = 3.9 nm; Ru = 3.0 nm) with a fine distribution on the graphene sheets. The synthesis was achieved by mixing the graphene with a solution of the metal in acetone and stirring the mixture by ultrasonication. After collecting and drying, the hybrid materials were treated with 4% H_2 in N_2 at 250 °C for 3 h, to reduce the metal nanoparticles.[48]

Centrifuge

In 2014, Markelonis *et al*. showed the possibility to employ a common laboratory centrifuge to deposit uniform films of Au and PbS nanoparticles on different types of materials, from flexible to rigid sheets as well as flat and rough surfaces. The synthesis involves the placement of the chosen support on the bottom of a vial followed by addition of a well-dispersed solution of the colloidal nanoparticles. The mixture was at this point centrifuged, leading to the formation of uniformly supported metal nanoparticles, the thickness of the film correlated to the concentration of the colloidal nanoparticles solution employed (Figure 13).[49]

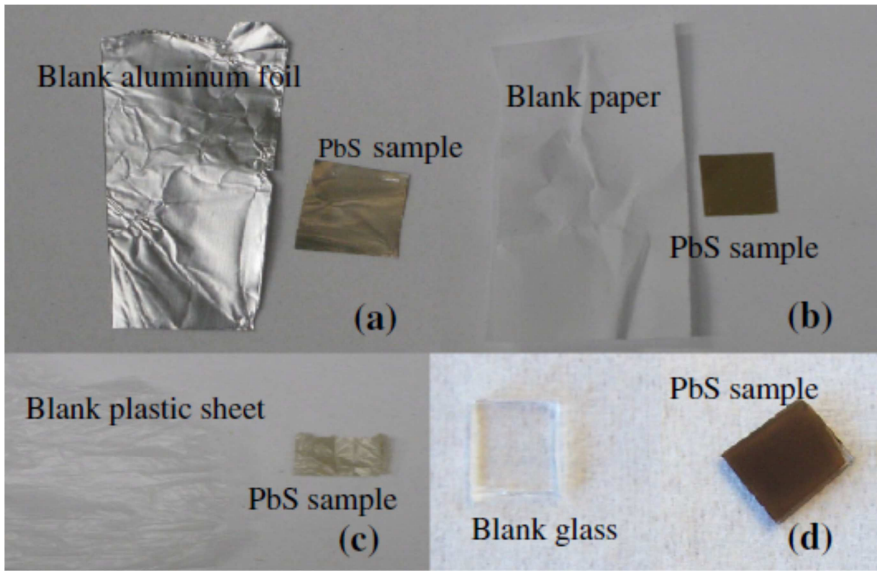

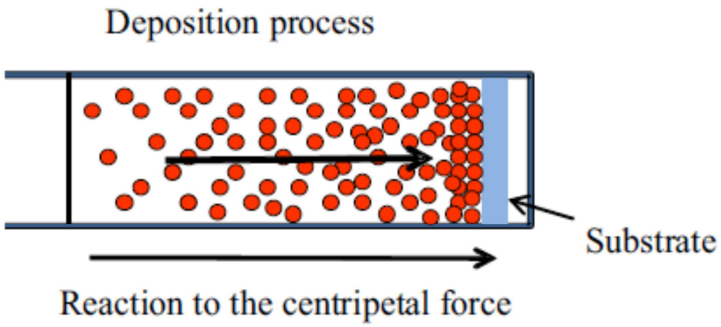

Figure 13 Upper panel: PbS NPs deposited by centrifugation method on different substrates. Left: blank substrates and right: PbS NPs deposited on a) aluminium foil, b) paper, c) plastic sheet and d) glass. Bottom panel: Schematic diagram to illustrate the centrifuge deposition process. Adapted from Reference [49], with permission of Springer

1.3 Applications

Supported metal nanoparticles have been successfully applied in a great variety of different fields. A small overview of the most relevant uses of these nanohybrids is presented in the following section.

Sensors

Metal-graphene nanocomposites have found various applications as electrochemical energy storage and sensing due to their large electrochemically active surface areas, which are able to efficiently increase the electron transfer between the electrode and the detected molecules, leading to more rapid and sensitive response than traditional sensors.[36,50,51] Determination of hydrogen peroxide (H_2O_2) in biological systems is of high importance in biology, biomedicine and environmental protection, being a by-product of several biological and chemical processes (*i.e*. pharmaceutical, paper and chemical industries). In biological systems, hydrogen peroxide can generate reactive oxygen species (ROS) that, in excess, can cause different diseases (*i.e*. Parkinson, Alzheimer, heart attack and cancer).[50] Similarly, detection of glucose in blood serum is particularly important in the control of diabetes mellitus, a current worldwide health problem. In 2012, Zhang *et al*. developed a new nanohybrid material composed of Ag nanoparticles deposited on graphene, employing tannic acid as reducing agent. The nanocomposite was then immobilized on the surface of a glassy carbon electrode (GCE) by addition of chitosan to form a modified electrode (chitosan/Ag NPs-G/GCE), evaluated for the sensing of H_2O_2 and glucose. The Ag NPs-G nanocomposites exhibit high electrocatalytic activity for the reduction of H_2O_2, being the current response of the modified chitosan/Ag NPs-G/GCE electrode significantly higher than the current obtained with the bare electrode. For the detection of glucose, the enzyme glucose oxidase (GOD) was immobilized on the already described electrode.

The detection mechanism involves the oxidation of glucose in the presence of oxygen by GOD leading to the formation of H_2O_2, that is electrochemically detected. A good linear relationship was observed between the current response and the glucose concentration, with a detection limit of 100 µmol/L, which enabled the modified electrode to be successfully used for the detection of glucose in blood samples.[51] In 2014, Maji *et al*. developed a hybrid material composed of well-dispersed small (~ 3 nm) Au NPs deposited over reduced graphene oxide (rGO) sheets covered with periodic mesoporous silica (PMS) (rGO-PMS@AuNPs). The nanocomposite was successfully employed as an electrode material to fabricate a sensor for the detection of H_2O_2 and glucose in biological samples (human urine). Additionally, as a result of the very low achievable detection limit (60 nM), it was used also for the detection of H_2O_2 released by cancer cells (Figure 14).[50]

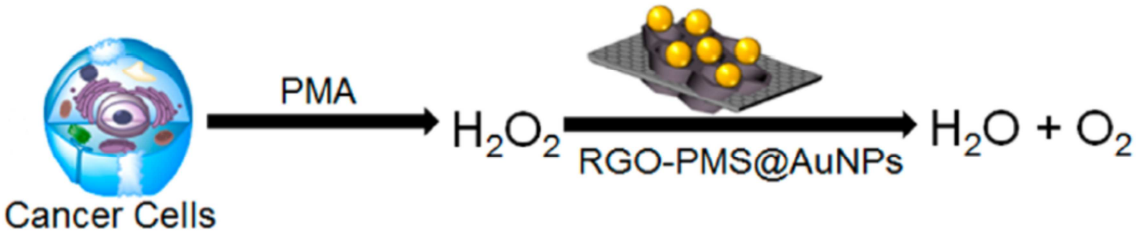

Figure 14 Schematic diagram for in vitro detection of H_2O_2. Adapted with permission from Reference [50]. Copyright © 2014 American Chemical Society.

Different cell lines were employed, human embryonic kidney cells (HEK 293), human cervical cancer cells (HeLa) and human hepatoma cancer cells (HepG2) together with a stimulating agent, the phobol 12-myristate-13-acetate (PMA), which induces the generation of hydrogen peroxide from tumour cells in a short time period. The RGO-PMS@AuNPs was demonstrated to be sensitive and reliable in the detection of H_2O_2 generated by tumour cells, allowing the distinction between normal and cancerous cell lines.[50]

The surface-enhanced Raman scattering (SERS) has attracted great attention for its microanalytical abilities, allowing the detection of analyte with high sensitivity and low detection limits. In 2011, Han *et al*. prepared silver-coated magnetic nanospheres (Fe_3O_4/Ag) that serve as a SERS substrate and can also be easily handled by applying an external magnetic field. Malachite green (MG) is a fungicide and antiseptic used in aquaculture industry but suspected to be genotoxic and carcinogenic, making its monitoring in water at trace level particularly important.[52] This scenario has been selected to evaluate the SERS-property of the silver-coated magnetic nanospheres.[53] The SERS signal obtained for this hybrid materials were much stronger than the one detected for the bare microspheres. A quantitative analysis was also made. Stock solutions of the MG were firstly mixed with the Fe_3O_4/Ag. A sample solution was then dropped on a glass slide, dried and analysed by Raman spectroscopy, using the relative Raman intensity to quantitatively evaluate the MG content.

A good linear relationship was observed in the concentration range of 10-350 ppb, demonstrating that the microspheres can be used to detect MG in water, in concentration as low as 10 ppb. The Fe_3O_4/Ag microspheres were also used to develop a SERS-based optofluidic system (Figure 15), where the microspheres and the MG analytes were mixed in a microfluidic channel and the SERS analysis was performed under continuous flow conditions. A mini-solenoid was introduced in the system, in order to generate a magnetic field that can trap the microsphere in the channel. In this way, they could adsorb the analyte molecules and be effective. A valve system was also introduced to regulate the flows. First, the microspheres were introduced and trapped on the channel. Afterwards, the analyte was circulated through the channel and absorbed on the microspheres. Here, "hot spots" generated by Fe_3O_4/Ag were detected by SERS.[52]

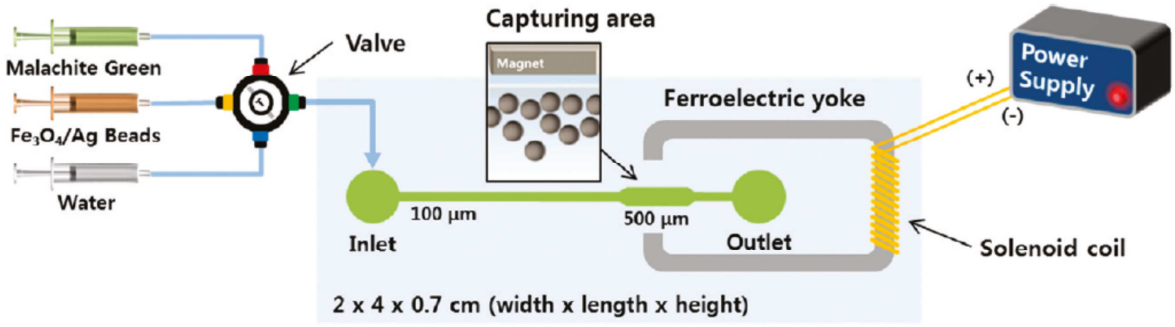

Figure 15 Layout of a SERS-based optofluidic sensor integrated with a solenoid. Adapted with permission from Reference [52]. Copyright © 2011 American Chemical Society.

Fuel cells

The current increase in energy consumption combined with the depletion of fossil fuel reserves and the environmental concerns associated with green-house gas emissions have motivated the development of alternative energy sources. Fuel cells, such as proton exchange membrane fuel cells (PEMFCs) and direct methanol fuel cells (DMFCs) are considered one of the most promising class of energy conversion devices allowing high densities and efficiencies.[54] Fuel cells might play a key role as possible future energy sources for zero-emission vehicles, distributed home power generators and power source for small electronics.[55] Fuel cells consist in an electrochemical device that is able to convert chemical energy of fuels (*i.e*. hydrogen, methanol, formic acid and ethanol) to electricity by separating the electron flow from the mass transport of two main chemical reactions involved, fuel oxidation on the anode and oxygen reduction on the cathode (Figure 16).[54]

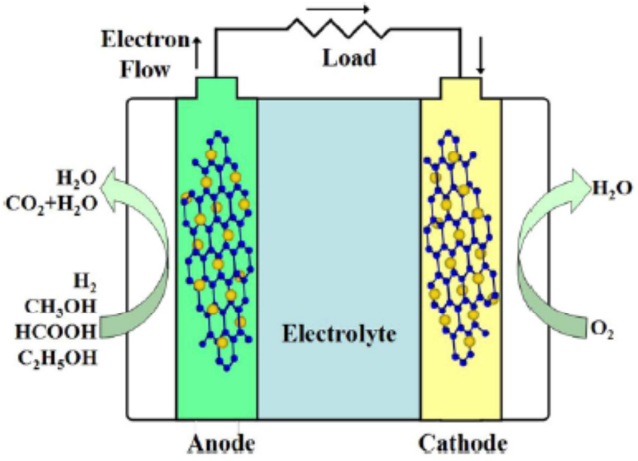

Figure 16 Schematic representation of a fuel cell. Adapted with permission from Reference [54]. Copyright © 2014 American Chemical Society.

In 2011, Qiu *et al*. described a new hybrid nanomaterial composed of small (~ 4.6 nm) and well-dispersed Pt nanoparticles on functionalized graphene sheets, successfully employed in a direct methanol fuel cell (DMFC) where methanol is oxidized with oxygen to carbon dioxide and water, generating electricity. Platinum is the most widely used catalyst in fuel cells and graphene has been used as support for these applications due to the high conductivity and surface area. The synthesised nanocomposite exhibits high electrochemical activity for methanol oxidation and oxygen reduction. Moreover, good tolerance towards CO was observed.[56]

Photocatalysis

Metal nanoparticles supported on semiconductor materials have been extensively studied for a variety of photocatalytic reactions. In 2011, Tsukamoto *et al*. studied the oxidation mechanism under visible-light irradiation of small Au nanoparticles (< 5 nm) deposited on the interface of anatase/rutile TiO_2 particles. Au nanoparticles are characterized by a strong light absorption in the visible region that generate oscillation of free electrons, known as surface plasmon resonance (SPR). In a general mechanism of visible-light-driven oxidation (Figure 17), surface plasmon resonance transfers electrons from Au nanoparticles to the semiconductor support conduction band and the positively charged Au nanoparticles receive electrons from a substrate that is in this way oxidized. Simultaneously, the electrons in the conduction band of the support are consumed by oxygen reduction.[57]

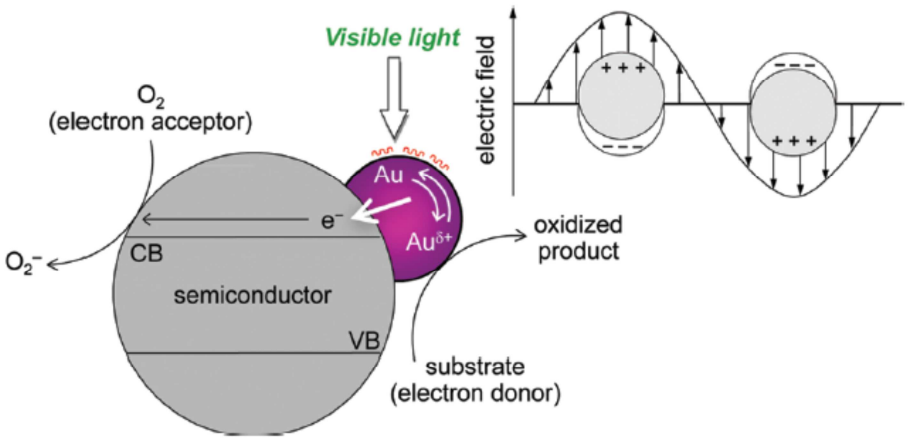

Figure 17 Proposed mechanism for visible-light-driven aerobic oxidation by Au particles supported on semiconductor particles. Adapted with permission from Reference [57]. Copyright © 2012 American Chemical Society.

It was demonstrated that small Au nanoparticles are required to observe a photocatalytic activity and also their position on the support influences the entire process. In fact, the Au nanoparticles need to be located at the interface of the anatase/rutile TiO_2 particles in order to obtain an active joint site that facilitates the electron transfer, leading to an efficient transformation. Applying the described nanocomposite, the oxidation of alcohols was performed at room temperature using sunlight. This opens the way to the design of more efficient photocatalysts that can be applied in a range of organic transformations.[57] Supported metal nanoparticles can also be applied to the photodegradation of toxic pollutants. In 2010, Hu *et al*. evaluated the photocatalytic activity of silver-silver iodide nanoparticles supported on alumina (Ag-AgI/Al_2O_3) for the degradation of phenolic compounds that are highly toxic and difficult to degrade (*i.e.* 2-chlorophenol (2-CP), 2,4-dichlorophenol (2,4-DCP) and trichlorophenol (TCP)). Different irradiation wavelengths (λ) were tested and comparison with AgI/Al_2O_3 was done to understand the reaction mechanism. Firstly, pollutants were absorbed on the surface of the nanocomposite under dark conditions. Subsequently, degradation (dechlorination) and mineralization (degradation of by-products) was carried out in an aqueous dispersion. The Ag-AgI/Al_2O_3 demonstrated to be an effective and stable plasmon induced catalyst that could be recycled for six consecutive runs. A two electron process was involved in the reaction. A first electron transfer occurred from photoexcited Ag nanoparticles to the AgI conduction band, leading to the formation of $O_2^{\cdot-}$ species and plasmon induced positive holes h^+, responsible of the pollutants degradation. A second electron transfer occurs from the pollutants to the Ag nanoparticles that resulted in this way significantly stable.[58]

Catalysis

Heterogeneous catalysis has been extensively studied in the past decades due to several related advantages such as easy separation from the reaction mixture, minimized metal contamination, recyclability, eco-friendliness and more economic transformations.[59] Several examples of supported metal nanoparticles employed in catalytic reactions are present in the most recent literature. In 2014, Deng *et al*. developed efficient hydrogen evolution reaction (HER) electrocatalysts by encapsulating 3d transition metals Fe, Co and FeCo nanoparticles on *N*-doped carbon nanotubes (NCNTs). The production of hydrogen is important for the development of technologies related to energy supply (*i.e*. hydrogen fuel cells). A general mechanism for the production of hydrogen by HER in acid media involves three steps: 1) absorption of an H atom by combination of a proton and an electron, 2) formation and desorption of an H_2 molecule by reaction of an H atom with a proton from the electrolyte and an electron from the CNT or 3) formation and desorption of an H_2 molecule by combination of two H atoms. Extraordinary catalytic activity was observed for this nanocomposite, showing, moreover, long-term durability.[60]

Similarly, Chen *et al*. immobilised small and well-dispersed Pd nanoparticles on graphene oxide sheets, employing the nanocomposite for the electro-oxidation of formic acid and ethanol. The nanohybrid showed superior catalytic activity compared to standard Pd/C electrode in both transformations. Moreover, high stability was exhibited, being still active after 100 potential cycles.[61]

Important catalytic reactions are also the hydrogenation of multiple carbon-carbon bonds and their formation. Liu *et al*. embedded Pd nanoparticles on the inner surface of carbon nanotubes and employed the nanocatalyst for the Suzuki-Miyaura cross-coupling reaction. The Pd nanoparticles were found uniformly distributed on the carbon surface and exhibited an enhanced sinter-resistance compared to the commercially available CNTs-supported Pd catalyst. In fact, no decrease in the catalytic activity was observed after 4 runs.[62]

α-β-Alkynyl ketones are an important class of compounds present in biologically active molecules and in intermediates of natural products. They can be obtained by the metal-catalysed Sonogashira coupling of terminal alkynes and aryl iodides in the presence of CO. Liu *et al*. applied immobilized Pd nanoparticles on iron oxide nanobeads to catalyse this transformation. A broad scope was investigated, including aryl iodides bearing both electron-withdrawing and electro-donating group in *ortho*, *meta* and *para* position. In all the cases, the desired product was afforded in good yields. Moreover, the nanocatalyst exhibited high stability and recyclability, being still active after seven consecutive runs.[63] Palladium is often used as catalysis in an exceedingly array of reactions, among those, hydrogenation and coupling reactions play an important role in pharmaceutical and chemical industries. In 2014, Linhardt *et al*. immobilised Pd nanoparticles on magnetic nanobeads previously modified with an ionic liquid, capable of stabilizing the nanoparticles through electrostatic interactions or coordination. The obtained nanocatalyst was firstly successfully applied in the hydrogenation of *trans*-stilbene with molecular hydrogen.

High yields were obtained in short reaction times and working at room temperature. Furthermore, the catalyst could be recycled for at least 11 runs without loss of activity and it was also possible to vary the substrates, from different olefins to nitro derivates.[64]

1.4 Conclusions

In combination with the development of nanoscience and the possibility to work and manipulate materials on a nano-scale, the rising environmental concerns and growing demand for energy and fast consumption of organic fuels, have created the need to promote "green" and sustainable processes. The immobilisation of metal nanoparticles on a variety of solid supports, leading to the formation of nanomaterials that can be recycled, allows a reduction of the generated waste. Furthermore, the synthesis of these nanocomposites can be achieved employing naturally occurring materials as supports and also methodologies that use alternative energy input (*i.e*. ultrasound and microwave). The development of more efficient catalytic system is one of the most intensely investigated topics, of particular importance is the simplification and shortening of reaction protocols that would enable increased productivities. The use of nanocatalysts, particularly those employing magnetic supports, show great promise at fulfilling these objectives. As a consequence of their easy separation from reaction media, the development of nanosystems that can be recycled for several consecutive runs without loss of activity is now a hot topic. At the same time, supported metal nanoparticles provide significant contributions in biomedical applications, allowing to detect molecules connected to human diseases in biological samples.

In conclusion, substantial advances have been made in the last years in nanoscience regarding the synthesis and applications of supported metal nanoparticles and the on-going research will surely lead to the creation of improved nanosystems with an even broader application range.

Objectives

Goal of the present doctoral thesis developed at the University of Regensburg and at the Institut Català d'Investigació Química was the synthesis of magnetic nanocatalysts that can be easily recovered from the reaction mixture just applying an external magnetic field and recycled for consecutive runs. The deposition of metal nanoparticles (Pd, Pt, Au and Ni) on the surface of two different magnetic supports, iron oxide and carbon-coated cobalt nanobeads, was investigated. Different deposition methods were considered aiming to obtain small and catalytically active supported metal nanoparticles. The activity of the synthesised nanocomposites was afterwards evaluated for a wide range of reactions, from Suzuki-Miyaura cross-coupling to hydrogenation of C-C double bonds and nitro-derivatives. Once the catalytic activity was proved, the recyclability of the nanocomposites and the metals leaching in the final product was evaluated.

1.5 References

[1] G. M. Whitesides, *Small* **2005**, *1*, 172–179.

[2] J. M. Campelo, D. Luna, R. Luque, J. M. Marinas, A. A. Romero, *ChemSusChem* **2009**, *2*, 18–45.

[3] R. Luque, R. S. Varma in *Sustainable Preparation of Metal Nanoparticles: Methods and Applications*, The Royal Society of Chemistry, **2013**.

[4] C. A. Mirkin, *Small* **2005**, *1*, 14–16.

[5] M. Chen, Y. Cai, Z. Yan, D. W. Goodman, *Journal of the American Chemical Society* **2006**, *128*, 6341–6346.

[6] A. M. Doyle, S. K. Shaikhutdinov, S. D. Jackson, H. Freund, *Angewandte Chemie International Edition* **2003**, *42*, 5240–5243.

[7] D. Barkhuizen, I. Mabaso, E. Viljoen, C. Welker, M.Claeys, E. Van Steen, J. C. Q. Fletcher, *Pure and Applied Chemistry*, **2009**, *78*, 1759-1769

[8] T. N. Rostovshchikova, V. V. Smirnov, V. M. Kozhevin, D. A. Yavsin, M. A. Zabelin, I. N. Yassievich, S. A. Gurevich, *Applied Catalysis A: General* **2005**, *296*, 70–79.

[9] R. J. White, R. Luque, V. L. Budarin, J. H. Clark, D. J. Macquarrie, *Chemical Society Reviews* **2009**, *38*, 481–494.

[10] Y. Kobayashi, Y. Tadaki, D. Nagao, M. Konno, *Journal of Colloid and Interface Science* **2005**, *283*, 601–604.

[11] S. R. N. Jha, *Nanoscale* **2010**, *2*, 806–810.

[12] K. A. Wepasnick, B. A. Smith, J. L. Bitter, F. D. Howard, *Analytical and Bioanalytical Chemistry* **2010**, *396*, 1003–1014.

[13] G. G. Wildgoose, C. E. Banks, R. G. Compton, *Small* **2006**, *2*, 182–193.

[14] R. Bi, X. Wu, F. Cao, L. Jiang, Y. Guo, L. Wan, *The Journal of Physical Chemistry C* **2010**, *114*, 2448–2451.

[15] H. C. Choi, M. Shim, S. Bangsaruntip, H. Dai, *Journal of the American Chemical Society* **2002**, *124*, 9058–9059.

[16] Y. Cheng, Y. Fan, Y. Pei, M. Qiao, *Catalysis Science & Technology* **2015**, *5*, 3903–3916.

[17] W. Hong, H. Bai, Y. Xu, Z. Yao, Z. Gu, G. Shi, *The Journal of Physical Chemistry C* **2010**, *114*, 1822–1826.

[18] S. S. S. Guo, *Journal of the American Chemical Society* **2012**, *134*, 2492–2495.

[19] P. V. Kamat, *The Journal of Physical Chemistry Letters* **2010**, *1*, 520–527.

[20] H. Vedala, D. C. Sorescu, G. P. Kotchey, A. Star, *Nano Letters* **2011**, *11*, 2342–2347.

[21] L. Shang,T. Bian, B. Zhang, D. Zhang, L. Wu, C. Tung, Y. Yin, T. Zhang, *Angewandte Chemie International Edition* **2014**, *53*, 250–254.

[22] S. Sarkar, E. Guibal, F. Quignard, A. K. SenGupta, *Journal of Nanoparticle Research* **2012**, *14*, 1–24.

[23] W. Dongwei, Y. Yongzhong, J. Xueping, Y. Chao, Q. Weiping, *Carbohydrate Research* **2010**, *345*, 74–81.

[24] G. V. Krylova, Y. I. Gnatyuk, N. P. Smirnova, A. M. Eremenko, V. M. Gun'ko, *Journal of Sol-Gel Science and Technology* **2009**, *50*, 216–228.

[25] Z. Jin, M. Xiao, Z. Bao, P. Wang, J. Wang, *Angewandte Chemie International Edition* **2012**, *51*, 6406–6410.

[26] V. Subramanian, E. E. Wolf, P. V. Kamat, *Journal of the American Chemical Society* **2004**, *126*, 4943–4950.

[27] R. K. Sharma, S. Dutta, S. Sharma, R. Zboril, R. S. Varma, M. B. Gawande, *Green Chemistry* **2016**, *accepted manuscript*.

[28] M. B. Gawande, R. Luque, R. Zboril, *ChemCatChem* **2014**, *6*, 3312–3313.

[29] J. A. Dahl, B. L. S. Maddux, J. E. Hutchison, James E., *Chemical Reviews* **2007**, *107*, 2228–2269.

[30] R. L. Puurunen, *Journal of Applied Physics* **2005**, *97*, 121301.

[31] C. Liu, C. Wang, C. Kei, Y. Hsueh, T. Perng, *Small* **2009**, *5*, 1535–1538.

[32] C. Marichy, M. Bechelany, N. Pinna, *Advanced Materials* **2012**, *24*, 1017–1032.

[33] M. B. Gawande, S. N. Shelke, R. Zboril, R. S. Varma, *Accounts of Chemical Research* **2014**, *47*, 1338–1348.

[34] E. A. Anumol, P. Kundu, P. A. Deshpande, G. Madras, N. Ravishankar, *ACS Nano* **2011**, *5*, 8049–8061.

[35] J. M. Campelo, T. D. Conesa, M. J. Gracia, M. J. Jurado, R. Luque, J. M. Marinas, A. A. Romero, *Green Chemistry* **2008**, *10*, 853–858.

[36] S. Guo, D. Wen, Y. Zhai, S. Dong, E. Wang, *ACS Nano* **2010**, *4*, 3959–3968.

[37] V. G. Pol, A. Gedanken, J. Calderon-Moreno, *Chemistry of Materials* **2003**, *15*, 1111–1118.

[38] K. S. Suslick, *IEEE Transactions on Ultrasonics, Ferroelectrics, and Frequency Control* **1986**, *33*, 143–147.

[39] V. G. Pol, D. N. Srivastava, O. Palchik, V. Palchik, M. A. Slifkin, A. M. Weiss, A. Gedanken, *Langmuir* **2002**, *18*, 3352–3357.

[40] M. J. Hampden-Smith, T. T. Kodas, *Chemical Vapor Deposition* **1995**, *1*, 8–23.

[41] M. Okumura, S. Nakamura, S. Tsubota, T. Nakamura, M. Azuma, M. Haruta, *Catalysis Letters*, *51*, 53–58.

[42] Q. Dai, J. Chen, L. Lu, J. Tang, W. Wang, *Nano Letters* **2012**, *12*, 4187–4193.

[43] C. A. Smyth, I. Mirza, J. G. Lunney, E.M. McCabe, *Applied Surface Science* **2013**, *264*, 31–35.

[44] J. Gonzalo, A. Perea, D. Babonneau, C. N. Afonso,N. Beer, J. P. Barnes, A. K. Petford-Long, D. E. Hole, P. D. Townsend, *Physical Review B* **2005**, *71*, 125420.

[45] G. D. M. Zhu, *The Journal of Physical Chemistry C* **2011**, *115*, 24743–24749.

[46] B. Liu, W. Zhang, F. Yang, H. Feng, X. Yang, *The Journal of Physical Chemistry C* **2011**, *115*, 15875–15884.

[47] B. Yoon, C. M. Wai, *Journal of the American Chemical Society* **2005**, *127*, 17174–17175.

[48] S. M. Choi, M. H. Seo, H. J. Kim, W. B. Kim, *Synthetic Metals* **2011**, *161*, 2405–2411.

[49] A. R. Markelonis, J. S. Wang, B. Ullrich, C. M. Wai, G. J. Brown, *Applied Nanoscience* **2014**, *5*, 457–468.

[50] S. K. Maji, S. Sreejith, A. K. Mandal, X. Ma, Y. Zhao, *ACS Applied Materials & Interfaces* **2014**, *6*, 13648–13656.

[51] Y. Zhang, S. Liu, L. Wang, X. Qin, J. Tian, W. Lu, G. Chang, X. Sun, *RSC Advances* **2012**, *2*, 538–545.

[52] B. Han, N. Choi, K. H. Kim, D. W. Lim, J. Choo, *The Journal of Physical Chemistry C* **2011**, *115*, 6290–6296.

[53] F. Bao, J. Yao, R. Gu, *Langmuir* **2009**, *25*, 10782–10787.

[54] M. Liu, R. Zhang, W. Chen, *Chemical Reviews* **2014**, *114*, 5117–5160.

[55] B. Fang, N. K. Chaudhari, M. Kim, J. H. Kim, J. Yu, *Journal of the American Chemical Society* **2009**, *131*, 15330–15338.

[56] J. Qiu, G. Wang, R. Liang, X. Xia, H. Yu, *The Journal of Physical Chemistry C* **2011**, *115*, 15639–15645.

[57] D. Tsukamoto, Y. Shiraishi, Y. Sugano, S. Ichikawa, S. Tanaka, T. Hirai, *Journal of the American Chemical Society* **2012**, *134*, 6309–6315.

[58] C. Hu, T. Peng, X. Hu, Y. Nie, X. Zhou, J. Qu, H. He, *Journal of the American Chemical Society* **2010**, *132*, 857–862.

[59] M. B. Gawande, P. S. Branco, R. S. Varma, *Chemical Society Reviews* **2013**, *42*, 3371–3393.

[60] J. Deng, P. Ren, D. Deng, L. Yu, F. Yang, X. Bao, *Energy & Environmental Science* **2014**, *7*, 1919–1923.

[61] X. Chen, G. Wu, J. Chen, X. Chen, Z. Xie, X. Wang, *Journal of the American Chemical Society* **2011**, *133*, 3693–3695.

[62] H. Liu, L. Zhang, N. Wang, D. S. Su, *Angewandte Chemie International Edition* **2014**, *53*, 12634–12638.

[63] J. Liu, X. Peng, W. Sun, Y. Zhao, C. Xia, *Organic Letters* **2008**, *10*, 3933–3936.

[64] R. Linhardt, Q. M. Kainz, R. N. Grass, W. J. Stark, O. Reiser, *RSC Advances* **2014**, *4*, 8541–8549.

Main Part

1. Magnetic supports: iron oxide and carbon-coated cobalt nanobeads

1.1 Introduction

Magnetic nanobeads have been extensively studied in the recent years because of their intrinsic properties and the useful application in catalysis. Due to the high surface area and the superparamagnetic behaviour, high catalyst loading and easy recovery and recyclability can be achieved. In the present work, two types of magnetic support have been employed. In 2007, Stark *et al.* reported a new one-step, large scale process via reducing flame spray pyrolysis for the synthesis of nanobeads characterized by a cobalt core and a graphene-like coating (Co/C) (Figure 1a) that protect the core from oxidation and can be easily functionalized, either covalently or non-covalently. Moreover, these versatile nanobeads show high air and thermal stability, as well as high magnetisation (158 emu/g), which allows the removal from the reaction mixture within seconds (Figure 1b).[1]

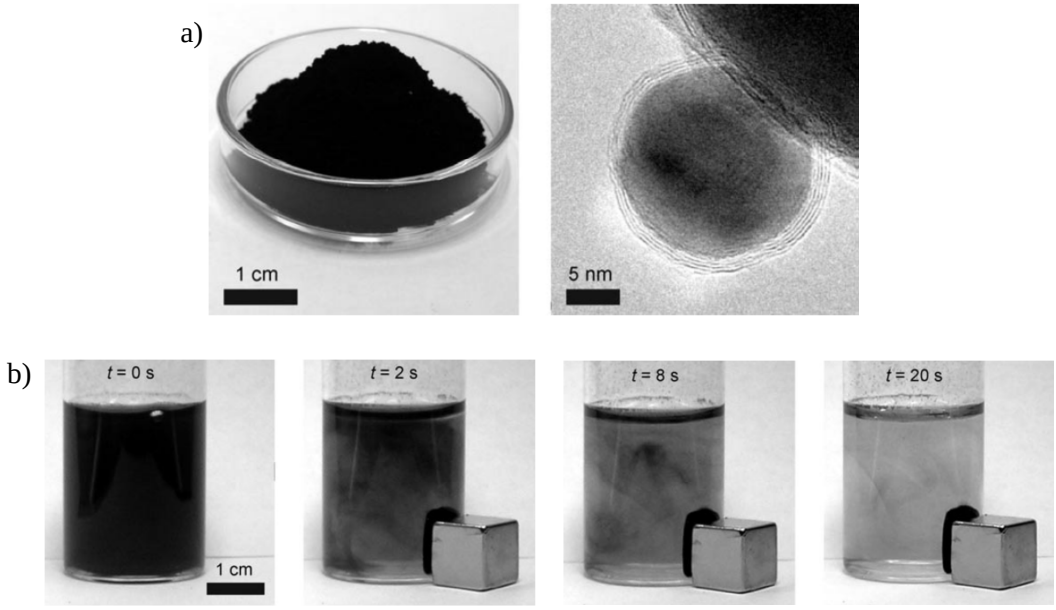

Figure 1 a) Left: Photograph of about 5 g of air-stable, carbon-coated nanomaterial. Right: Transmission electron microscopy image of the powder shows two to four homogeneous graphene layers coating the metallic cobalt core. b) Separation of cobalt nanoparticles from a suspension (1 g/L) in water by a commercial neodymium magnet (B = 1.4 T). Photographs were taken at indicated times after placement of the magnet. Figures adapted with permission from Reference [1]. Copyright © 2007, Wiley-VCH Verlag GmbH & Co. KGaA, Weinheim.

On the other hand, monodisperse, well-defined spherical iron oxide (Fe_3O_4) nanobeads with an average diameter of 5.6 ± 1.3 nm (Figure 2) were obtained by thermal decomposition of $Fe(acac)_3$ in the presence of oleic acid and oleylamine as surfactant agents.[2,3] A straightforward surface functionalization with covalently supported ligands and organocatalyst, was achieved grafting a propyltrimethoxysilane bearing an azido or amino moiety.[4]

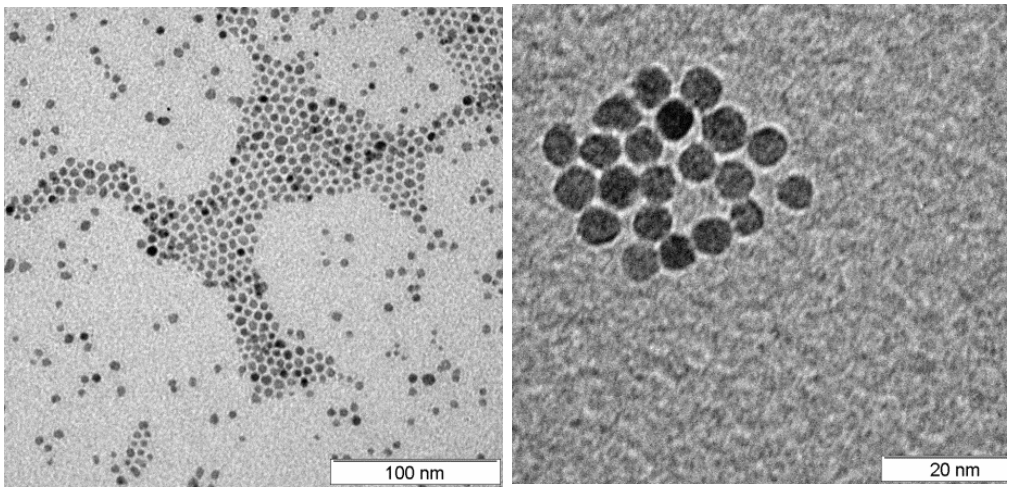

Figure 2 Transmission electron microscopy images of iron oxide nanoparticles with an average diameter of 5.6 ± 1.3 nm at different magnifications.

1.2 Outline

The following chapters demonstrate possibilities to depose different metal nanoparticles on magnetic supports, ensued by the evaluation of the catalytic activity. The recyclability of the catalyst and a possible functionalization to minimize metals leaching were also investigated for the material described in Chapter 2, that was able to promote Suzuki C-C coupling in high yields.

1.3 References

[1] R. N. Grass, E. K. Athanassiou, W. J. Stark, *Angewandte Chemie International Edition* **2007**, *46*, 4909–4912.

[2] S. Sun, H. Zeng, D. B. Robinson, S. Raoux, P. M. Rice, S. X. Wang, G. Li, *Journal of the American Chemical Society* **2004**, *126*, 273–279.

[3] S. Sun, H. Zeng, *Journal of the American Chemical Society* **2002**, *124*, 8204–8205.

[4] P. Riente, C. Mendoza, M. A. Pericas, *Journal of Material Chemistry* **2011**, *21*, 7350–7355.

2. Pd@Co/C and Pd@SiO_2@Co/C nanobeads: evaluation of the catalytic activity for the Suzuki-Miyaura coupling reaction and recyclability test

The activity of a catalyst composed of palladium nanoparticles (NPs) deposited on the surface of carbon-coated cobalt (Co/C) nanobeads has been investigated. The Suzuki-Miyaura C-C cross-coupling of phenylboronic acid and different aryl halides was chosen as a test reaction. Full conversion of the starting material was achieved using aryl iodides and bromides. Moreover, the catalyst could be reused for six consecutive runs without a significant loss in the activity. A modification of the magnetic nanobeads consisting in a silica coating grown around the graphene shell and incorporating a Pd complex, has also been studied. The catalytic activity and recyclability of the new catalyst were afterwards compared with the previous one.

2.1 Introduction

Palladium is one of the most commonly used transition metal in catalytic transformations, in particular for the formation of new carbon-carbon bonds.[1–3] High activities under mild reaction conditions employing small amounts of catalysts have been demonstrated.[4] Moreover, the catalytic activity can be easily tuned by the use of different ligands and additives.[1] The Suzuki-Miyaura coupling, consisting in the cross-coupling of an arylboronic acid and an organohalide, is one of the most versatile and powerful methods for the synthesis of new carbon-carbon bond among all the palladium catalysed reactions. The availability and sustainability of the boronic acids used as starting material,[5] the low toxicity of the by-products formed, the mild reaction conditions and the tolerance to a wide range of substrate and functional groups,[5,6] make this coupling one of the most widely applied reactions for the formation of biaryl skeletons, a very common substructure in pharmaceutical and natural products.[1,5] A general catalytic cycle (Figure 1) involves first an oxidative addition step of an organohalide **2** to a Pd(0) catalyst that leads to the formation of a Pd(II) intermediate **3**. This is the rate-determining step and the reactivity decreases in the following order: I > Br > Cl.[7] The Pd(II) intermediate **3** reacts afterwards with a base to give intermediate **4,** which undergoes transmetallation with an organoboronate **5** to form the organo palladium species **6**. The following reductive elimination releases the desired product **7** and regenerates the original catalyst **1**.

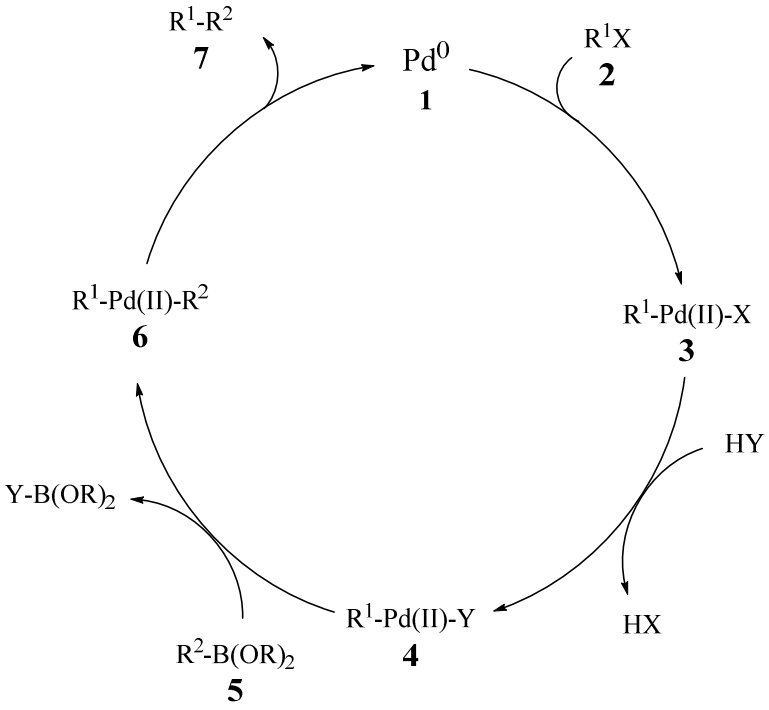

Figure 1 Schematic representation of the Suzuki-Miyaura coupling reaction mechanism.

Although homogeneous palladium catalysts have been extensively investigated because of their extraordinary catalytic activity, their separation from the reaction medium is often complicated.[8] Thus, big interest has grown around the use of heterogeneous catalysts that can replace homogeneous systems.[9] For this purpose, several different supports such as polymers,[10] mesoporous materials,[11] ionic liquids,[12] carbon[6,13] and Al_2O_3[14] have been explored. However, also in these cases the recovery by filtration and ultracentrifugation is not straightforward. Magnetic nanobeads with a high surface-to-volume ratio and superparamagnetic behaviour constitute a promising alternative and, in recent years, broad attention has been focused on their use as supports for Pd catalysts.[2,8] In our group, carbon-coated cobalt nanobeads developed in 2007 by Stark *et al*. and described in the previous chapter have been extensively investigated.[15–17] In 2010 a palladium complex was non-covalently grafted on the graphene-like coating of the cobalt nanobeads and was demonstrated to be able to dissociate from the nanobeads during the hydroxycarbonylation of aryl halides at 100 °C and recaptured at room temperature.[16] The catalyst could then be recovered from the reaction mixture applying an external magnetic field. A different functionalization was developed by Schätz *et al*. that covalently immobilized the nitroxyl radical 2,2,6,6-tetramethylpiperidine-1-oxyl (TEMPO) on the carbon shell of the cobalt nanobeads.[18] The new heterogeneous catalyst was active for the oxidation of primary and secondary alcohols and could be reused for at least six runs.

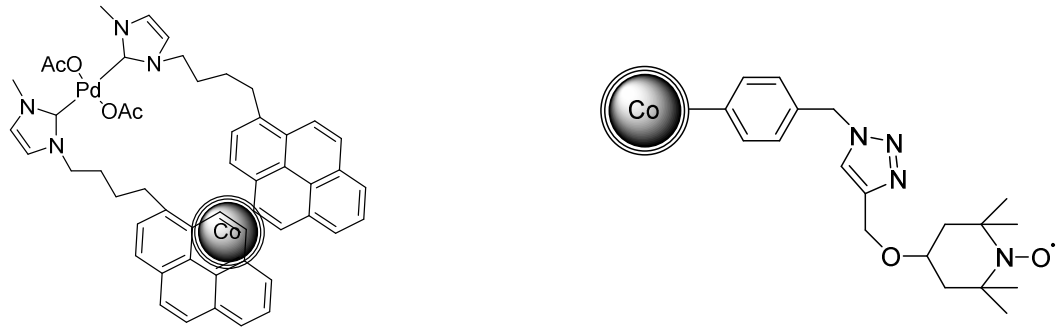

8 **9**

Figure 2 Non covalently immobilized Pd-NHC complex[16] and covalently grafted TEMPO[18] on carbon-coated cobalt nanobeads.

In 2014 an innovative catalytic system composed of Pd nanoparticles deposited on the surface of the carbon-coated cobalt nanobeads was developed by Kainz *et al.*[19] The catalyst exhibited high catalytic activity and good recyclability in hydrogenation reactions at room temperature. Hence, the aim of the present study was to investigate the activity and recyclability of this catalyst for the Suzuki-Miyaura coupling reaction.

A comparison between conventional and microwave heating was also made. In the recent years, microwave (MW) has become a popular and useful heating source in organic chemistry. Reduced reaction times, fast heating, clean transformations and increased reaction yields and selectivity, are the main advantages of this technology.[22] While in the traditional conductive heating the reaction mixture temperature depends on the conductivity of the various materials that have to be warmed up, in microwave irradiation, employing vessels transparent to microwaves, all the heat is generated in the interior of the sample, leading to a faster and more efficient methods. Metals leaching in the final products has also been evaluated and an additional silica coating over the carbon shell of the cobalt nanobeads has been considered in order to reduce the amount of metals released during the reaction.

2.2 Results and discussion

In 2014 Kainz *et al*. developed a new hybrid catalytic system by direct deposition of palladium nanoparticles on the surface of the carbon-coated cobalt nanobeads (Pd@Co/C) produced by Stark *et al*.[19,20] and described in the previous chapter. These seemed to be an appropriate support due to the reported carbon stabilization of metal nanoparticles through π-interactions.[21] Thermal decomposition under microwave irradiation of the complex $Pd_2(dba)_3 \cdot CHCl_3$ (Figure 3) led to the formation of Pd nanoparticles on the surface of the magnetic support in only 2 minutes. Catalyst **11** has been fully characterized[19] and the presence of Pd(0) instead of Pd(II) nanoparticles was confirmed by X-ray powder diffraction (XRD). Well-dispersed 5-10 nm Pd nanoparticles with high catalytic activity for double bond hydrogenation were obtained when the metal loading was fixed to 0.015 mmol/g.

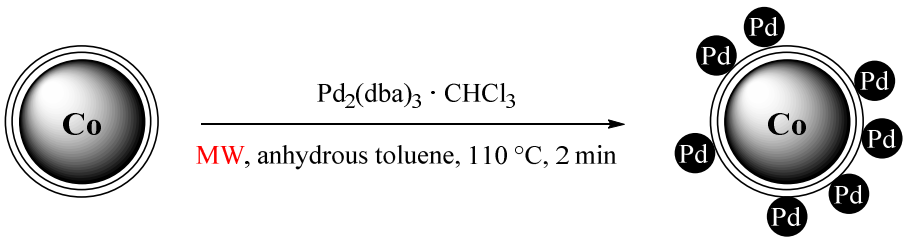

10 **11**

Figure 3 Schematic representation of microwave deposition of Pd nanoparticles on carbon-coated cobalt nanobeads. Co/C nanobeads **10** were dispersed by sonication in a $Pd_2(dba)_3 \cdot CHCl_3$ solution in anhydrous toluene and heated to 110 °C for 2 min by microwave irradiation.

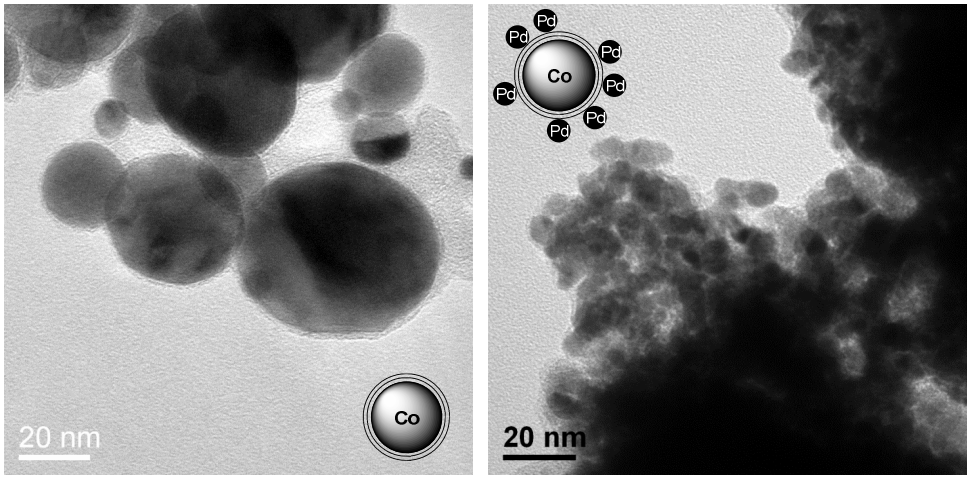

Figure 4 Left: TEM picture of original Co/C nanobeads **10**. Right: TEM pictures of Pd@Co/C nanobeads **11** (Pd loading: 0.015 mmol/g). Figure adapted with permission from Reference [19]. Copyright © 2013, Wiley-VHC Verlag GmbH & Co. KGaA, Weinheim.

In the present work, catalyst **11** was reproduced keeping a Pd loading of 0.015 mmol/g and its catalytic activity for the Suzuki-Miyaura coupling reaction has been investigated. First, different reaction conditions were screened for the coupling of phenylboronic acid **12** and 4-iodoanisole **13**; these results are summarized in Table 1. The use of toluene afforded low yields (entries 1 and 2) and was therefore deemed as not a good solvent for this transformation. Other organic solvents and mixtures of these with water were tested. The use of a mixture of water/ethanol 1:1 afforded the best result (entry 8). Running the reaction in only water, resulted in low isolated yield, probably due to the inadequate dispersibility of the catalyst **11** in this solvent. Interestingly, the minimum amount of catalyst required to obtain full conversion of the starting material was found to be only 0.1 mol%, validating the good activity of Pd@Co/C catalyst **11**. Moreover, the isolation of a clean product without the need of further chromatographic purification was achieved by simple extraction with EtOAc. In addition, the ability of recovering the catalyst applying an external magnetic field and decanting the reaction mixture, enabled a simple and fast reaction protocol. In fact, the higher purity of the products can be attributed to the homogeneous in-situ heating.[23] As shown in Table 1, the use of microwave irradiation, reduced the reaction time for the investigated transformation, obtaining full conversion of the starting material after only 5 minutes.

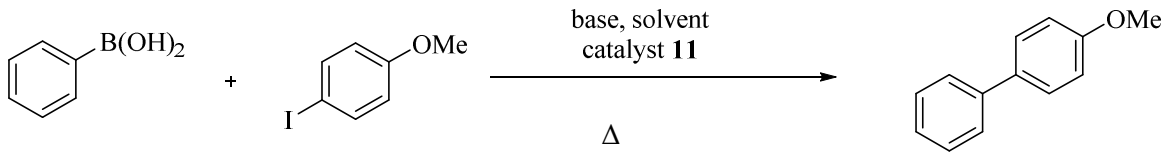

12 **13** **14**

entry	cat. amount	solvent	base	heating	T (°C)	time	yield[a]
1[c]	0.4%	toluene	Cs_2CO_3	conventional	100	overnight	10%
2[c]	0.4%	toluene	Cs_2CO_3	MW	100	45 min	28%
3[c]	0.2%	MeOH	K_3PO_4	conventional	100	4 h	50%
4[c]	0.2%	DMF/water	K_2CO_3	conventional	100	2 h	65%
5[c]	0.2%	THF/water	K_2CO_3	conventional	100	4 h	43%
6[b]	0.2%	EtOH/water	K_3PO_4	conventional	100	2 h	85%
7[b]	0.2%	EtOH/water	K_3PO_4	MW	100	5 min	90%
8[b]	0.1%	EtOH/water	K_3PO_4	MW	100	5min	98%
9[c]	0.05%	EtOH/water	K_3PO_4	MW	100	10 min	65%
10	0.1%	water	K_3PO_4	MW	100	30 min	-
11	-	EtOH/water	K_3PO_4	MW	100	5 min	-

Table 1 Phenylboronic acid **12** (0.55 mmol) was reacted with 4-iodoanisole **13** (0.5 mmol) in 3 ml of solvent adding 1 mmol base and different amounts of catalyst **11**. [a] Yield after product isolation. [b] Product isolated by extraction with EtOAc. [c] Yield after chromatographic purification.

After the successful coupling between arylboronic acids and aryl iodides, the Suzuki-Miyaura reaction of phenylboronic acid **12** and 4-bromoanisole **15** was investigated. In addition, in view of the good results previously achieved working with microwave irradiation, only this heating source was used in the subsequent studies.

As summarized in Table 2, full conversion of the starting material was obtained after a slight increase of the catalyst loading, the temperature and reaction time. The reaction is still fast and simple, requiring only 15 min at 120 °C and 0.3 mol% of catalyst **11**. Moreover, also in this case a clean product was isolated by extraction with EtOAc, without the need of any further purification.

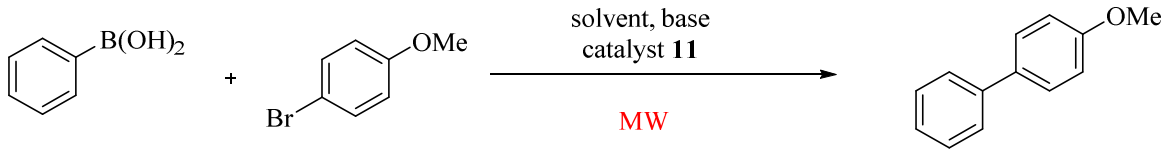

12 **15** **14**

entry	cat. amount	solvent	base	T (°C)	time	yield[a]
1[c]	0.1%	EtOH/water	K_3PO_4	100	40 min	50%
2[c]	0.1%	EtOH/water	K_3PO_4	120	20 min	54%
3[b]	0.2%	EtOH/water	K_3PO_4	120	15 min	86%
4[b]	0.3%	EtOH/water	K_3PO_4	120	15 min	98%

Table 2 Phenylboronic acid **12** (0.55 mmol) was reacted with 4-bromoanisole **15** (0.5 mmol) in 3 ml of solvent adding 1 mmol base and different amount of catalyst **11**. [a] Yield after product isolation. [b] Product isolated by extraction with EtOAc. [c] Yield after chromatographic purification

Next, we wished to evaluate the activity of catalyst **11** for the coupling reaction of phenylboronic acid **12** and 4-chloroacetophenone **16**. It is well known that aryl chlorides are difficult substrates in cross-coupling reactions due to the strength of the C-Cl bond.[6] 4-chloroacetophene **16** was chosen as aryl halide due to the presence of the activating electron withdrawing (EWG) group. Unfortunately the activity of catalyst **11** for this transformation was not as good as in the previous cases. In Table 3 are summarized all the reaction conditions that have been screened. No improvements were observed after increasing catalyst amount, temperature and reaction time. In fact, in each attempt several side products, including the homocoupling of 4-chloroacetophenone **16**, were found. The highest attainable isolated yield of the desired 4-acetylbiphenyl **17** was only 10% (entry 5).

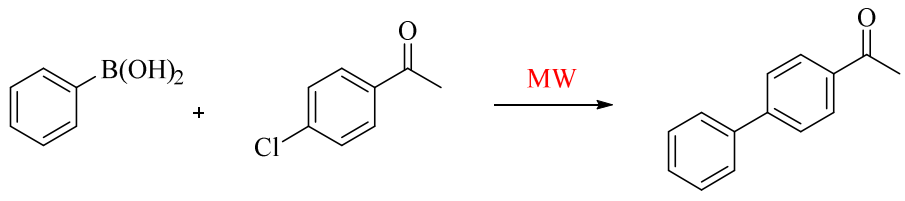

12 **16** **17**

Entry	cat amount	solvent	base	heating	T (°C)	time	yield
1	0.3%	EtOH/water	K_3PO_4	MW	125	30 min	-
2	0.4%	EtOH/water	K_3PO_4	MW	125	30 min	-
3[a,b]	0.4%	EtOH/water	K_3PO_4	MW	120-150	3 h	-
4[a]	0.6%	EtOH/water	K_3PO_4	MW	130-140	3 h	-
5[a]	1%	EtOH/water	K_3PO_4	MW	130-140	5 h	10%
6	2%	EtOH/water	K_3PO_4	MW	130	1 h	-
7	4%	EtOH/water	K_3PO_4	MW	130	1 h	-
8	1%	DMF/water	Cs_2CO_3	MW	130	1 h	-
9	1%	DMF/EtOH/water	K_3PO_4	MW	130	1 h	-

Table 3 Phenylboronic acid **12** (0.55 mmol) was reacted with 4-chloroacetophenone **16** (0.5 mmol) in 3 ml of solvent adding 1 mmol base and different amount of catalyst **11**. [a] Reaction temperature was increased from 120 °C to 150 °C, at a rate of 10 °C/min. [b] It has not been possible to reach temperatures higher than 150 °C because of black leaching from the magnetic nanobeads to the reaction mixture.

Considering the tendency for the formation of homocoupling product of 4-chloroacetophenone **16**, the activity of catalyst **11** for the Ullmann reaction was investigated. This transformation, reported for the first time in 1901, is an additional important and versatile route to construct biaryl units present in a large variety of organic compounds.[24] The reaction conditions tested for this transformation are shown in Table 3. Unfortunately, catalyst **11** showed only modest activity in this transformation. No full conversion of the starting material could be achieved, the highest isolated yield of 4,4'-diacetylbiphenyl **18** being only 35% (entry 6).

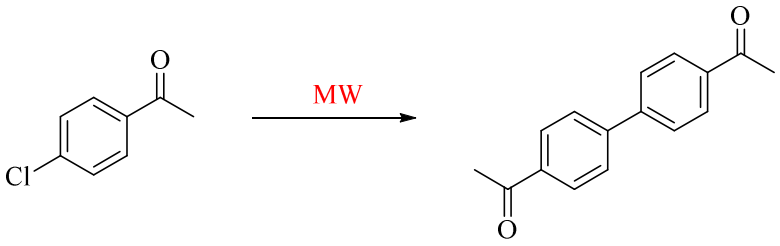

16 **18**

entry	cat amount	solvent	base	T (°C)	time	yield[a]
1	0.3%	EtOH/water	K_3PO_4	120	1 h	-
2	0.5%	EtOH/water	K_3PO_4	120	1 h	-
3	0.5%	DMSO	K_3PO_4	120	5 h	-
4	0.5%	EtOH/water	K_3PO_4	130	2 h	-
5	0.5%	DMF/water	K_3PO_4	130	1 h	25%
6	1%	DMF/water	K_3PO_4	130	2h	35%
7	1%	DMF/water	Et_3N	130	3 h	10%
8	1%	NMP/water	K_2CO_3	130	2 h	-
9	1%	MeCN/water	K_3PO_4	130	2 h	-
10	1%	EtOH/water	Et_3N	130	2 h	11%

Table 4 4-chloroacetophenone **16** (1 mmol) was heated in 3 ml of solvent adding 1.5 mmol base and different amount of catalyst **11**. [a] Isolated yield after chromatographic purification.

Recyclability of catalyst **11** in the Suzuki-Miyaura coupling of phenylboronic acid **12** and 4-bromoacetophenone **19** was investigated, under the reaction conditions previously found to lead to full conversion of the starting materials (Figure 5). After each reaction, the catalyst was recovered with an external magnet, washed several times with water and EtOAc, dried under vacuum and reused in the following reaction. As is possible to observe in Figure 5, catalyst **11** is characterized by good recyclability, being still active after six runs.

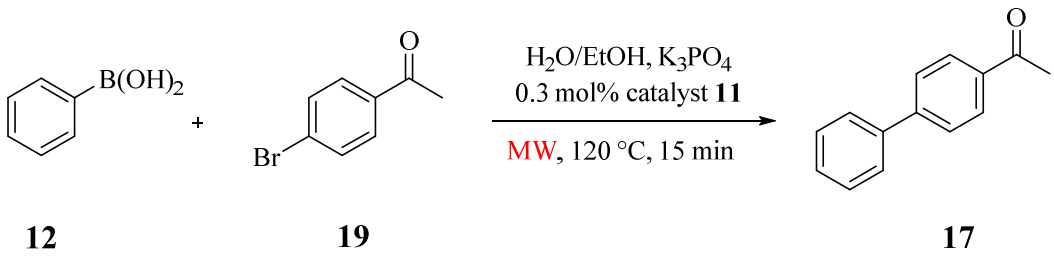

12 **19** **17**

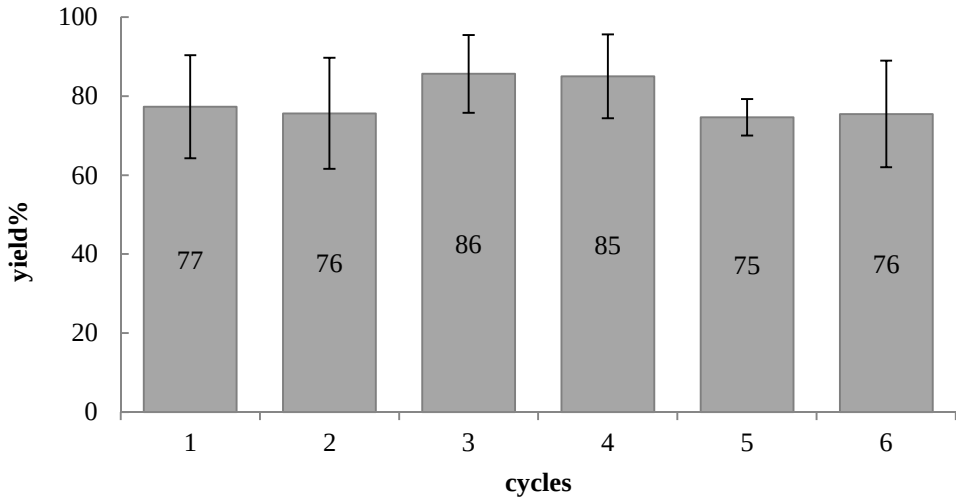

Figure 5 Recycling experiments with catalyst **11** in the Suzuki-Miyaura coupling of phenyl boronic acid **12** and 4-bromoacetophenone **19.** Displayed bars with relative standard deviations are the average of three different results obtained for the same reaction. Yields are given in % at the centre of every single column. Catalyst **11** was recovered with a magnet after each run, washed 4 times with water and EtOAc, dried under vacuum and directly used in the following reaction.

Taking in consideration that an advantage of working with an heterogeneous catalyst is the possibility to avoid heavy metal contamination of the final products, the amount of Pd and Co leached during the Suzuki-Miyaura coupling was evaluated. The 4-acetylbiphenyl **17** products isolated during the recyclability test, were analysed by ICP-OES and the results obtained are shown in Table 5. Since these products belong to an important class of compounds for pharmaceutical industries, metal contamination should lay below very strict limits, typically under 10 ppm.[25,26] As reported in Table 5, the amount of Pd and Co present in the final products is well over the allowed limits. These results are in disagreement with those obtained in the previous work of Kainz *et al.*[19] where the same catalyst **11** was used for the double bond hydrogenation at room temperature. In this case the amount of metals contamination was found to be below the required limits.

This difference in behaviour can be ascribed to the higher reaction temperature applied in the present study that could affect the final metal leaching from the heterogeneous catalyst.

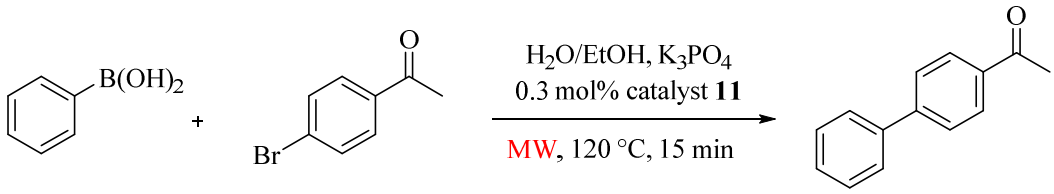

12 **19** **17**

Run	Pd leaching [ppm][a]	Co leaching [ppm][a]
1	52.78	394.6
2	49.13	143.8
3	30.78	80.35
4	19.00	56.82
5	38.24	114.9
6	43.14	151.3

Table 5 Metal leaching evaluation. 4-acetylbiphenyl **17** products obtained from the Suzuki-Miyaura coupling of phenylboronic acid **12** and 4-bromoacetophenone **19** in a mixture of water/EtOH 1:1 (3 ml) under microwave irradiation, have been analysed by ICP-OES. [a] Values expressed in µg metal per g of product.

A functionalization of the carbon coated Co nanobeads **10** and a new metal deposition have been investigated by Soraia Fernandes, a member of our group. With this modification, consisting in a silica coating around the magnetic nanobeads, a decrease in metals leaching could be achieved as it has already been demonstrated.[27] Moreover, it would allow a higher Pd loading on the magnetic nanobeads, improving the reaction protocol as less amount of material would be used. The synthesis shown in Figure 6 consists of a first diazonium-mediated functionalization of the graphene-like shell, followed by the growing of a silica coating around the nanobeads and simultaneous incorporation of the complex $Pd_2(dba)_3 \cdot CHCl_3$ by ultrasonication.

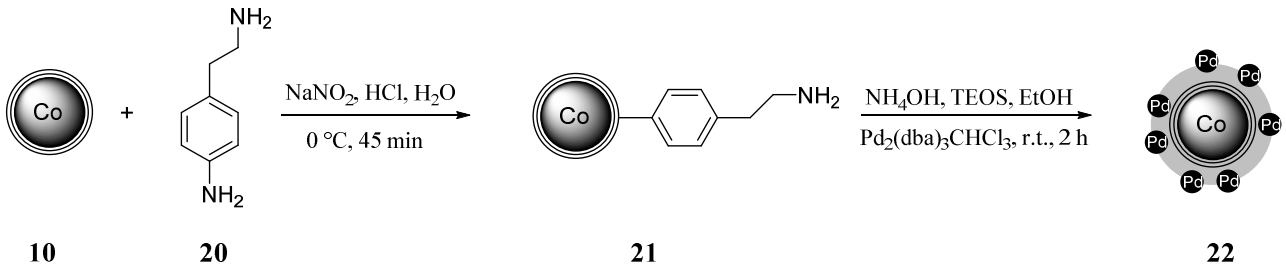

10 **20** **21** **22**

Figure 6 Schematic representation of the silica coating functionalization of the carbon-coated cobalt nanobeads **10** and incorporation of the complex $Pd_2(dba)_3 \cdot CHCl_3$ to form the new catalyst Pd@SiO_2@Co/C NPs **22**. All the reaction steps were performed by ultrasonication.

In Figure 7a the TEM pictures of the new catalyst Pd@SiO_2@Co/C NPs **22** are shown. It is possible to observe that the silica shell is not growing around each single carbon-coated nanobeads **10**, but is incorporating more than one, forming a magnetic cluster. The presence of a palladium complex was confirmed by XPS measurements and a loading of 0.107 mmol/g quantified by ICP-OES.

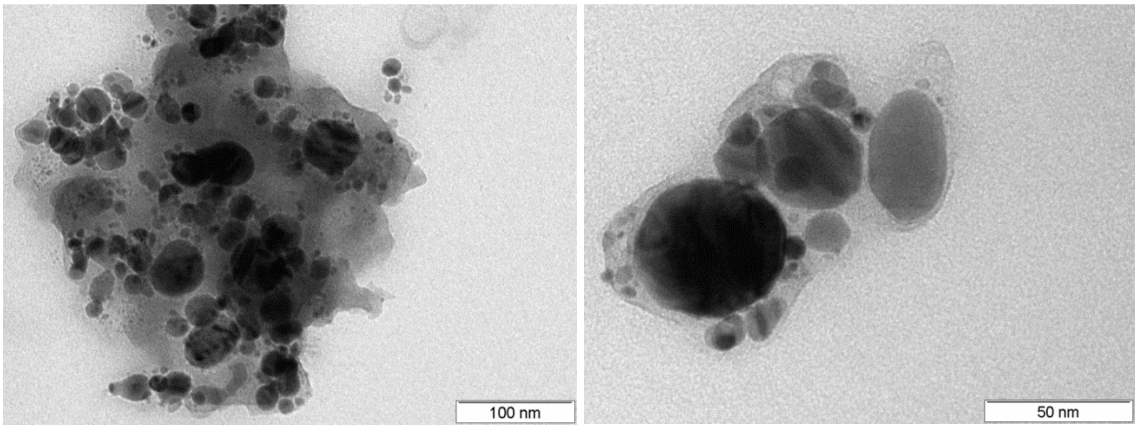

Figure 7 TEM picture of Pd@SiO_2@Co/C NPs (Pd loading of 0.107 mmol/g) **22** at different magnification. Is it possible to observe that the silica shell is growing around more than one carbon coated cobalt nanobead **10**, forming a sort of magnetic cluster.

The thus synthesised catalyst **22**, was also tested for the Suzuki-Miyaura reaction. First, the coupling between phenylboronic acid **12** and two different aryl iodides was evaluated (Table 6), using the same reaction conditions that lead to full conversion of the starting material with the previous catalyst **11**. High catalytic activity was exhibited for this transformation and, also in this case, a clean product could be isolated just by extraction with EtOAc without the need of any further purification. The presence of a strongly deactivating group led to no conversion of the starting material (entry 3).

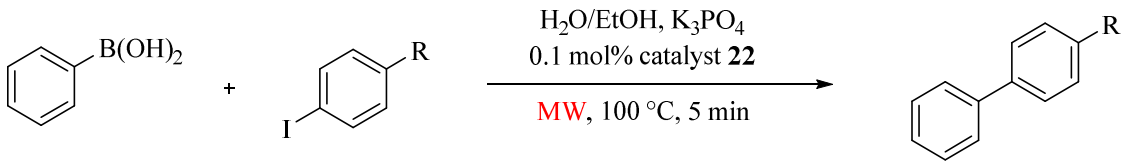

12 **23-25** **26-28**

entry	aryl iodide	product	yield[a]
1	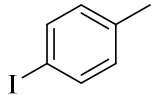 **23**	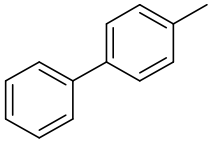 **26**	95%
2	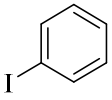 **24**	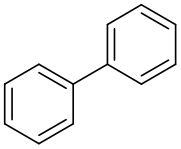 **27**	84%
3	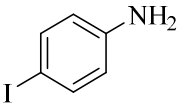 **25**	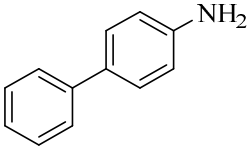 **28**	-

Table 6 Phenylboronic acid **12** (0.55 mmol) was reacted with aryl iodide (0.5 mmol) owing different functional group in *para* position (**23-25**). in 3 ml of solvent adding 1 mmol base and 0.1mol% of catalyst **22**. [a] Yield after product isolation by extraction with EtOAc.

Motivated by the good activity of catalyst **22** for the coupling between phenylboronic acid and aryl iodides, the Suzuki-Miyaura coupling of phenyl boronic acid **12** and aryl bromides with different functional group in *para* position was investigated (Table 7). High yields were achieved also in this transformation and, once more, clean products could be isolated by simple extraction with EtOAc. Oddly, no conversion of the starting material was achieved when an ester or carboxylic acid was present in the substrate (entries 8 and 9).

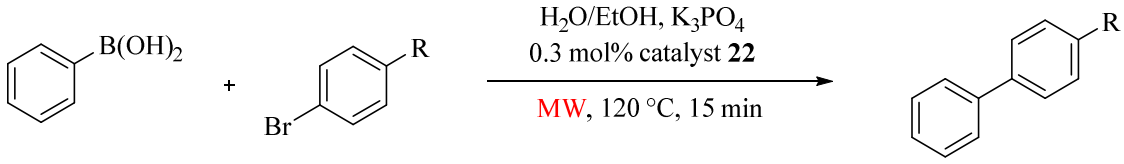

12 **15;19;29-35** **14;18;27;36-41**

entry	aryl bromide	product	yield[a]
1	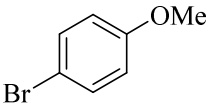 **15**	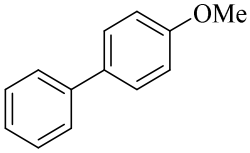 **14**	95%
2	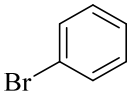 **29**	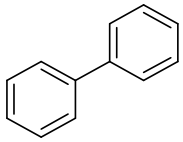 **27**	55%
3	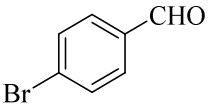 **30**	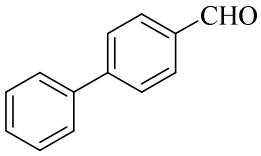 **36**	86%
4	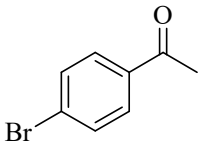 **19**	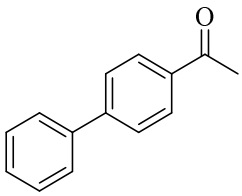 **17**	68%
5	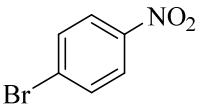 **31**	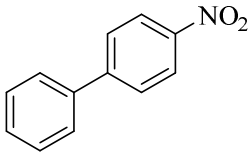 **37**	96%

entry	Aryl bromide	Product	yield[a]
6	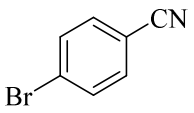 **32**	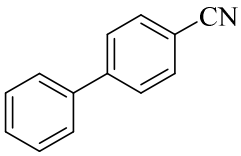 **38**	95%
7	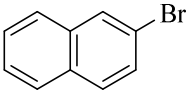 **33**	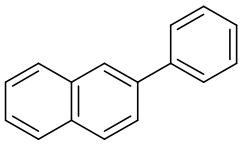 **39**	68%
8	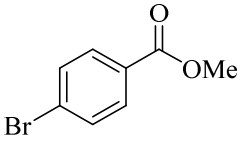 **34**	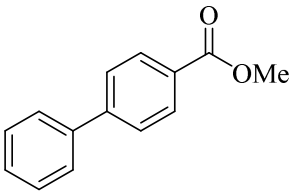 **40**	-
9	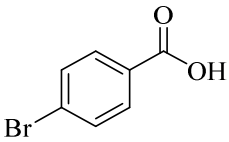 **35**	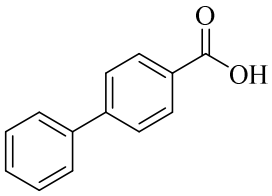 **41**	-

Table 7 Phenylboronic acid **12** (0.55 mmol) was reacted with different aryl bromide (0.5 mmol) owing different functional group in *para* position (**15;19;29-35**) in 3 ml of solvent adding 1 mmol base and 0.3 mol% of catalyst **22**. [a] Yield after product isolation by extraction with EtOAc.

The coupling of phenylboronic acid **12** and 4-chloroacetophenone **16** was also tested under the previously optimized conditions (Table 3, entry 5). Unfortunately, also in this case, the catalyst is not able to activate aryl chlorides and no conversion of the starting material was achieved. The next step was the evaluation of the recyclability of catalyst **22** in the Suzuki-Miyaura coupling of phenylboronic acid **12** and 4-bromoanisole **15.** After each reaction, the catalyst was recovered with an external magnet, washed several times with water and EtOAc, dried under vacuum and reused in the following reaction (Figure 8).

Unlike catalyst **11**, good catalytic activity was exhibited only until the 4th run. Afterwards, lower conversions of the starting material were observed and it was necessary to isolate the product by chromatographic purification.

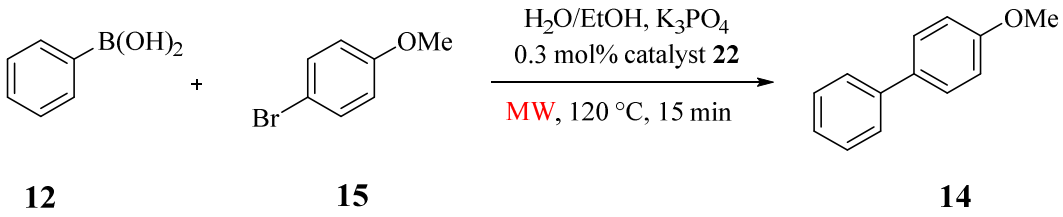

12 **15** **14**

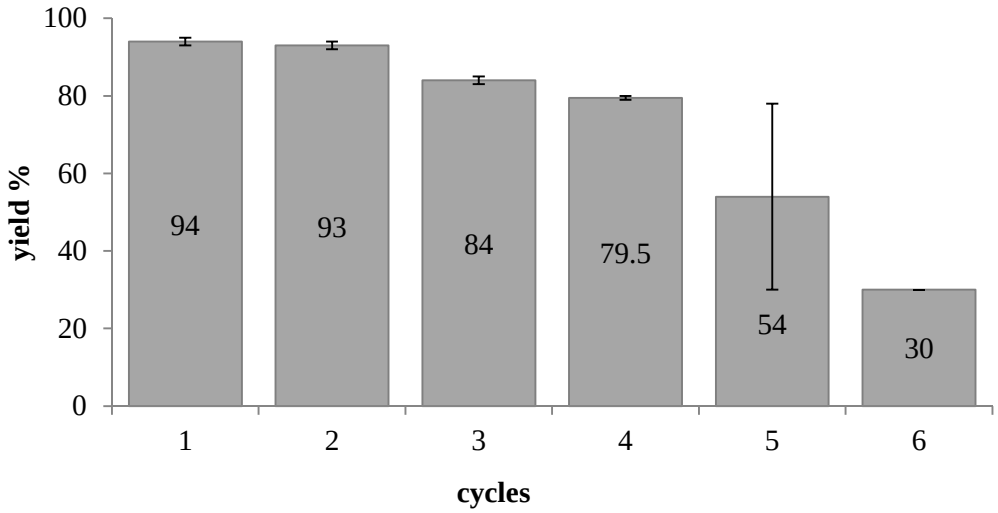

Figure 8 Recycling experiments with catalyst **22** in the Suzuki-Miyaura coupling of phenylboronic acid **12** and 4-bromoanisole **15.** Displayed bars with relative standard deviations are the average of two different results obtained for the same reaction. Yields are given in % at the centre of every single column. Catalyst **22** was recovered with a magnet after each run, washed 4 times with water and EtOAc, dried under vacuum and directly used in the following reaction.

The isolated products were afterwards analysed by ICP-OES in order to assess the amount of metals leached during the reaction, evaluating in this way the role of the additional silica coating. In Table 8 the results obtained are shown. As previously stated, the amount of metals should not exceed 10 ppm and working with the new catalyst **22**, the Pd values are all below the allowed limits. In the case of Co however, even though it is significantly decreased, the amount leached during the reaction is still out of the required range.

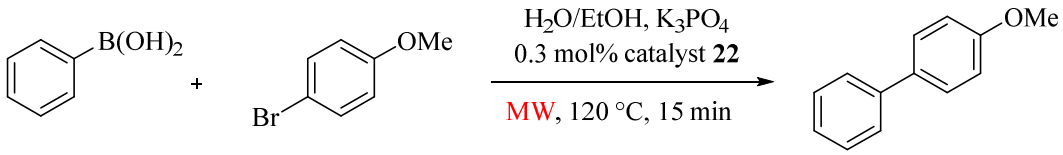

12 **15** **14**

Run	Pd leaching [ppm][a]	Co leaching [ppm][a]
1	6.048	7.48
2	1.070	5.81
3	1.106	7.62
4	0.401	11.23
5	1.417	3.027
6	1.038	30.165

Table 8 Metal leaching evaluation. 4-methoxybiphenyl **14** products obtained from the Suzuki-Miyaura coupling of phenyl boronic acid **12** and 4-bromoanisole **15** in a mixture of water/EtOH 1:1 (3 ml) under microwave irradiation, have been analysed by ICP-OES. [a] Values expressed in µg metal per g of product.

To better highlight the difference between the activities of the two catalysts (**11** and **22**) described in this chapter, a graphic comparison of the results obtained is shown in Figure 9 (a-c). We can conclude that Pd@Co/C NPs **11** are characterized by high catalytic activity for the Suzuki-Miyaura coupling of phenylboronic acid and an aryl iodide and bromide. An equally good activity was found in the case of Pd@SiO_2@Co/C NPs **22**, being the catalyst a Pd complex incorporated in the silica shell instead of Pd(0) nanoparticles. Catalyst **11** exhibits better recyclability compared to catalyst **22**, for which yields drop after the 4th run (Figure 9a). The silica shell characterizing the Pd@SiO_2@CO/C NPs **22** has an evident effect on the metal leaching. Pd amounts found in the final products are considerably decreased working with this catalyst (Figure 9b), while for the Co values, even though definitely improved, they are still out of the allowed limits.

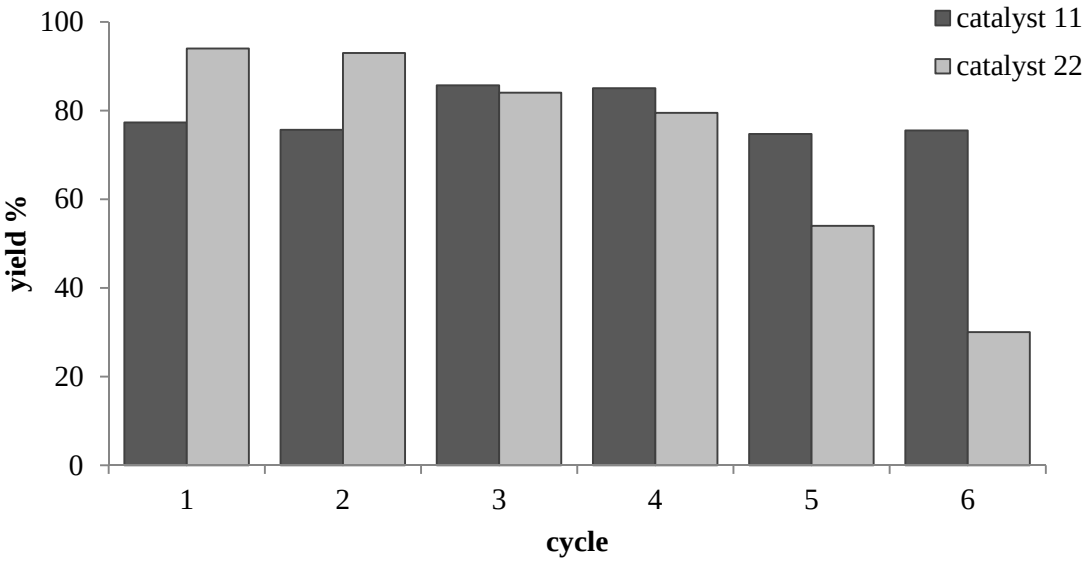

Figure 9a Comparison between the recyclability of the two catalysts investigated in the present study. Pd@Co/C NPs **11** can be recycled for six runs without a significant loss in the activity while working with the Pd@SiO_2@Co/C NPs **22**, the activity drops after the 4^{th} run.

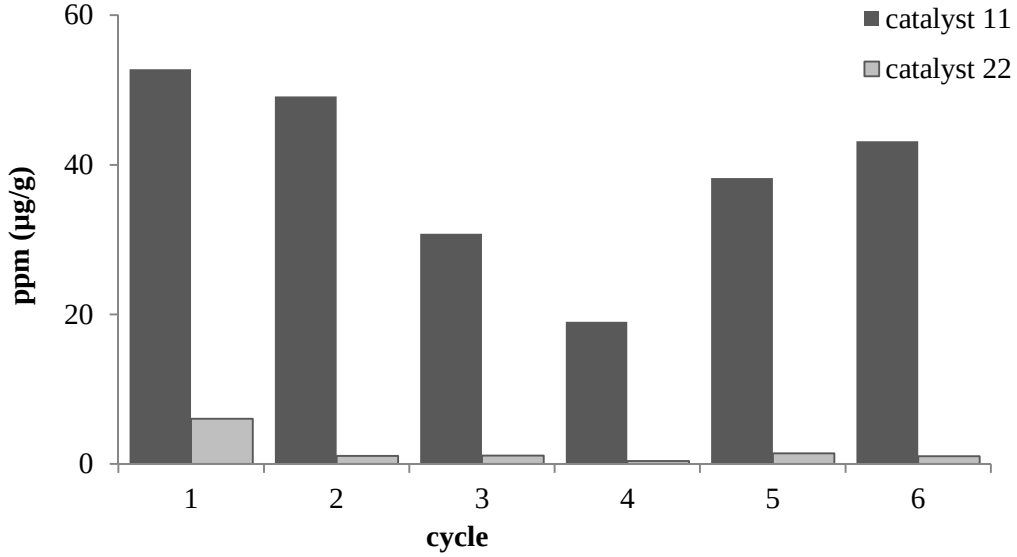

Figure 9b Comparison of the amount of Pd released by the catalyst in the final products. Working with catalyst Pd@SiO_2@Co/C NPs **22** definitely decreases the ppm of metal leached during the reaction.

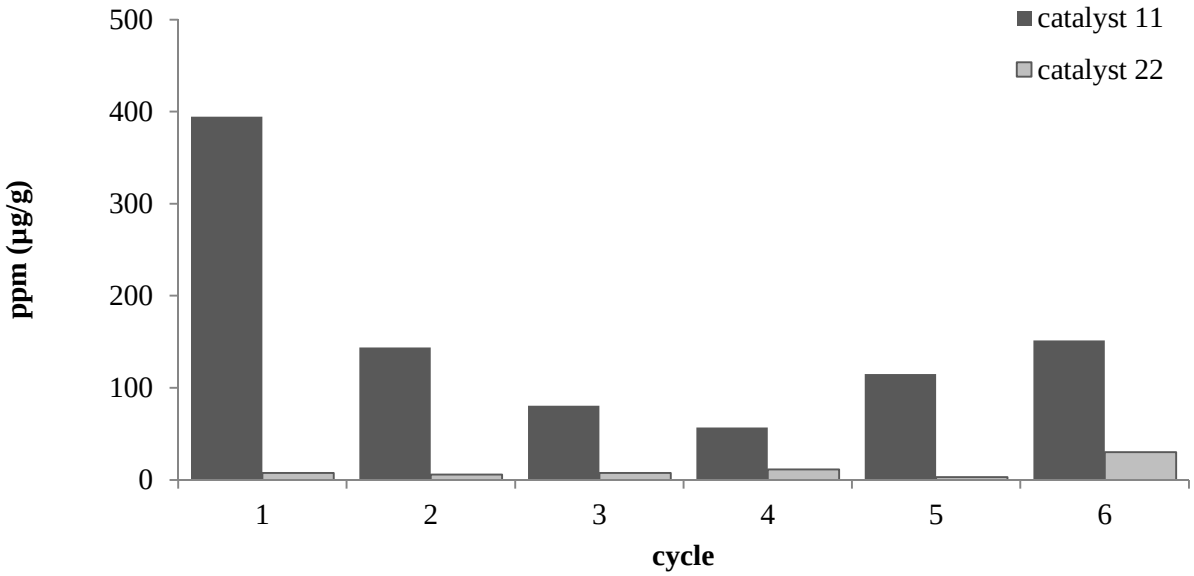

Figure 9c Comparison of the amount of Co released by the catalyst in the final products. Working with catalyst Pd@SiO_2@Co/C NPs **22** definitely decreases the ppm of metal leached during the reaction even if still out of the allowed range.

2.3 Conclusions

In summary, a Pd@Co/C catalyst was successfully applied in the Suzuki-Miyaura coupling of phenylboronic acid with aryl iodides and bromides. High yields were achieved working with low catalyst loadings (0.1 and 0.3 mol% respectively) and in short reaction times (5 and 15 min each) applying microwave irradiation. The catalyst could be recycled for at least six runs without a significant loss in activity.

The activity of a new catalyst derived from a modification of the graphene coated nanobeads and characterized by a Pd(0) complex incorporated into a silica shell grown around the carbon coating of the magnetic nanobeads, was investigated. In this case, high yields were also achieved in the Suzuki-Miyaura coupling of phenylboronic acid and aryl iodides and bromides, applying the previously optimized reaction conditions. The recyclability of the catalyst was not as good as the previous one, the yield dropping after the 4^{th} run. Anyway, the advantages achieved with this functionalization were a higher metal loading on the support but keeping the same high catalytic activity and a decreased metal leaching from the heterogeneous catalyst into the final products.

2.4 Experimental section

Material and methods

Carbon coated cobalt nanobeads (Co/C, 20.5 m^2/g, mean particles size ≈ 40 nm) were purchased from Turbobeads Llc, Switzerland. Prior to use, they were washed in a concentrated HCl/water mixture (1:1) 5 times for 24 h. Acid residues were removed by washing with millipore water (x5) and the particles were dried at 50 °C in a vacuum oven. The magnetic nanobeads were dispersed using an ultrasound bath (Sonorex RK 255 H-R, Bandelin) and recovered with the aid of a neodymium-based magnet (15 x 30 mm). All commercially available compounds were used as received. IR-ATR spectroscopy was carried out on a Biorad Excalibur FTS 3000. Elemental microanalysis (LECO CHN-900) was carried out by the micro analytic Department at the University of Regensburg and by the Universidad Complutense de Madrid. Transmission electron microscopy was carried out by Dr. Daniela Paunesco from ETH, Zurich; by Prof. Josef Zweck from the Department of Physic of the University of Regensburg and by the Microscopy Unit of Universitat Rovira i Virgili, Tarragona. Inductively coupled plasma optical emission spectrometry was carried out by University of Regensburg (Spectro Analytical Instruments ICP Modula EOP), by Universidad de Alicante and by MEDAC Ltd, United Kingdom. XPS measurements were performed by Thomas Meier from the Department of Physic at the University of Regensburg and by SuSoS, Switzerland. Pd@Co/C nanoparticles **11** were prepared following a previously reported procedure.[19] NMR spectra were recorded with a Bruker AV 300 spectrometer. Chemical shifts (δ) are reported in ppm and coupling constants (*J*) are reported in Hertz (Hz). The signals in the spectra are described as singlet (s), doublet (d), triplet (t) and multiplet (m).

Palladium nanoparticles deposited on the graphene-like shell of cobalt nanobeads (11)

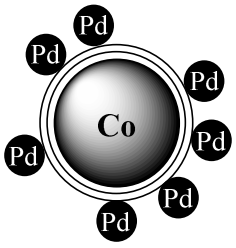

500 mg Co/C nanobeads **10**, $Pd_2(dba)_3 \cdot CHCl_3$ (3.88 mg, 7.5 µmol) and anhydrous toluene (3 ml) were introduced in a microwave vessel under nitrogen atmosphere. The reaction mixture was sonicated in an ultrasonic bath for 10 min and then heated in a microwave oven to 110 °C for 2 min. The catalyst was recovered by an external magnet, the solution decanted and the nanoparticles washed with DCM (5 x 3 ml). After drying under vacuum, the metal loading was evaluated by ICP-OES (0.015 mmol/g).

Functionalization of the graphene-like coating of cobalt nanobeads by diazonium chemistry (21)

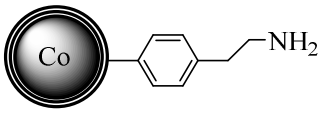

1 g Co/C nanobeads **10** (0.17 mmol/g of C), 4-(2-aminoethyl)aniline (224 µl, 1.7 mmol, 10 equiv), conc. HCl (1.7 ml) and water (23 ml) were introduced in a round bottom flask and the reaction mixture was sonicated in an ultrasonic bath for 15 min. The dispersion was cooled to 0 °C in an ice/water bath before generation of the diazonium species *in situ* by adding dropwise a cooled solution of $NaNO_2$ (176 mg, 2.55 mmol, 15 equiv in 23 ml water). The slurry was sonicated for additional 30 min at room temperature. The nanoparticles were collected by a magnet and the supernatant decanted. The magnetic nanobeads were carefully washed with a 1 M solution of NaOH (3 x 20 ml) and water (3 x 20 ml). When the pH was neutral, the nanobeads were additionally washed with acetone (3 x 15 ml) and Et_2O (2 x 15 ml). After freeze-drying under vacuum, the nitrogen loading was evaluated by microelemental analysis (0.14 mmol/g).

Palladium complex incorporation in the silica shell growing around the graphene-like coating of cobalt nanoparticles (22)

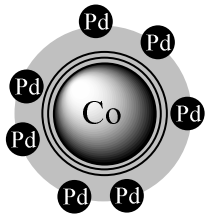

100 mg of Co/C-NH_2 nanobeads **21**, aqueous ammonia (32%, 16 ml) and EtOH (200 ml) were introduced in a round bottom flask and the reaction mixture was sonicated in an ultrasonic bath for 30 min. Afterwards, tetraethyl orthosilicate (TEOS) was added (0.1 ml) and the sonication was continued for an additional 1 h. Then, $Pd_2(dba)_3 \cdot CHCl_3$ (20 mg, 0.019 mmol) was added to the reaction mixture and the sonication was continued for 1 h. Once the catalyst was collected with an external magnet and the reaction mixture decanted, the nanobeads were thoroughly washed with water (7 x 40 ml). After drying under vacuum, the Pd loading was evaluated by ICP-OES (0.107 mmol/g).

General procedure for the Suzuki-Miyaura coupling of phenylboronic acid and an aryl halide using Pd@Co/C catalyst 11 under conventional heating (GP1)

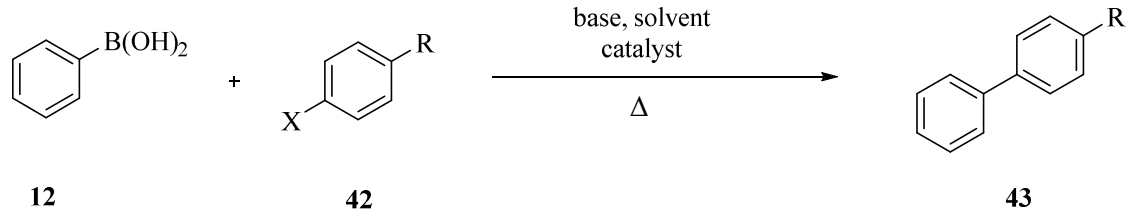

12 **42** **43**

GP1. The desired amount of Pd@Co/C **11**, phenylboronic acid (0.55 mmol), aryl halide (0.5 mmol), base (1 mmol) and solvent (3 ml) were introduced into a Schlenk tube. The reaction mixture was heated to the desired temperature in an oil bath and vigorously stirred. The reaction progress was monitored by TLC and the heating was stopped when no further conversion of the starting material was observed. Once cooled down to room temperature, the catalyst was collected with a magnet and the supernatant decanted in a separation funnel. The nanobeads were washed with water (3 x 3 ml) and EtOAc (3 x 3 ml) and dried under vacuum. The solvent collected from the washing step was also added to the separation funnel and the product was isolated by extraction with EtOAc (3 x 15 ml). The organic phase was dried over $MgSO_4$ and the solvent evaporated under vacuum, checking the crude material by ^1H NMR analysis. For isolation of the products, the crude mixture was purified by column chromatography.

General procedure for the Suzuki-Miyaura coupling of phenylboronic acid and an aryl halide using Pd@Co/C catalyst 11 and Pd@SiO_2@Co/C catalyst 22 under microwave irradiation (GP2)

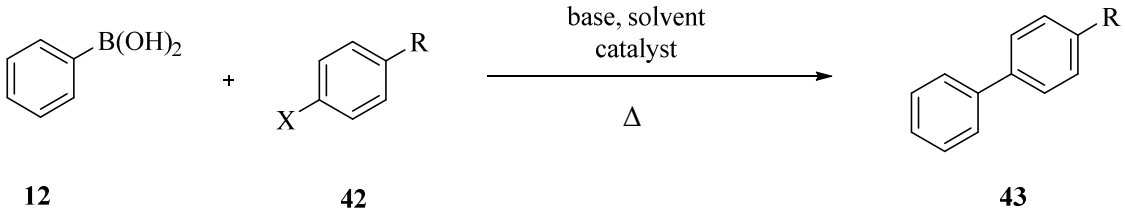

12 **42** **43**

GP2. The desired amount of Pd@Co/C **11** or Pd@SiO_2@CO/C **22**, phenylboronic acid (0.55 mmol), aryl halide (0.5 mmol), base (1 mmol) and solvent (3 ml) were introduced into a microwave vessel. The reaction mixture was vigorously stirred for 5 min and heated to the desired temperature under microwave irradiation. The reaction progress was monitored by TLC and the heating was stopped when no further conversion of the starting material was observed. Once cooled down to room temperature, the catalyst was collected with a magnet and the supernatant decanted in a separation funnel. The nanobeads were washed with water (3 x 3 ml) and EtOAc (3 x 3 ml) and dried under vacuum.

The solvent collected from the washing step was added to the separation funnel and the product was isolated by extraction with EtOAc (3 x 15 ml). The organic phase was dried over $MgSO_4$ and the solvent evaporated under vacuum to give a crude material that was submitted to ^1H NMR analysis. In case of not achieving full conversion of the starting material, the product was isolated from the crude mixture by column chromatography.

For the recycling experiments, the nanoparticles were separated by an external magnet and after magnetic decantation, they were washed with water (3 x 3 ml) and EtOAc (3 x 3 ml). After drying under vacuum, the catalyst was reused for further runs.

General procedure for the Ullmann homo-coupling of 4-chloroacetophenone using Pd@Co/C 11 (GP3)

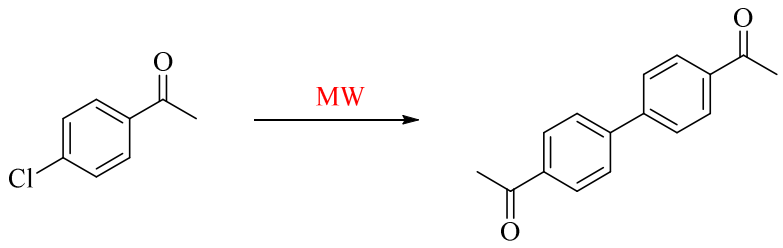

16 **18**

GP3. The desired amount of Pd@Co/C **11**, 4-chloroacetophene (1 mmol), base (1.5 mmol) and solvent (3 ml) were introduced into microwave vessel. The reaction mixture was stirred vigorously for 5 min and heated to the desired temperature under microwave irradiation. The reaction progress was monitored by TLC and the heating was stopped when no further conversion of the starting material was observed. Once cooled down to room temperature, the catalyst was collected with a magnet and the supernatant decanted in a separation funnel. The nanobeads were washed with water (3 x 3 ml) and EtOAc (3 x 3 ml) and dried under vacuum. The solvent collected from the washing step was also added to the separation funnel and the product was isolated by extraction with EtOAc (3 x 15 ml). The organic phase was dried over $MgSO_4$ and the solvent was evaporated under vacuum to give a crude material that was submitted to ^1H NMR analysis.

For isolation of the products, the crude mixture was purified by column chromatography.

NMR Data

All products are literature-known and all spectroscopic data match with those reported in the literature.

4-Methoxybiphenyl (14)

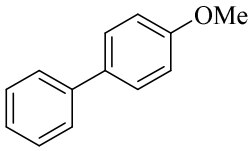

Synthesised according to the general procedure **GP2**.

^{1}H NMR (300 MHz, $CDCl_3$): δ = 7.58-7.52 (m, 4H), 7.45-7.39 (m, 2H), 7.34-7.28 (m, 1H), 7.00 (d, *J* = 8.8, 2H), 3.86 (s, 3H); **^{13}C NMR** (75 MHz, $CDCl_3$): δ = 159.1, 140.8, 133.8, 128.7, 128.1, 126.7, 126.6, 114.2, 55.3.

4-Acetylbiphenyl (17)

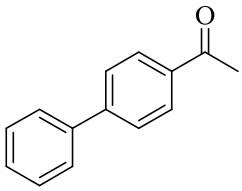

Synthesised according to the general procedure **GP2**.

^{1}H NMR (300 MHz, $CDCl_3$): δ = 8.04 (d, *J* = 8.5, 2H), 7.72-7.61 (m, 4H), 7.51-7.38 (m, 3H), 2.65 (s, 3H); **^{13}C NMR** (75 MHz, $CDCl_3$): δ = 197.8, 145.8, 139.9, 135.8, 128.9, 128.9, 128.3, 127.3, 127.3, 26.7.

4-Methylbiphenyl (26)

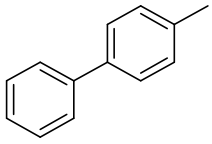

Synthesised according to the general procedure **GP2**.

^{1}H NMR (300 MHz, $CDCl_3$): δ = 7.65-7.62 (m, 2H), 7.54-7.48 (m, 2H), 7.47-7.40 (m, 2H), 7.37-7.30 (m, 1H), 7.29-7.24 (m, 2H), 2.41 (s, 3H); **^{13}C NMR** (75 MHz, $CDCl_3$): δ = 135.7, 132.8, 129.5, 128.8, 128.0, 127.0, 127.0, 21.1

Biphenyl (27)

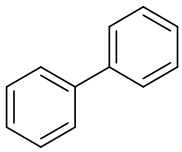

Synthesised according to the general procedure **GP2**.

^{1}H NMR (300 MHz, $CDCl_3$): δ = 7.64-7.61 (m, 4H), 7.50-7.44 (m, 4H), 7.40-7.35 (m, 2H);

^{13}C NMR (75 MHz, $CDCl_3$): δ = 141.3, 128.8, 127.3, 127.2.

Biphenyl-4-carboxaldehyde (36)

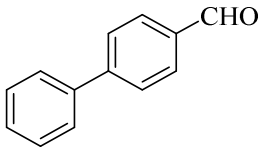

Synthesised according to the general procedure **GP2**.

^{1}H NMR (300 MHz, $CDCl_3$): δ = 10.07 (s, 1H), 7.96 (d, *J* = 8.21, 2H), 7.76 (d, *J* = 7.7, 2H), 7.65 (m, 2H), 7.52-7.41 (m, 3H); **^{13}C NMR** (75 MHz, $CDCl_3$): δ = 192.0, 147.2, 139.7, 135.2, 130.3, 129.0, 128.5, 127.7, 127.4.

4-Nitrobiphenyl (37)

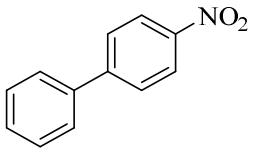

Synthesised according to the general procedure **GP2**.

^{1}H NMR (300 MHz, $CDCl_3$): δ = 8.30 (d, *J* = 8.8, 2H), 7.74 (d, *J* = 8.8, 2H), 7.65-7.59 (m, 2H), 7.54-7.44 (m, 3H); **^{13}C NMR** (75 MHz, $CDCl_3$): δ = 147.6, 147.0, 138.7, 129.2, 128.9, 127.8, 127.4, 124.1.

4-Cyanobiphenyl (38)

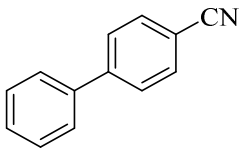

Synthesised according to the general procedure **GP2**.

^{1}H NMR (300 MHz, $CDCl_3$): δ = 7.76-7.66 (m, 4H), 7.62-7.57 (m, 2H), 7.52-7.40 (m, 3H); **^{13}C NMR** (75 MHz, $CDCl_3$): δ = 145.6, 139.1, 132.6, 129.1, 128.6, 127.7, 127.2, 119.9, 110.9.

2-Phenylnaphtalene (39)

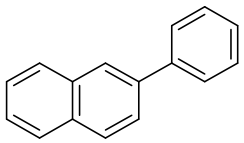

Synthesised according to the general procedure **GP2**.

^{1}H NMR (300 MHz, $CDCl_3$): δ = 8.05 (s, 1H), 7.95-7.85 (m, 3H), 7.78-7.71 (m, 3H), 7.55-7.46 (m, 4H), 7.42-7.34 (m, 1H); **^{13}C NMR** (75 MHz, $CDCl_3$): δ = 134.5, 131.6, 127.7, 127.3, 127.1, 126.9, 126.5, 126.3, 126.2, 125.2, 124.8, 124.7, 124.5

2.5 References

[1] S. Paul, M. M. Islam, S. M. Islam, *RSC Advances* **2015**, *5*, 42193–42221.

[2] M. Gholinejad, M. Razeghi, C. Najera, *RSC Advances* **2015**, *5*, 49568–49576.

[3] S. Sobhani, Z. Zeraatkar, F. Zarifi, *New Journal of Chemistry* **2015**, *39*, 7076–7085.

[4] J.-C. Hierso, J. Boudon, M. Picquet, P. Meunier, *European Journal of Organic Chemistry* **2007**, 583–587.

[5] X. Sun, Y. Zheng, L. Sun, H. Su, C. Qi, *Catalysis Letters* **2015**, *145*, 1047–1053.

[6] L. Duan, R. Fu, Z. Xiao, Q. Zhao, J. Wang, S. Chen, Y. Wan, *ACS Catalysis* **2015**, *5*, 575–586.

[7] N. Miyaura, A. Suzuki, *Chemical Reviews* **1995**, *95*, 2457–2483.

[8] P. P. Latha, M. Bhatt, S. L. Jain, *Tetrahedron Letters* **2015**, *56*, 5718–5722.

[9] A. Balanta, C. Godard, C. Claver, *Chemical Society Reviews* **2011**, *40*, 4973–4985.

[10] E. D. Sultanova, V. V. Salnikov, R. K. Mukhitova, Y. F. Zuev, Y. N. Osin, L. Y. Zakharova, A. Y. Ziganshina, A. I. Konovalov, *Chemical Communications* **2015**, *51*, 13317–13320.

[11] A. Berenguer, T. M. Sankaranarayanan, G. Gomez, I. Moreno, J. M. Coronado, P. Pizarro, D. P. Serrano, *Green Chemistry* **2016**, *18*, 1938-1951

[12] J. Restrepo, R. Porcar, P. Lozano, M. I. Burguete, E. García-Verdugo, S. V. Luis, *ACS Catalysis* **2015**, *5*, 4743–4750.

[13] A. Ohtaka, J. M. Sansano, C. Nájera, I. Miguel-García, Á. Berenguer-Murcia, D. Cazorla-Amorós, *ChemCatChem* **2015**, *7*, 1841–1847.

[14] V. A. Kondratenko, C. Berger-Karin, E. V. Kondratenko, *ACS Catalysis* **2014**, *4*, 3136–3144.

[15] R. Linhardt, Q. M. Kainz, R. N. Grass, W. J. Stark, *RSC Advances* **2014**, *4*, 8541–8549.

[16] S. Wittmann, A. Schätz, R. N. Grass, W. J. Stark, O. Reiser, *Angewandte Chemie International Edition* **2010**, *49*, 1867–1870.

[17] S. Fernandes, C. M. Eichenseer, P. Kreitmeier, J. Rewitzer, V. Zlateski, R. N. Grass, W. J. Stark, O. Reiser, *RSC Advances* **2015**, *5*, 46430–46436.

[18] A. Schätz, R. N. Grass, W. J. Stark, O. Reiser, *Chemistry – A European Journal* **2008**, *14*, 8262–8266.

[19] Q. M. Kainz , R. Linhardt , R. N. Grass , G. Vilé , J. Pérez-Ramírez, W. J. Stark , O. Reiser, *Advanced Functional Materials* **2014**, *24*, 2020–2027.

[20] R. N. Grass, E. K. Athanassiou, W. J. Stark, *Angewandte Chemie International Edition* **2007**, *46*, 4909–4912.

[21] S. Chandra, S. Bag, P. Das, D. Bhattacharya, P. Pramanik, *Chemical Physics Letters* **2012**, *519–520*, 59–63.

[22] L. Perreux, A. Loupy, *Tetrahedron* **2001**, *57*, 9199–9223.

[23] M. Larhed, C. Moberg, A. Hallberg, *Accounts of Chemical Research* **2002**, *35*, 717–727.

[24] G. Cravotto, M. Beggiato, A. Penoni, G. Palmisano, *Tetrahedron Letters* **2005**, *46*, 2267–2271.

[25] V. L. Budarin, P. S. Shuttleworth, J. H. Clark, R. Luque, *Current Organic Synthesis* **2010**, *7*, 614–627.

[26] C. E. Garrett, K. Prasad, *Advanced Synthesis & Catalysis* **2004**, *346*, 889–900.

[27] Q. Liu, Z. Xu, J. A. Finch, R. Egerton, *Chemistry of Materials* **1998**, *10*, 3936–3940.

3. Deposition of platinum and gold nanoparticles on the graphene-like coating of cobalt nanobeads and evaluation of their catalytic activity

The deposition of noble metals (Pt and Au) nanoparticles on the surface of carbon-coated cobalt nanobeads was investigated. The study could lead to the development of a catalyst containing an expensive metal that can be easily recovered from the reaction mixture and recycled for more than one run, achieving a cheap and fast reaction performance. Different synthetic pathways were employed in order to obtain ultra-small catalytically active metal nanoparticles with an average diameter of 3-5 nm. The catalytic activity of the synthesized materials was tested for secondary alcohol oxidation and hydrogenation of both nitro derivates and double C-C double bonds.

3.1 Introduction

Noble metals nanoparticles, with their unique physical and chemical properties that differentiate them from the bulk materials,[1] have attracted a wide interest in the recent years and have been applied in different fields, from catalysis[2] to sensing,[3] biomedicine[4] and nanoelectronics.[5] Due to the high cost of these metals and the growing need of developing environmentally-friendly and sustainable catalytic systems, deposition of metal nanoparticles on solid supports that can be easily recovered and recycled, have been extensively investigated. Deposition of gold and platinum nanoparticles on carbon nanotubes and related materials or, alternatively, on magnetic supports is widely reported. The aim of the present work is to combine the qualities of these two different materials, depositing gold and platinum nanoparticles on the graphene-like coating of cobalt nanobeads (**10**) previously described. On one hand, magnetically separable nanocatalyst can be easily and rapidly separated from the reaction mixture by applying an external magnetic field, allowing recyclability and decreasing costs and, on the other hand, carbon-based materials are one of the most applied support for metals nanoparticles due to their outstanding characteristics *i.e*. large surface area, high strength and the ability to increase the contact between reactant and catalytic sites.[6] An additional goal is the development of an easy and fast synthetic pathway without employing procedures that require long reaction times at high temperatures (*e.g*. calcination and annealing processes)[7] or particular instrumentations (*e.g*. laser vaporization deposition). Gold in the bulk form has been historically considered catalytically inert as it is inactive towards chemisorption of oxygen and hydrogen.[8] Lately, the catalytic activity of this metal once the particle size is reduced to few nanometres has been revealed, the performance being strongly dependent on the size and shape of the nanoparticles. Also platinum-based nanosystems have found a large application because of their high catalytic activity and stability.[9] A wide range of organic transformations are catalysed by these two metals from alcohol oxidation to hydrogenation of both C-C double bonds and nitro groups,[10] employing molecular H_2 and O_2. This type of catalytic transformations are highly attractive since they represent the main goals of green chemistry: high activity, recyclability and minimization of by-products and waste. Nitroarenes are known to be harmful industrial waste with long degradation times and their removal is an important concern for public health.[12] Hydrogenation with $NaBH_4$ was demonstrated to be an effective choice leading to the formation of aminoarenes that found a wide application in synthetic organic chemistry and in the manufacture of antipyretics, analgesics[13] and in the industrial production of polymers.[11] The widely accepted mechanism was proposed by Haber in 1898 and is shown in Figure 1.[14] The hydrogenation is characterized by a first reduction step of the nitro group to a nitroso group, followed by the addition of a second equivalent of hydrogen to form an hydroxylamine. A further addition of hydrogen leads to the formation of the final aniline derivative. An important feature of the employed catalyst is to avoid accumulation of the intermediates and the developing of side reactions (*e.g*. hydroxylamine and nitroso compound condensation).

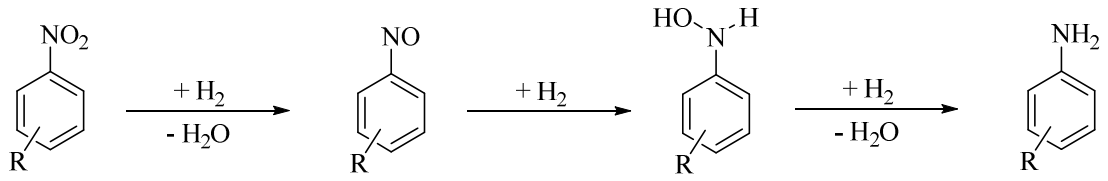

Figure 1 Schematic representation of the reduction mechanism of nitro derivatives proposed by Haber in 1898.

Selective alcohol oxidation is another important class of transformation in organic chemistry, leading to the formation of building blocks applied in the synthesis of various drugs, agro-chemicals and fragrances.[15] Moreover, catalytic oxidation is a significant green alternative to the use of metal-based oxidants such as permanganate and manganese dioxide that are a major source of waste and problematic by-products.[16,17]

Encouraging precedents have been recently reported. In 2012, Yang *et al*. developed a catalyst composed of Pt nanoparticles deposited on engineered carbon nanotubes (CNTs) by incipient wetness impregnation. The nanocatalyst was employed in the hydrogenation of chloronitrobenzene showing, in comparison to platinum nanoparticles supported on activated carbon, lower activity for C-Cl hydrogenolysis and higher selectivity to chloroaniline due to the advantageous porosity of the support.[7] Kumar *et al*., in 2013, synthesised new carbon nanotube-gold nanohybrids. Multiwall carbon nanotubes (MWCNTs) were decorated twice with polymers, obtaining a two-layer assembly on which monodispersed gold nanoparticles with an average diameter of 3 nm were deposited. The nanohybrid showed high catalytic activity for the oxidation of diverse alcohols at room temperature and under mild conditions. Under anhydrous conditions, primary alcohols were converted to the corresponding aldehyde while the presence of water in the reaction mixture led to the formation of the acid derivatives. The catalyst could also be reused for consecutive reactions without any loss in the catalytic activity.[18]

3.2 Results and discussion

Considering the increasing need of developing green and sustainable catalytic systems, the deposition of gold and platinum nanoparticles on the graphene-like coating of cobalt nanobeads **10** previously described, was investigated. The study would lead to the synthesis of a catalyst that can be easily and quickly recovered from the reaction mixture by applying an external magnetic field and can be recycled for several consecutive runs. The recyclability of these catalysts composed of expensive noble metals, would decrease the cost of the performing such reactions.

An important key factor working with metal nanoparticles, is the ability to synthesise small and shaped nanomaterials, exploiting their affinity for carbonaceous surfaces that discriminate the magnetic support employed in the present work. Different synthetic pathways were evaluated and are described in the subsequent sections. Bearing in mind the previously described catalyst Pd@Co/C NPs **11** showing the highest activity with a metal loading of 0.015 mmol/g, in most of the following described attempts was planned to achieve the same final metal loading. Selected samples were analysed by TEM and XPS.

3.2.1 Deposition of Au nanoparticles on graphene-coated cobalt nanobeads and evaluation of their catalytic activity

Considering the reported high similarity of the carbon coating of the cobalt nanobeads **10** with carbon nanotubes,[19] a first attempt of deposition of gold nanoparticles on the surface of the magnetic nanobeads was done taking in consideration the work of Choi *et al*. that reported a spontaneous metal nanoparticles formation on singlewalled carbon nanotube (SWCNT) by direct redox reaction between the metal ions and the carbon nanotubes. In the cited work, Au nanoparticles with an average size of 7 nm were formed on the sidewalls of the CNTs in short reaction times.[20] In Figure 2 is shown a scheme of the reproduced synthesis employing the carbon-coated cobalt nanobeads **10**. These were stirred for 1 hour in a water/EtOH solution of the Au salt, collected by an external magnet, washed several times with water and dried under vacuum. The amount of gold deposited on the carbon shell of the magnetic nanobeads was evaluated by ICP-OES. The synthesis did not lead to the expected results, the final gold incorporation in the nanocatalyst **44**, being only 22%. TEM pictures of the sample (Figure 3) show a tendency of the gold nanoparticles to agglomerate and to distribute without a regular size on the surface of the magnetic nanobeads.

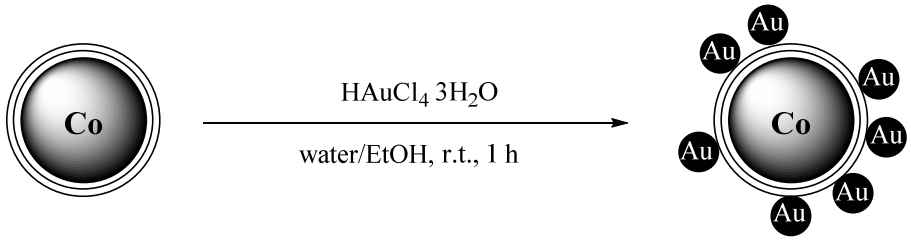

10 **44**

Figure 2 Schematic representation of the synthesis of catalyst **44**. Carbon-coated cobalt nanobeads **10** were stirred in a gold water/EtOH solution for 1 hour. Afterwards the catalysts was collected with a magnet, the reaction mixture decanted and the nanobeads washed several times with water before being dried under vacuum. Au loading of 0.005 mmol/g was evaluated by ICP-OES (22% incorporation)

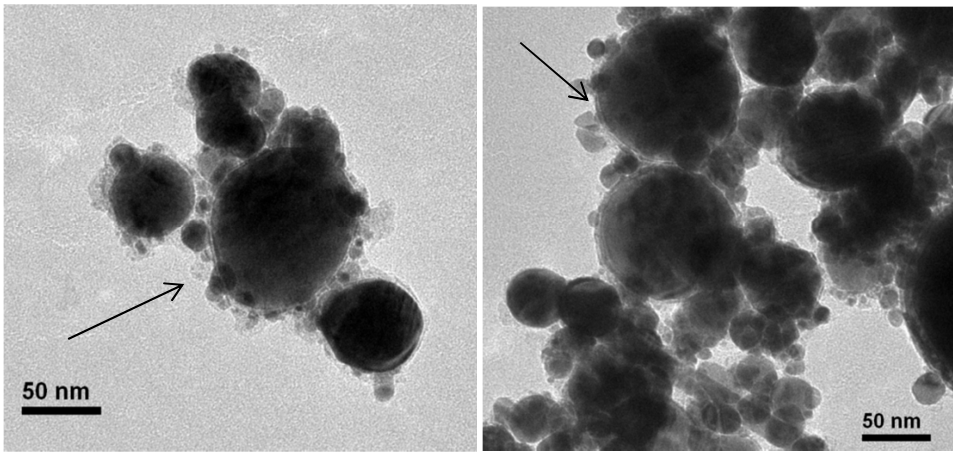

Figure 3 TEM pictures of catalyst **44**. The arrows indicate the tendency of the gold nanoparticles to agglomerate on the surface of the magnetic nanobeads **10** without a regular size distribution.

A modification of the aforementioned synthesis was afterwards assayed, adding a reducing agent (Figure 4) to evaluate upcoming differences. An improvement in the final gold incorporation was achieved, obtaining a 90% value.

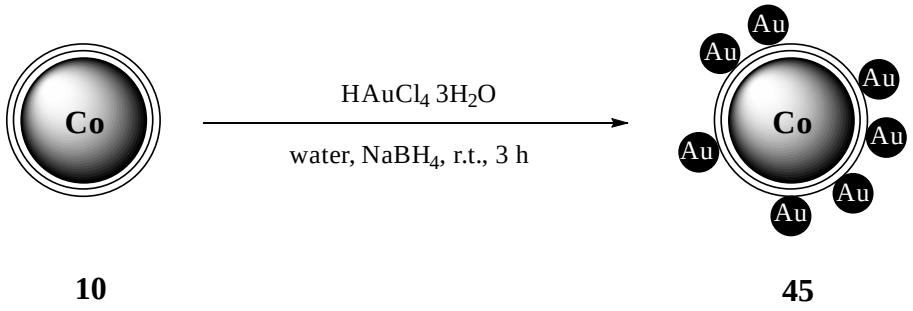

Figure 4 Schematic representation of the synthesis of Au@Co/C NPs catalyst **45**. The magnetic nanobeads **10** were stirred in a gold aqueous solution for 30 minutes. $NaBH_4$ was added and the stirring continued for 2 hours. Au loading of 0.047 mmol/g was evaluated by ICP-OES (90% incorporation)

In 2003, Jiang *et al*. reported a simple and versatile method to deposit gold nanoparticles on multiwall carbon nanotubes (MWCNTs) through surface absorption of anionic or cationic polyelectrolytes. Citric acid was used not just as a reducing agent of $HAuCl_4$ but also as a dispersant to modify the surface of the CNTs[21] (Figure 5a). Application of this method to our case led to a 60% gold incorporation on the magnetic nanocatalyst **46** (Figure 5b). However, TEM pictures in Figure 6 show gold nanoparticles without a regular size and distribution over the carbon shell of the magnetic nanobeads.

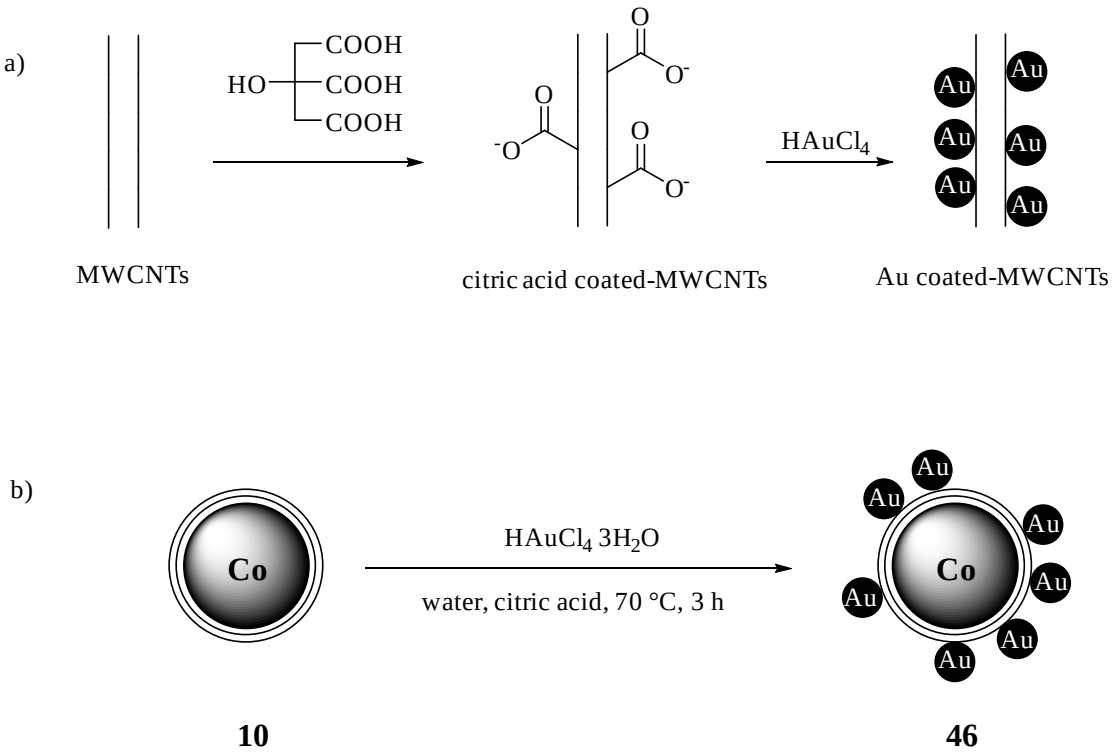

Figure 5 a) Schematic representation of the process for immobilizing gold nanoparticles on the surface of MWCNTs by absorption of citric acid via electrostatic interaction. b) Illustrative scheme of the synthesis of the catalyst **46** by applying the same principle shown in picture 5a. Au loading of 0.009 mmol/g was evaluated by ICP-OES (60% incorporation)

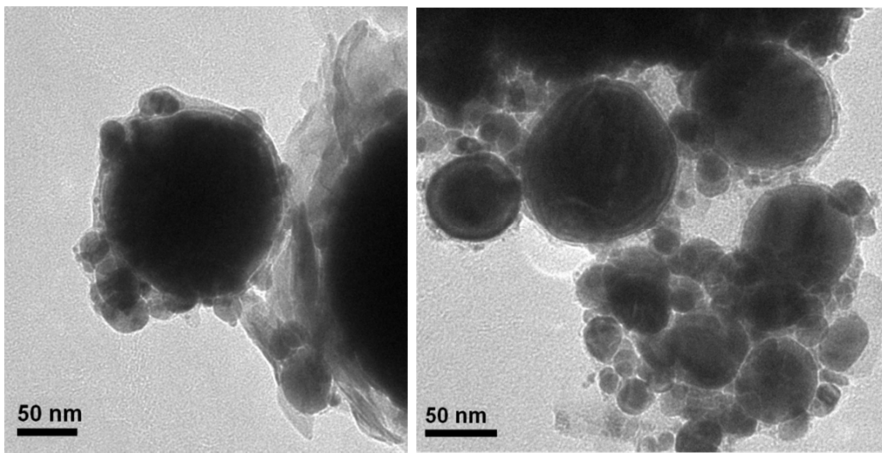

Figure 6 TEM pictures of catalyst **46**. It is possible to observe gold nanoparticles with an average size > 10 nm and with the tendency to agglomerate instead of regularly distribute over the carbon shell of the magnetic nanobeads.

A new attempt consisting in the synthesis of gold colloids followed by deposition on the carbon coating of the magnetic nanobeads was also investigated (Figure 7). Stable gold nanoparticles **47** were synthesised in an acidic aqueous gold solution by addition of $NaBH_4$ as reducing agent and stabilizer,

employing a defined molar ratio of Au/reducing agent in order to obtain nanoparticles in the range of 4-6 nm.[22] The magnetic nanobeads **10** were afterwards added to the solution leading to the formation of the nanocatalyst **48** with a final 70% gold incorporation.

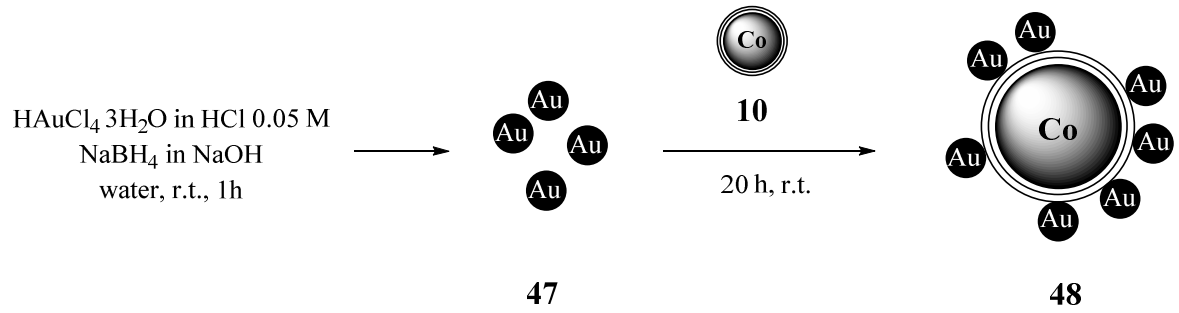

Figure 7 Schematic representation of the synthesis of catalyst **48**. Gold nanoparticles **47** were previously synthesised by addition of $NaBH_4$ to an acidic solution of $HAuCl_4 \cdot 3H_2O$. The magnetic nanobeads **10** were then added to the solution and stirred overnight leading to the formation of the nanocatalyst **48**. Au loading of 0.029 mmol/g was evaluated by ICP-OES (70 % incorporation)

A different pathway for the synthesis of gold colloids was afterwards evaluated. In 2001, Gittins *et al.* developed a new facile method for the synthesis of spherical gold nanoparticles with an average size of 5 nm through phase transfer from organic to aqueous media by using a 4-dimethylamino pyridine.[23] The cobalt nanobeads were stirred overnight with the gold nanoparticles solution thus obtained, achieving the synthesis of catalyst **50** (Figure 8). TEM pictures of the sample manifest also in this case, the formation of big agglomerates around the magnetic nanobeads (Figure 9).

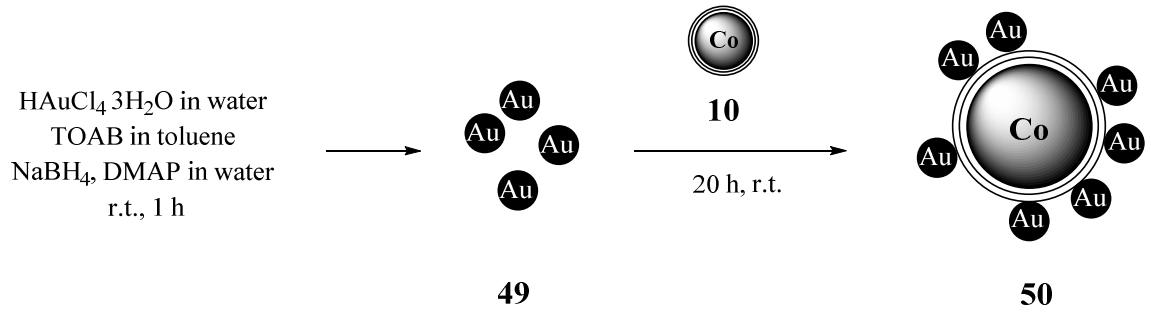

Figure 8 Scheme of the synthesis of catalyst **50**. Gold nanoparticles **49** were previously synthesised by addition of a solution of trioctylammonium bromide (TOAB) in toluene to an aqueous solution of $HAuCl_4 \cdot 3H_2O$. $NaBH_4$ was afterwards added and the final phase transfer from organic to aqueous media was driven by the addition of an aqueous DMAP solution. The magnetic nanobeads **10** were then added and the slurry stirred overnight leading to the formation of the nanocatalyst. Au loading of 0.04 mmol/g was evaluated by ICP-OES. It was not possible to evaluate the level of incorporation, since the initial gold concentration was unknown.

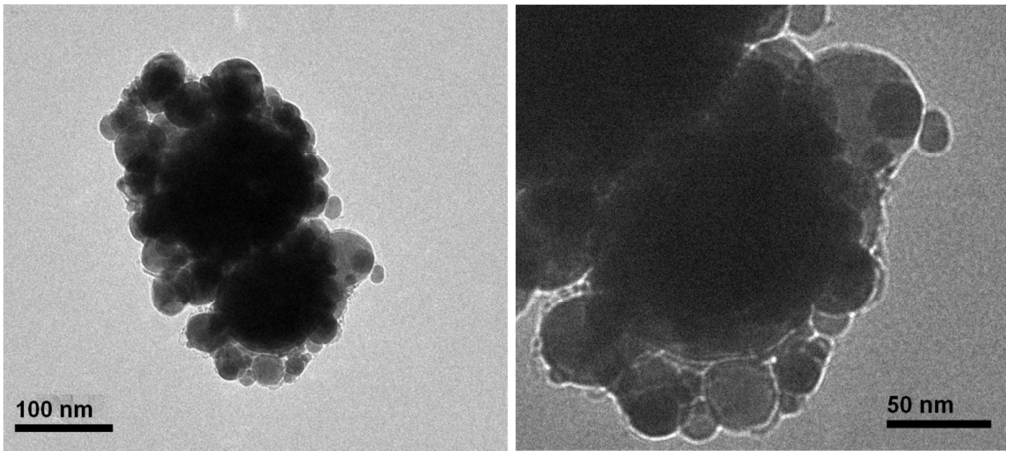

Figure 9 TEM pictures of the sample. It is possible to observe the formation of big gold agglomerate around the carbon-coated magnetic nanobeads.

An additional trial was made considering the work of Zhang from 2013, where a capping agent is also employed in the synthesis of carbon supported gold nanoparticles[24] (Figure 10). Polyvinylpyrrolidone (PVP) was added to the reaction mixture as a stabilizer and shape directing agent in the synthesis of the gold nanoparticles. This synthetic pathway led to the incorporation of the 63% of gold in the final nanocatalyst **51**. TEM pictures in Figure 11 show the formation, once more, of big gold clusters difficult to distinguish from the cobalt nanobeads.

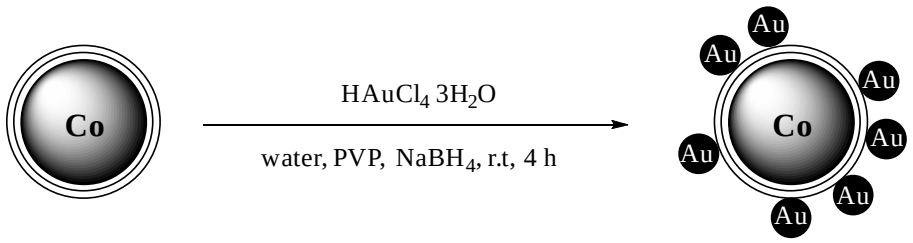

10 **51**

Figure 10 Scheme of the synthesis of catalyst **51** by gold nanoparticles deposition on the magnetic nanobeads **10**. The support was sonicated in an aqueous gold solution. PVP and $NaBH_4$ were afterwards added to the slurry and the sonication continued for additional 4 hours. Au loading of 0.03 mmol/g was evaluated by ICP-OES (63% incorporation).

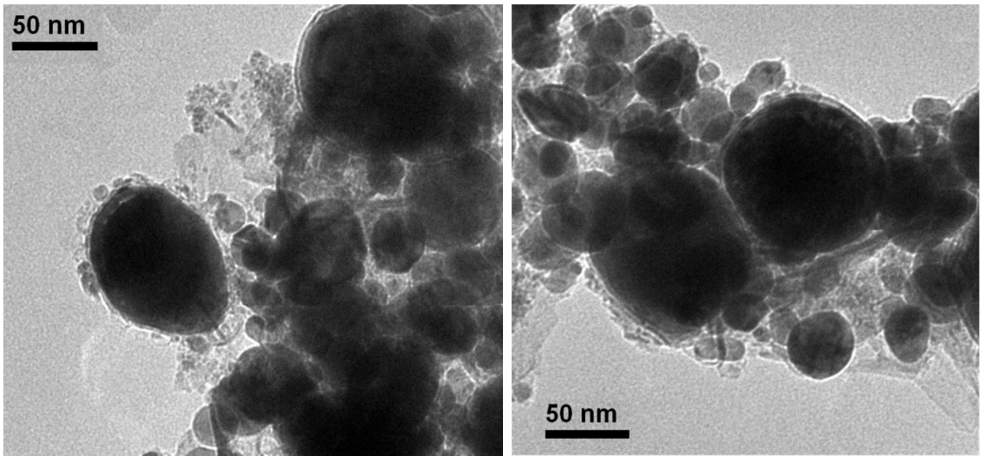

Figure 11 TEM pictures of the sample. Gold nanoparticles are agglomerating in big clusters, being almost impossible to distinguish them from the cobalt nanobeads **10**.

The activity of the synthesised nanocatalysts was tested for the oxidation of diphenylmethanol **52**. Different reaction conditions were investigated, varying the reaction times, temperatures and catalyst loadings (Table 1). The test reaction was run several times employing different bases as additive: NaOH (entries 1 and 2), K_2CO_3 (entries 4 and 6) and Cs_2CO_3 (entry 5). The reaction temperature was raised from ambient temperature to 120 °C but no conversion of the starting material was observed. The addition of H_2O_2 (entries 7 and 8) as an oxidizer did not lead to the formation of the desired product either. A final trial was made running the reaction in MeOH without addition of a base but also in this case no product was formed. The absence of catalytic activity is probably connected to the formation of gold agglomerates instead of nanoparticles with an average diameter of 5 nm, which remarkably influencies the catalytic activity. Thus, considering the unpromising results, a new deposition method was investigated.

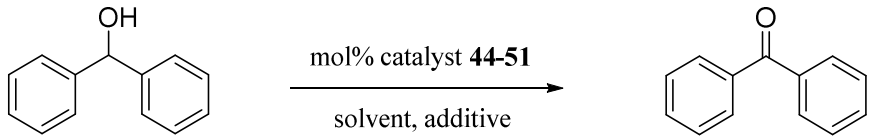

52 **53**

entry	cat amount	solvent	additive	O_2	T (°C)	time
1	0.3%	water	0.5 mmol NaOH	✓	r.t.	over-night
2	0.3%	water	1 mmol NaOH	✓	120	8 h
3	0.3%	toluene	-	✓	110	8 h
4	0.7%	toluene	1 mmol K_2CO_3	✓	120	6 h
5	0.7%	toluene	1 mmol Cs_2CO_3	✓	r.t.	8 h
6	0.3%	water	1 mmol K_2CO_3	✓	r.t.	8 h
7	0.3%	EtOH	0.5 mmol H_2O_2	-	r.t.	8 h
8	0.3%	water	0.5 mmol H_2O_2	-	100	6 h
9	0.3%	MeOH	-	✓	r.t.	over-night
10	0.8%	MeOH	-	✓	r.t.	over-night
11	0.7%	MeOH	-	✓	80	8 h

Table 1 Diphenylmethanol **52** (0.5 mmol) was stirred under an O_2 atmosphere with the indicated amount of base and catalyst in 3 ml of solvent. In entries 7 and 8, the oxidizer H_2O_2 was employed so the reaction was not run under O_2 atmosphere.

As already known, the synthesis of an active gold catalyst is considerably elaborate, being correlated to several parameters as morphology, dimension and dispersion on the support. A new attempt was made, preparing Au nanoparticles in the presence of a stabilizing agent and the subsequent immobilization.[25] A solution of gold and PVP in a known molar ratio that leads to the formation of nanoparticles with an average diameter of 5 nm, was prepared. Afterwards, a solution of $NaBH_4$ was added, observing the solution colour change from yellow to ruby red, confirming the formation of Au(0) nanoparticles. After acidification to pH 2, the support was added, stirring vigorously until the gold solution turned transparent (Figure 12).

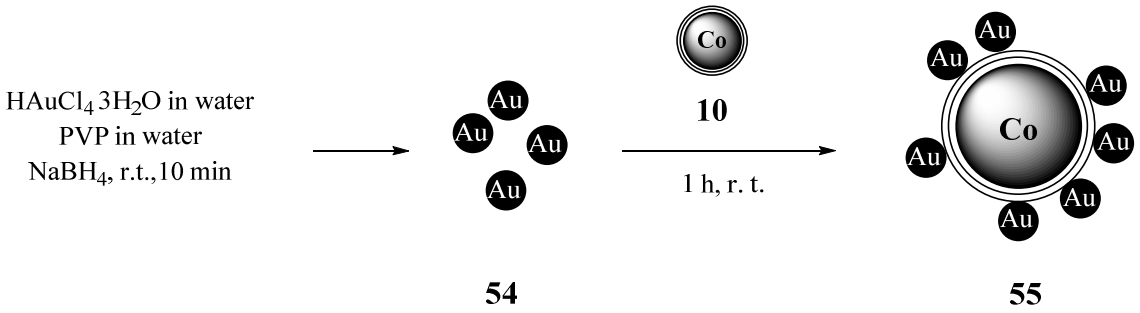

Figure 12 Schematic representation of the synthetic pathways for the synthesis of the nanocatalyst **55.** Gold nanoparticles **54** were prepared by addition of PVP and $NaBH_4$ to an aqueous gold solution. A change in the colour from light yellow to ruby red was observed after addition of the reducing agent, confirming the formation of the Au(0) nanoparticles **54**. After acidification to pH = 2, the magnetic nanobeads **10** were added to the solution and stirred until a transparent solution was obtained. Au loading of 0.048 mmol/g was evaluated by ICP-OES (98% incorporation)

To confirm the formation of gold nanoparticles with an average diameter of 5 nm, the prepared gold solution was characterized by UV-Vis analysis and TEM pictures (Figures 13 and 14) before addition of the magnetic support **10**. The analysis of the UV-Vis spectra gave a preliminary idea about the average size of the gold nanoparticles, the nanocluster with dimension above 7 nm being characterized by a sharp and intense plasmon absorption band close to 525 nm.[26,27] In this case, observing the spectra in Figure 13, it is possible to establish the formation of gold nanoparticles smaller than 5 nm, being the plasmon absorption at 520 nm quite broad. The size of the nanoparticles was then confirmed by TEM pictures (Figure 14), in which gold nanoparticles smaller than 5 nm are recognizable showing the typical grid-like surface appearance.

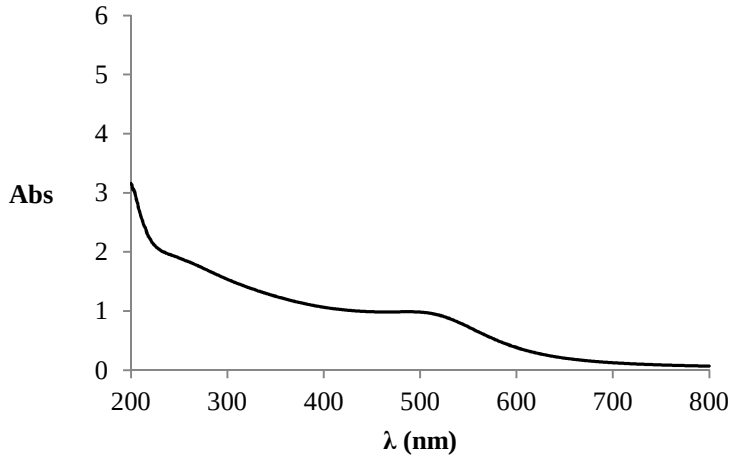

Figure 13 UV-vis spectrum of gold nanoparticles **54** before addition of the magnetic nanobeads **10**. The spectrum shows the typical broad plasmon absorption band at 525 nm of nanoparticles with average size below the 5 nm.

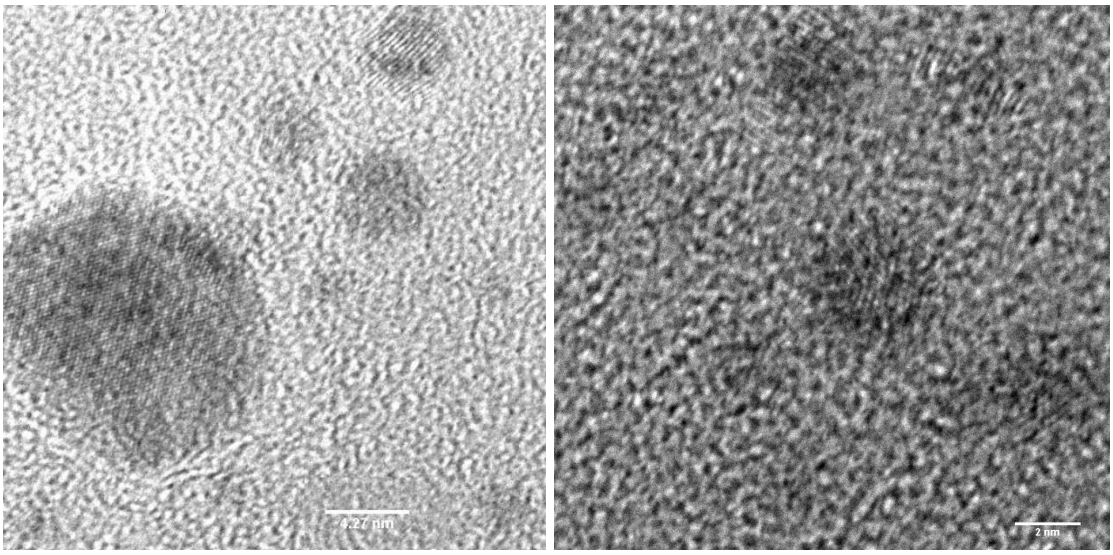

Figure 14 TEM pictures of gold nanoparticles **54**. It is possible to observe the typical grid-like surface appearance and dimension below 5 nm of the synthesised gold nanoparticles.

The final nanocatalyst **55** was afterwards analysed by TEM (Figure 15), observing the presence of small gold nanoparticles on the carbon shell of the magnetic nanobeads. Moreover, XPS analysis confirmed the presence of Au(0) nanoparticles.

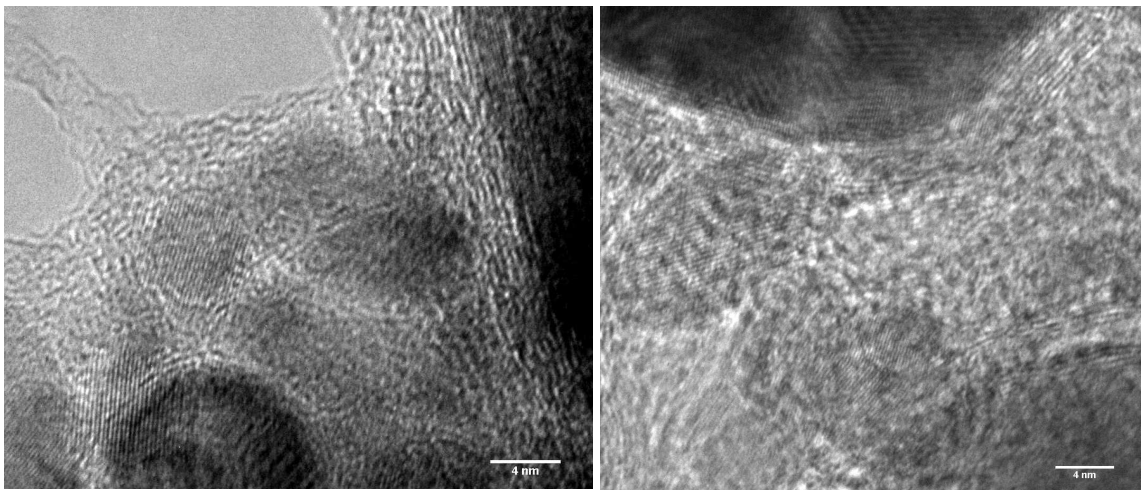

Figure 15 TEM picture of the nanocatalyst **55** Au@Co/C NPs. It is possible to observe the presence of small gold nanoparticles on the carbon shell of the magnetic nanobeads. The metal nanocluster can be recognized by the typical grid-like surface appearance.

Preliminary studies on the thus synthesised nanocatalyst **55** were made evaluating the catalytic activity in the hydrogenation of *para*-nitrophenol **56** (Figure 16). The test reaction was performed employing 0.5 mol% of catalyst **55** using water as a solvent and $NaBH_4$ as reducing agent.

Already after 15 min it was possible to observe the reaction mixture colour changing from bright yellow to colourless indicating that hydrogenation had occurred. The reaction was performed also in the absence of the catalyst and no change in the colour solution was noticed. Problems were encountered during the isolation and characterization of the *para*-aminophenol **57**, being difficult to remove the remaining $NaBH_4$. Moreover, black leaching from the magnetic support was detected.

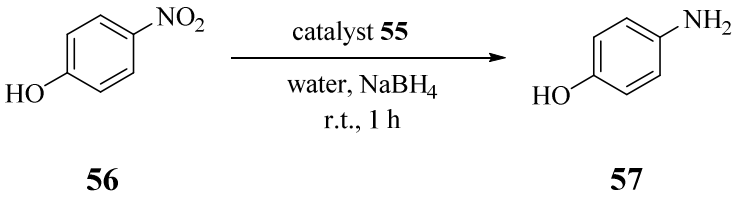

56 **57**

Figure 16 Hydrogenation of *para*-nitrophenol **56**. 0.5 mmol of *para*-nitrophenol were stirred in 6 ml of water at room temperature for 1 h adding 5 mmol $NaBH_4$ and 0.5 mol% of catalyst **55**. It was possible to observe a change in the colour of the reaction mixture from bright yellow to colourless.

Despite the detected leaching during the previous runs a recyclability test was performed, employing the catalyst for two consecutive hydrogenation reactions. The catalyst did not show activity in the second run, probably being deactivated by $NaBH_4$. Considering the problems encountered with the hydrogenation of *para*-nitrophenol **56**, catalyst **55** was tested also for the oxidation of diphenylmethanol **52** (Figure 17) but no conversion of the starting material was observed.

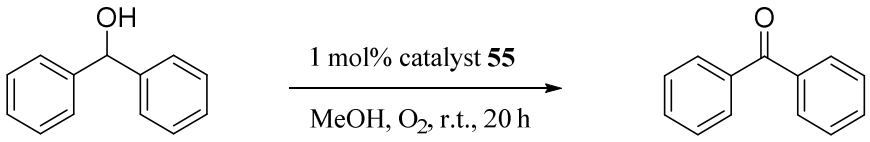

52 **53**

Figure 17 Diphenylmethanol **52** (0.5 mmol) was stirred under O_2 with 1 mol% of catalyst **55** in 3 ml MeOH at room temperature for 20 h.

Being the tested reactions only a preliminary study on the activity of catalyst **55**, this can be considered an interesting starting point in the development of a magnetic supported gold catalyst, employing an easy and simple reaction protocol. Further investigations could lead to a more active catalyst that can be easily recovered from the reaction mixture and recycled for consecutive reactions. In addition, an interesting synthesis that could be better investigated, is the incorporation of Au nanoparticles on polyethylenimine (PEI) functionalised carbon-coated cobalt nanobeads **59** (Au@PEI-Co/C) (Figure 18). The PEI functionalised magnetic nanobeads **58**, developed in our group, form a

stable dispersion in water with no tendency to agglomerate[28] and can be considered a good support for metal nanoparticles due to the presence of several amino groups that cap and stabilize metal nanoparticles. Moreover, even if the magnetisation is reduced because of the presence of the polymer, it is still possible to quickly collect them from the reaction mixture by applying an external magnetic field.[28] A first attempt is shown in Figure 18. High incorporation percentage (80%) was achieved and the presence of the polymer coating, which extends the total surface area of the magnetic support, allowed an increased metal loading, leading to an improvement in the reaction protocol as less material can be employed.

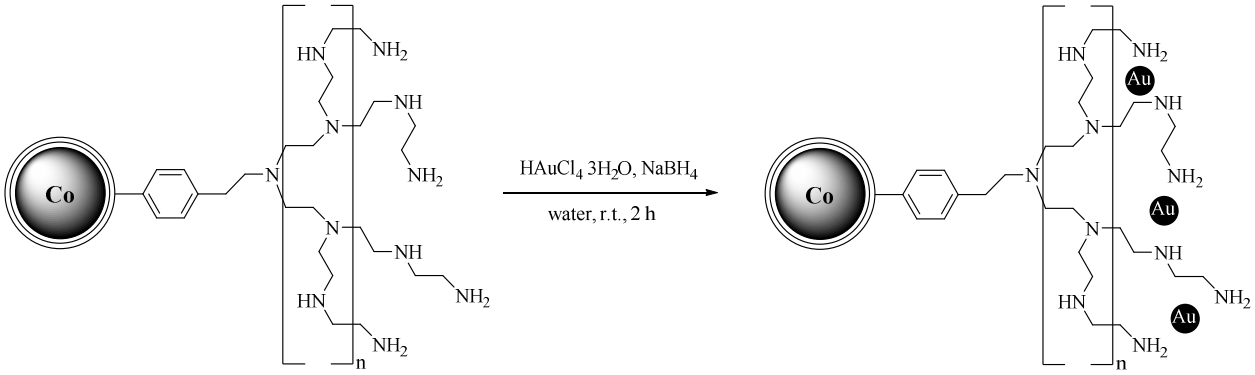

58 **59**

Figure 18 Gold nanoparticles incorporation on PEI coated Co/C nanobeads **58**. The polymer functionalised magnetic nanobeads **58** were stirred in an aqueous solution of $HAuCl_4 \cdot 3H_20$ for 30 min. $NaBH_4$ was added and the stirring continued for 2 h. Au loading of 0.8 mmol/g evaluated by ICP-OES (80% incorporation).

3.2.2 Deposition of Pt nanoparticles on graphene-coated cobalt nanobeads and evaluation of their catalytic activity

Preliminary studies were made regarding the deposition of platinum nanoparticles on the carbon-coated cobalt nanobeads. As already mentioned in the previous paragraph, considering the reported high similarity of the carbon coating of the cobalt nanobeads **10** to carbon nanotubes,[19] a first attempt of deposition of platinum nanoparticles on the surface of the magnetic nanobeads was done once more taking in consideration the work by Choi *et al*. that reported a spontaneous metal nanoparticles formation on SWCNTs by direct redox reaction between the metal ions and the carbon nanotubes.[20]
In Figure 19 is shown a scheme of the reproduced synthesis.
The magnetic nanobeads **10** were stirred for one hour in a water/EtOH solution of the Pt salt, collected by an external magnet, washed several times with water and finally dried under vacuum. The amount of platinum deposited on the carbon shell of the magnetic nanobeads was evaluated by ICP-OES.

In this case the synthesis was successful, leading to high metal incorporation (90%) in the final catalyst **60**. As it was observed in the previous case, the TEM pictures of the sample (Figure 20) show a tendency of the platinum nanoparticles to agglomerate forming big clusters.

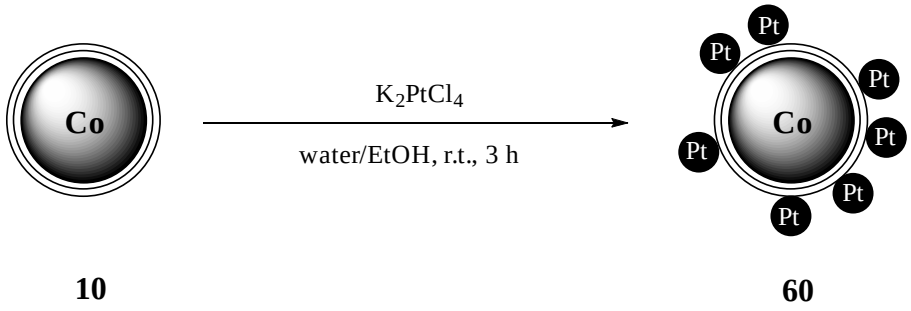

10 **60**

Figure 19 Schematic representation of a synthetic pathway for the deposition of platinum nanoparticles on the carbon coating of cobalt nanobeads **10**. These were stirred in a water/EtOH solution of the Pt salt for 3 hours. Afterwards the catalysts was collected by an external magnetic field, the reaction mixture decanted and the nanobeads washed several times with water before being dry under vacuum. Pt loading of 0.02 mmol/g was evaluated by ICP-OES (90% incorporation)

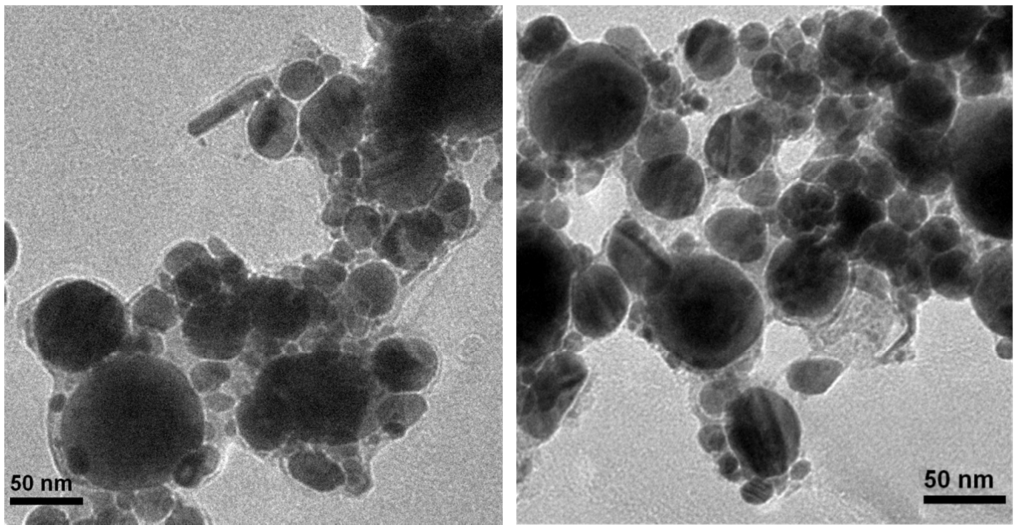

Figure 20 TEM pictures of the sample. It is possible to observe platinum nanoparticles agglomerating in big clusters.

Also in this case, a modification of the aforementioned synthetic pathway was investigated, adding a reducing agent (Figure 21) to evaluate upcoming differences in the catalytic activity. A high metal incorporation of 90% was, once again, obtained.

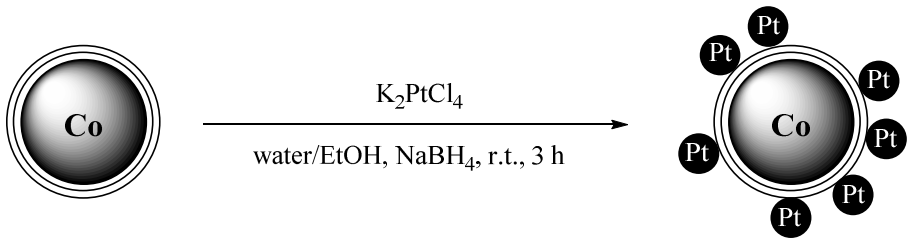

10 **61**

Figure 21 Schematic representation of the synthesis of Pt@Co/C NPs catalyst **61**. The magnetic nanobeads **10** were stirred in a platinum solution for 30 minutes. $NaBH_4$ was added and the stirring continued for 2 hours. Pt loading of 0.02 mmol/g was evaluated by ICP-OES (90% incorporation).

The catalytic activity of the synthesised catalysts was tested for both hydrogenation of nitrobenzene **62** and *trans*-stilbene **64.** In the first case, the hydrogenation was performed under H_2 in a Schlenk tube at atmospheric pressure. Only traces of the desired product were detected running the reaction in EtOH at 40 °C and employing catalyst **61** (Table 1, entry 3). No further reaction conditions were screened, adducing the insufficient catalytic activity connected to the formation of big platinum cluster on the magnetic nanobeads.

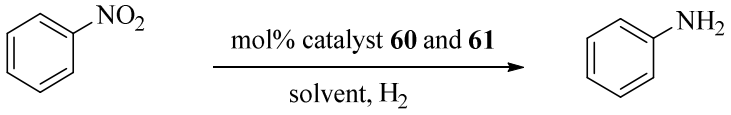

62 **63**

entry	cat. amount	solvent	H_2	T (°C)	time	yield
1	0.3%	EtOH	✓	40	8 h	-
2	0.3%	EtOAc	✓	r.t.	8 h	-
3	0.5%	EtOH	✓	40	8 h	traces
4	0.5%	EtOAc	✓	r.t.	8 h	-

Table 2 Nitrobenzene **62** (0.5 mmol) was stirred under H_2 with the indicated amount of catalyst **60** or **61** in 3 ml of solvent. Traces of the product were detected only in entry 3. Because of the low conversion no isolation of the product was possible.

The hydrogenation of *trans*-stilbene **64** was performed under H_2 in both Schlenk tube and autoclave at different pressure values (Table 3) to evaluate upcoming improvements. The tested reaction conditions were those applied in a previous work from our group,[29] where a magnetically supported Pd catalyst was successfully employed for the same transformation.

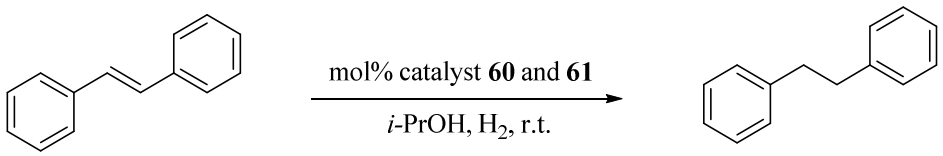

64 **65**

entry	cat. amount	time	autoclave	yield
1	0.3%	6 h	-	-
2	0.3%	6 h	✓ (20 bar)	-
3	0.5%	6 h	✓ (40 bar)	-
4	1%	20 h	-	-

Table 3 t*rans*-Stilbene **64** (0.5 mmol) was stirred under H_2 with the indicated amount of catalyst **60** or **61** in 3 ml *i*-PrOH at room temperature for the indicated time. In entries 2 and 3 an autoclave was employed to run the reaction under H_2 at higher pressure (20 and 40 bar respectively). No conversion of the starting material was observed.

As is it possible to observe in Table 3, no conversion of the starting material was observed applying the indicated reaction conditions with both the synthesised catalysts **60** and **61**. Also, performing the reaction in an autoclave that allows working at higher pressure, did not lead to an improvement in the transformation. The absence of catalytic activity was ascribed to the presence of big non-active platinum clusters on the surface of the magnetic nanobeads. For this reason, no further reaction conditions were tested, considering necessary to be able firstly to obtain a catalyst composed of small platinum nanoparticles with a potentially higher activity. After this, optimized reaction conditions could be investigated. Later on, XPS analysis of the sample, exhibited the presence of Pt(II) instead of Pt(0), additionally minimizing the activity of the catalyst. Further research needs to be done in order to be able to obtain an active platinum supported catalyst. In this direction, as previously described for the gold supported nanocatalyst, an interesting functionalization that could be examined is the incorporation of Pt nanoparticles on PEI-coated magnetic nanobeads. A preliminary study has been done on the platinum uploading on this material, leading to a high incorporation percentage (83%) and higher metal loading (Figure 22).

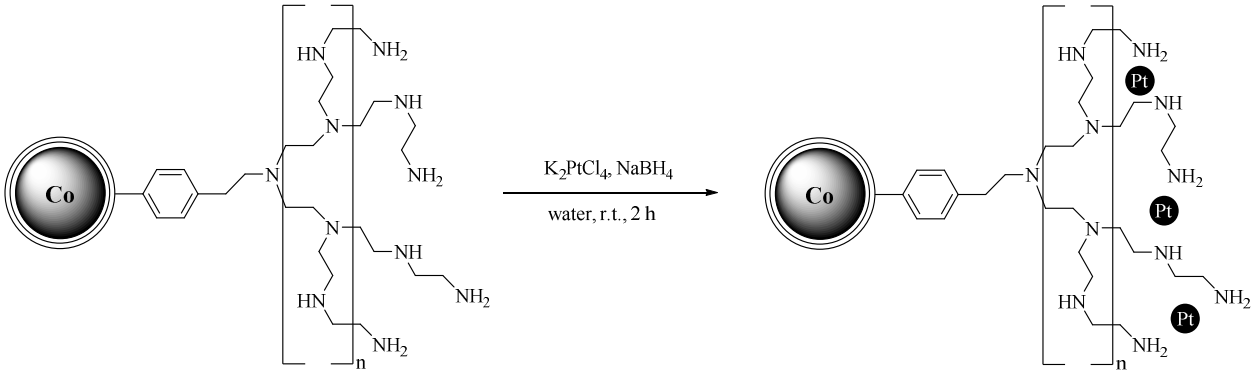

58 **66**

Figure 22 Platinum nanoparticles incorporation on PEI coated Co/C nanobeads **58**. The polymer functionalised magnetic nanobeads **58** were stirred in an aqueous solution of K_2PtCl_4 for 30 min. $NaBH_4$ was added and the stirring continued for 2 h. Pt loading of 0.92 mmol/g evaluated by ICP-OES (83% incorporation).

3.3 Conclusions

In this chapter, the deposition of nanoparticles of the noble metals Au and Pt was investigated ensued by the evaluation of the catalytic activity. The difficulties in synthesising an active catalyst of these metals are well known, as an appreciable activity is observed only when really small nanoparticles are obtained. Different synthetic pathways were evaluated, firstly considering a direct deposition of the nanoparticles on the magnetic nanobeads, exploiting the high similarity of the carbon coating present in the support with carbon nanotubes. Under these conditions, big clusters of the metals were obtained often being difficult to distinguish them from the magnetic support. Further investigations were made and the synthesis of small Au nanoparticles with an average diameter of 5 nm deposited on the magnetic nanobeads was achieved. Preliminary studies on the activity were made and the catalyst was able to promote the hydrogenation of *para*-nitrophenol. However, further investigation is needed in order to optimize the reaction conditions, improve the recyclability and to broaden the reaction scope. Regarding the supported Pt catalyst, more difficulties have been encountered in the attempt of synthesising small nanoparticles. More studies are needed in order to obtain an active catalyst.

3.4 Experimental section

Material and methods

Carbon coated cobalt nanobeads (Co/C, 20.5 m^2/g, mean particles size ≈ 40 nm) were purchased from Turbobeads Llc, Switzerland. Prior to use, they were washed in a concentrated HCl/water mixture (1:1) 5 times for 24 h. Acid residues were removed by washing with millipore water (x5) and the particles were dried at 50 °C in a vacuum oven. The magnetic nanobeads were dispersed using an ultrasound bath (Sonorex RK 255 H-R, Bandelin) and recovered with the aid of a neodymium-based magnet (15 x 30 mm). All commercially available compounds were used as received. IR-ATR spectroscopy was carried out on a Biorad Excalibur FTS 3000. Elemental microanalysis (LECO CHN-900) was carried out by the micro analytic Department at the University of Regensburg. Transmission electron microscopy was carried out by Dr. Daniela Paunesco from ETH, Zurich and by Prof. Josef Zweck from the Department of Physics of the University of Regensburg. Inductively coupled plasma optical emission spectrometry was carried out by University of Regensburg (Spectro Analytical Instruments ICP Modula EOP). XPS measurements were performed by Thomas Meier from the Department of Physic at the University of Regensburg and by SuSoS, Switzerland. NMR spectra were recorded with a Bruker AV 300 spectrometer. Gas chromatography was recorded on Fisons Instruments GC8000 equipped with a capillary (30 m x 250 µm x 0.25 µm) and flame ionization detector. TLC were performed on silica gel 60 F254 plates and detection was carried out under UV light. Absorption spectra were recorded in a Varian Cary BIO 50 UV/VIS/NIR spectrometer with temperature control using 1 cm quartz cuvette (Hellma).

Gold nanoparticles deposited on the graphene-like shell of cobalt nanobeads (44)

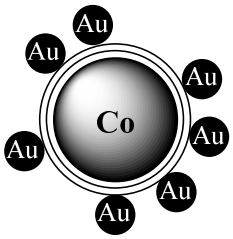

300 mg Co/C nanobeads **10**, $HAuCl_4 \cdot 3H_2O$ (2 mg, 4.82 µmol) and a water/EtOH mixture 1:1 (4 ml) were introduced in a Schlenk tube. The reaction mixture was stirred for 1 h. The catalyst was recovered by an external magnet, the solution decanted and the nanoparticles were washed with water (5 x 4 ml). After drying under vacuum, the metal loading was evaluated by ICP-OES (0.005 mmol/g; 22% incorporation).

Gold nanoparticles deposited on the graphene-like shell of cobalt nanobeads (45)

200 mg Co/C nanobeads **10**, $HAuCl_4 \cdot 3H_2O$ (4.3 mg, 0.01 mmol) and a water/EtOH mixture 1:1 (4 ml) were introduced in a Schlenk tube. The reaction mixture was stirred for 30 min followed by addition of $NaBH_4$ (2 mg, 0.05 mmol) and additionally stirred for 2 h.
The catalyst was recovered by an external magnet, the solution decanted and the nanoparticles washed with water (5 x 4 ml). After drying under vacuum, the metal loading was evaluated by ICP-OES (0.05 mmol/g; 90% incorporation).

Gold nanoparticles deposited on the graphene-like shell of cobalt nanobeads (46)

300 mg Co/C nanobeads **10**, sodium citrate dihydrate (1.6 mg, 4.41 µmol) and water (2 ml) were introduced in a Schlenk tube. The reaction mixture was stirred for 30 min, followed by dropwise addition of an aqueous solution of $HAuCl_4 \cdot 3H_2O$ (1.7 mg, 4.41 µmol). The slurry was stirred for additional 3 h at 70 °C.
The catalyst was recovered by an external magnet, the solution decanted and the nanoparticles washed with water (5 x 4 ml). After drying under vacuum, the metal loading was evaluated by ICP-OES (0.009 mmol/g; 60% incorporation).

Gold nanoparticles deposited on the graphene-like shell of cobalt nanobeads (48)

Firstly, gold colloids **47** were synthesised. $HAuCl_4 \cdot 3H_2O$ (3.6 mg, 8 µmol) and 1 ml of a 0.05 M HCl solution were added to a Schlenk tube followed by addition of water (6 ml).
The mixture was stirred for 30 min and afterwards $NaBH_4$ (0.3 mg, 8 µmol) in a 0.05 M NaOH solution (1 ml) was added. The solution was stirred for an additional 1 h and, afterwards, 200 mg of Co/C nanobeads **10** were added and the stirring continued for 20 h at 60 °C. The catalyst was recovered by an external magnet, the solution decanted and the nanoparticles were washed with water (5 x 10 ml). After drying under vacuum, the metal loading was evaluated by ICP-OES (0.029 mmol/g; 65% incorporation).

Gold nanoparticles deposited on the graphene-like shell of cobalt nanobeads (50)

Gold colloids **49** were synthesised by Dr. Adela Carrillo following the procedure described in the work of Gittins *et al*.[23] 0.3 ml of the aforementioned Au nanoparticles solution was diluted with 4 ml water. Then, 100 mg Co/C nanobeads **10** were added and the mixture was stirred for 20 h at room temperature.

The catalyst was recovered by an external magnet, the solution decanted and the nanoparticles washed with water (5 x 5 ml). After drying under vacuum, the metal loading was evaluated by ICP-OES (0.04 mmol/g).

Gold nanoparticles deposited on the graphene-like shell of cobalt nanobeads (51)

500 mg Co/C nanobeads **10** and a 0.25 mM aqueous solution of $HAuCl_4 \cdot 3H_2O$ (9.84 mg, 0.025 mmol) were added to a round bottom flask and stirred for 1 h. An aqueous solution of PVP (5%, K-30 40 kDa; 5 g) was added and the stirring continued for additional 30 min. A 100 mM aqueous solution of $NaBH_4$ (18.19 mg, 0.5 mmol) was rapidly injected into the mixture under vigorously stirring and the slurry was aged for 3 h. The catalyst was recovered by an external magnet, the solution decanted and the nanoparticles washed with water (5 x 15 ml). After drying under vacuum at 60 °C, the metal loading was evaluated by ICP-OES (0.03 mmol/g, 63% incorporation).

Gold nanoparticles deposited on the graphene-like shell of cobalt nanobeads (55)

Firstly, gold nanoparticles **54** were synthesised. $HAuCl_4 \cdot 3H_2O$ (1.69 mg, 5 µmol) and water (10 ml) were added to a Schlenk tube. PVP (0.246 mg; Au:PVP = 1:0.125 wt/wt) was added to the solution and stirred vigorously for 3 min. An aqueous 0.1 M solution of $NaBH_4$ (0.8 mg, 0.02 mmol, $Au/NaBH_4$ = 1:4 mol/mol) was added and the solution stirred for some minutes, observing a change in the colour from yellow to ruby red (formation of Au(0) nanoparticles). The mixture was acidified to pH = 2 with H_2SO_4 and 100 mg Co/C nanobeads **10** were added. The slurry was sonicated for some minutes and afterwards stirred for 1 h, until a transparent solution was observed.
The catalyst was recovered by an external magnet, the solution decanted and the nanoparticles washed with water (5 x 6 ml). After drying under vacuum, the metal loading was evaluated by ICP-OES (0.048 mmol/g; 98% incorporation).

Carbon-coated cobalt nanobeads functionalized with a PEI-coating (58)

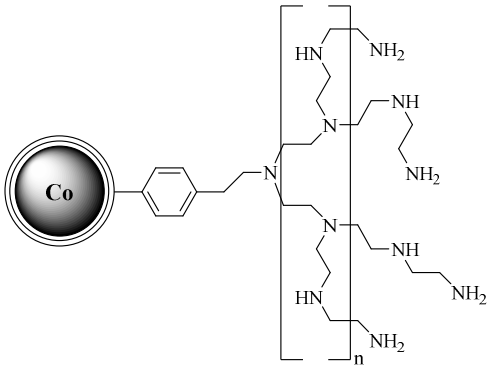

Firstly, the carbon-coated cobalt nanobeads **10** were functionalized by diazonium chemistry as already described in the previous chapter, obtaining NH_2-functionalized nanobeads **21** (N loading: 0.14 mmol/g determined by elemental microanalysis). 700 mg nanobeads **21** were sonicated in DCM (34 ml) for 10 min. Aziridine (5.08 ml, 1000 equiv, 98 mmol) and concentrated HCl (98 µl, 12 equiv, 1.176 mmol) were added and the slurry was stirred at 80 °C for 24 h. The nanobeads were recovered by an external magnet, the solution decanted and the nanobeads washed with DCM (5 x 20 ml) and water (2 x 10 ml). After freeze-drying under vacuum, the nanobeads were analysed by elemental microanalysis (N loading: 0.97 mmol/g).

Gold nanoparticles deposited on the PEI-coated cobalt nanobeads (59)

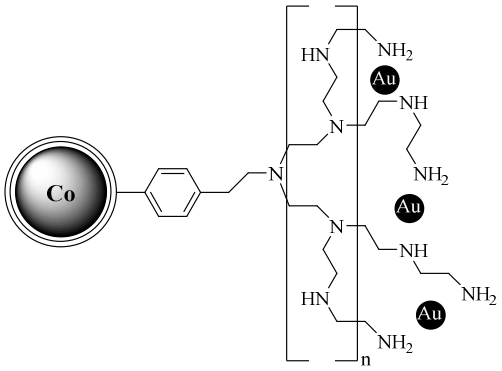

50 mg PEI-coated Co/C nanobeads **58,** $HAuCl_4 \cdot 3H_2O$ (20.4 mg, 0.052 mmol) and water (4 ml) were added to a Schlenk tube and the slurry was stirred for 30 minutes. $NaBH_4$ (23.7 mg, 0.625 mmol) was added and the stirring continued for 2 h. The catalyst was recovered by an external magnet, the solution decanted and the nanoparticles washed with water (5 x 5 ml). After drying under vacuum, the metal loading was evaluated by ICP-OES (0.8 mmol/g, 80% incorporation).

Platinum nanoparticles deposited on the graphene-like shell of cobalt nanobeads (60)

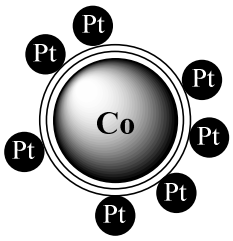

200 mg Co/C nanobeads **10**, K_2PtCl_4 (2 mg, 4 µmol) and a water/EtOH mixture 1:1 (4 ml) were introduced in a Schlenk tube. The reaction mixture was stirred for 3 h. The catalyst was recovered by an external magnet, the solution decanted and the nanoparticles washed with water (5 x 4 ml).

After drying under vacuum, the metal loading was evaluated by ICP-OES (0.02 mmol/g; 90% incorporation).

Platinum nanoparticles deposited on the graphene-like shell of cobalt nanobeads (61)

200 mg Co/C nanobeads **10**, K_2PtCl_4 (2.2 mg, 4 µmol) and a water/EtOH mixture 1:1 (4 ml) were introduced in a Schlenk tube. The reaction mixture was stirred for 30 min, followed by addition of $NaBH_4$ (2 mg, 0.05 mmol) and additional stirring for 2 h.
The catalyst was recovered by an external magnet, the solution decanted and the nanoparticles washed with water (5 x 4 ml). After drying under vacuum, the metal loading was evaluated by ICP-OES (0.023 mmol/g; 90% incorporation).

Platinum nanoparticles deposited on the PEI-coated cobalt nanobeads (66)

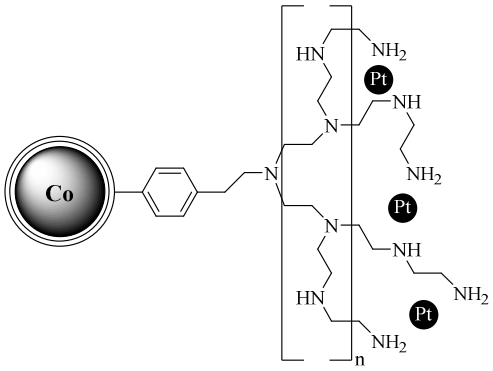

50 mg PEI-coated Co/C nanobeads **58**, K_2PtCl_4 (23.30 mg, 0.056 mmol) and water (4 ml) were added to a Schlenk tube and the slurry stirred for 30 minutes. $NaBH_4$ (23.7 mg, 0.625 mmol) was added and the stirring continued for 2 h. The catalyst was recovered by an external magnet, the solution decanted and the nanoparticles washed with water (5 x 5 ml). After drying under vacuum, the metal loading was evaluated by ICP-OES (0.92 mmol/g, 83% incorporation).

General procedure for the hydrogenation of diphenylmethanol 52 (GP4)

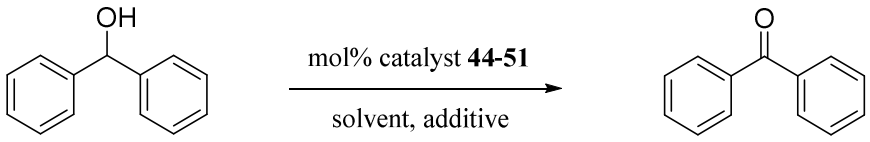

52 **53**

GP4. The desired amount of gold supported catalyst (**44**-**51**), diphenylmethanol (0.5 mmol) and solvent (3 ml) were introduced into a Schlenk tube together with the base and oxidizing agent (if employed). The reaction mixture was stirred vigorously under 1 atm H_2-atmosphere (balloon). The reaction progress was monitored by TLC. The catalyst was collected with a magnet and the supernatant decanted. The nanobeads were washed with water (3 x 4 ml) and dried under vacuum. The solvent collected was evaporated under vacuum to obtain a crude material that was analysed by ^{1}H NMR.

General procedure for the hydrogenation of *para*-nitrophenol 56 (GP5)

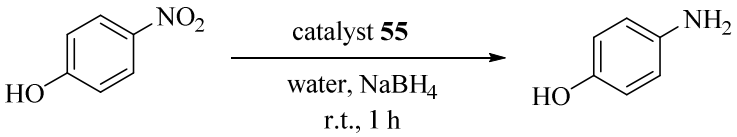

56 **57**

GP5. The desired amount of gold supported catalyst **55**, *para*-nitrophenol (0.5 mmol), water (6 ml) and $NaBH_4$ (5 mmol) were introduced into a Schlenk tube. The reaction mixture was stirred vigorously observing the colour change from a bright yellow to transparent. The catalyst was collected with a magnet and the supernatant decanted. The nanobeads were washed with water (3 x 4 ml) and dried under vacuum. The solvent collected was filtered twice and evaporated under vacuum, giving a crude material analysed by ^{1}H NMR.

General procedure for the hydrogenation of nitrobenzene 62 (GP6)

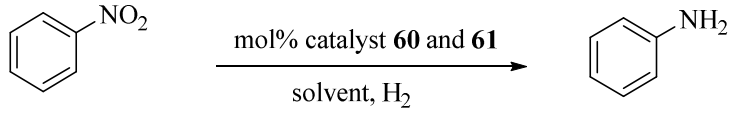

62 **63**

GP6. The desired amount of supported platinum catalyst (**60**-**61**), nitrobenzene (0.5 mmol) and solvent (3 ml) were introduced into a Schlenk tube. The reaction mixture was stirred vigorously under 1 atm of H_2 (balloon). The reaction progress was monitored by TLC. The catalyst was collected with a magnet and the supernatant decanted. The nanobeads were washed with water (3 x 4 ml) and dried under vacuum. The solvent collected was evaporated under vacuum to give a crude material that was analysed by ^{1}H-NMR.

General procedure for the hydrogenation of *trans*-stilbene 64 (GP7)

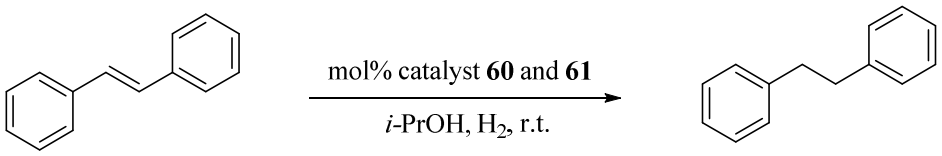

64 **65**

GP7. The desired amount of supported platinum catalyst (**60**-**61**), *trans*-stilbene (0.5 mmol), *i*-PrOH (3 ml) and dodecane (0.5 mmol) as an internal standard were introduced into a Schlenk tube. The reaction mixture was stirred vigorously under 1 atm of H_2 (balloon). Alternatively, the reactants were transferred to an autoclave and stirred rapidly at room temperature under 20 or 40 atm of hydrogen gas. The reaction progress was monitored by GC. The catalyst was collected with a magnet and the supernatant decanted. The nanobeads were washed with water (3 x 4 ml) and dried under vacuum. The solvent collected was evaporated under vacuum obtaining a crude material that was analysed by ^{1}H NMR.

3.5 References

[1] S. Das, B. B. Dhar, *RSC Advances* **2014**, *4*, 46285–46292.

[2] A. Corma, H. Garcia, *Chemical Society Reviews* **2008**, *37*, 2096–2126.

[3] K. Saha, S. S. Agasti, C. Kim, X. Li, V. M. Rotello, *Chemical Reviews* **2012**, *112*, 2739–2779.

[4] E. C. Dreaden, A. M. Alkilany, X. Huang, C. J. Murphy, M. A. El-Sayed, *Chemical Society Reviews* **2012**, *41*, 2740–2779.

[5] C. N. R. Rao, G. U. Kulkarni, P. J. Thomas, P. P. Edwards, *Chemical Society Reviews* **2000**, *29*, 27–35.

[6] Z. Sun, Y. Zhao, Y. Xie, R. Tao, H. Zhang, C. Huang, Z. Liu, *Green Chemistry* **2010**, *12*, 1007–1011.

[7] J. Yang, L. Ngaw, *Topics in Catalysis* **2012**, *55*, 663–667.

[8] X. Liu, L. He, Y. Liu, Y. Cao, *Accounts of Chemical Research* **2014**, *47*, 793–804.

[9] S. Kinayyigit, P. Lara, P. Lecante, K. Philippot, B. Chaudret, *Nanoscale* **2014**, *6*, 539–546.

[10] N. Raveendran Shiju, Vadim V. Guliants, *Applied Catalysis A: General* **2009**, *356*, 1–17.

[11] P. Lara, K. Philippot, *Catalysis Science & Technolology* **2014**, *4*, 2445–2465.

[12] Y. Choi, M. J. Choi, S. H. Cha, Y. S. Kim, S. Cho, Y. Park, *Nanoscale Research Letters* **2014**, *9*, 1–8.

[13] H. Yang, S. Li, X. Zhang, X. Wang, J. Ma, *Journal of Materials Chemistry A* **2014**, *2*, 12060–12067.

[14] E. Boymans, S. Boland, P. T. Witte, C. Müller, D. Vogt, *ChemCatChem* **2013**, *5*, 431–434.

[15] M. Kidwai, S. Bhardwaj, *Applied Catalysis A: General* **2010**, *387*, 1–4.

[16] R. L. Oliveira, P. K. Kiyohara, L. M. Rossi, *Green Chemistry* **2010**, *12*, 144–149.

[17] S. Kim, S. W. Bae, J. S. Lee, J. Park, *Tetrahedron* **2009**, *65*, 1461–1466.

[18] R. Kumar, E. Gravel, A. Hagege, H. Li, D. V. Jawale, D. Verma, I. N. N. Namboothiri, E. Doris, *Nanoscale* **2013**, *5*, 6491–6497.

[19] R. N. Grass, E. K. Athanassiou, W. J. Stark, *Angewandte Chemie International Edition* **2007**, *46*, 4909–4912.

[20] H. C. Choi, M. Shim, S. Bangsaruntip, H. Dai, *Journal of the American Chemical Society* **2002**, *124*, 9058–9059.

[21] L. Jiang, L. Gao, *Carbon* **2003**, *41*, 2923–2929.

[22] D. Padayachee, V. Golovko, B. Ingham, A. T. Marshall, *Electrochimica Acta* **2014**, *120*, 398–407.

[23] D. I. Gittins, F. Caruso, *Angewandte Chemie International Edition* **2001**, *40*, 3001–3004.

[24] D. Zhang, *Applied Mechanics and Materials* **2013**, *313-314*, 232–236.

[25] A. Villa, Di Wang, G. M. Veith, F. Vindigni, L. Prati, *Catalysis Science & Technolology* **2013**, *3*, 3036–3041.

[26] I. Hussain, S. Graham, Z. Wang, B. Tan, D. C. Sherrington, S. P. Rannard, A. I. Cooper, M. Brust, *Journal of the American Chemical Society* **2005**, *127*, 16398–16399.

[27] N. R. Jana, L. Gearheart, C. J. Murphy, *Langmuir* **2001**, *17*, 6782–6786.

[28] Q. M. Kainz, S. Fernandes, C. M. Eichenseer, F. Besostri, H. Korner, R. Muller, O. Reiser, *Faraday Discuss* **2014**, *175*, 27–40.

[29] Q. M. Kainz, R. Linhardt, R. N. Grass, G. Vilé, J. Pérez-Ramírez, W. J. Stark, O. Reiser, *Advanced Functional Materials* **2014**, *24*, 2020–2027.

4. Deposition of nickel nanoparticles on magnetic nanobeads and evaluation of their catalytic activity

In the present chapter, the deposition of nickel nanoparticles on two different magnetic supports was investigated. On the one hand, carbon-coated cobalt nanobeads **10** were employed, exploiting the tendency of this carbonaceous material to coordinate metal nanoparticles, leading to the synthesis of a supported Ni nanocatalyst whose activity was evaluated for the hydrogenation of nitro derivatives and C-C double bonds. On the other hand, the behaviour of iron oxide nanoparticles (already delineated in Chapter 1) as a suitable support for direct deposition of nickel nanoparticles, was considered. The stability of the nanocatalyst was expected to derived from the high affinity of nickel for the C-C double bonds present in large amount on the surface of the magnetic support. The activity of the thus obtained magnetic nanocatalyst was evaluated in the hydrogenation of nitro derivatives and the Suzuki-Miyaura cross-coupling reaction.

4.1 Introduction

From the point of view of sustainable chemistry, development of chemical transformations that minimize byproducts, waste and that avoid the use of not-abundant precious metals, is one of the most important goals in catalysis. To tackle this problem, the use of nickel has attracted wide attention in the recent years as an easily available and less expensive alternative to the more commonly used Pd, Rh, Ru, Pt and Au. Nickel nanoparticles demonstrated to be able to be competent catalysts for a number of transformations, including the reduction of several functional groups *e.g*. C-C multiple bonds,[1,2] sulfonate,[3] nitro derivatives,[4,5] aldehydes and ketones.[6,7] Moreover, high catalytic activity was exhibited in the Wittig-type olefination,[8] imine reduction,[9] Suzuki-Miyaura cross-coupling reaction[10,11] and for the *N*-alkylation of amines with alcohols.[12] Due to the spreading of nanotechnology, noteworthy progresses have also been made in the development of heterogeneous systems, employing solid supports that allow easy recovery and recycling of the catalyst.[10] In particular, the use of magnetic supports has been widely investigated due to their high surface-area, robustness, availability and easy recovery from the reaction mixture by just applying an external magnetic field.[13,14,15] Magnetic supported nickel catalysts also showed to be a good alternative to Raney Ni, extensively used as a heterogeneous catalyst despite possessing several disadvantages as being pyrophoric or not selective towards functional groups as C=O and NO_2, reducing all of them simultaneously.[16] Additionally, difficulties regarding dosage and deactivation after long-term storage are commonly encountered.[2]

The aim of the present chapter was the direct deposition of Ni nanoparticles on two different magnetic supports employing simple and fast synthetic protocols. In one case, cobalt nanobeads coated with a graphene-like shell comparable to carbon nanotube were employed. In 2015, Huang *et al*. deposited nickel nanoparticles on carbon nanofibers (CNFs). The synthesis required firstly the immersion of the nanofibers in a Ni nitrate solution, followed by a carbonization step in a vacuum tube furnace to reduce nickel nitrate to Ni(0) nanoparticles. The obtained catalysts were then applied in the hydrogenation of nitrotoluene,[17] resulting in high catalytic performance carrying out the reaction at 160 °C in an autoclave under a hydrogen atmosphere for 6 h. Similarly, Gunawan *et al*. supported Ni nanoparticles on carbon.[18] The synthesis was accomplished by reducing nickel ions with reducing gases (*e.g*. H_2, CH_4, CO) formed during the carbonization of tannins, in particular *o*-catechol, with microwave irradiation. The synthesised hybrid material showed Ni(0) nanoparticles uniformly dispersed on the carbon matrix, being a good candidate for heterogeneous catalysis.

The second support employed in the present study, was iron oxide nanobeads. In 2009, Polshettiwar *et al*. applied nano ferrite-supported Ni catalyst in hydrogenation and transfer hydrogenation reactions.[19] The catalyst was obtained by a two-step synthetic pathway. Firstly, the nano ferrite beads were sonicated with dopamine and the thus generated amine-functionalized nano ferrites were dispersed in a solution containing the Ni source and the reducing agent.

The magnetic nanocatalyst showed catalytic activity for hydrogenation of both alkynes and carbonyl compounds. An additional example of Ni nanoparticles supported on iron oxide nanobeads was developed by Sharma *et al*. in 2015.[20] Firstly, the magnetic nanoparticles were synthesised by a co-precipitation technique and, to avoid agglomeration, they were additionally coated with a silica shell that also provides suitable sites for a further functionalization of the surface. The hydroxy groups of the silica coating were reacted with 3-aminopropyltriethoxysilane and the amino moieties of the latter with thiophene-2 carboxaldehyde. On this resulting material were finally deposited nickel(II) species. The magnetic nanocatalyst was applied in the Suzuki-Miyaura coupling of phenylboronic acid and aryl halides, adding PPh_3 to reduce Ni(II) to Ni(0), leading to an active catalyst. The desired products were obtained in high yield and the catalyst could be used for six runs, without a significant metal leaching.

4.2 Results and discussion

The aim of the project was the development of a Ni-based, supported catalyst, synthesised by a simple and fast procedure. The presence of a magnetic support would allow the recovery of the catalyst from the reaction mixture by only applying an external magnetic field, gaining a very simple and quick reaction work-up. As a result, the catalyst could be recycled and used for consecutive reactions. TEM pictures and XPS analysis of selected samples were performed.

4.2.1 Nickel nanoparticles on Co/C nanobeads (Ni@Co/C)

For the deposition of nickel nanoparticles on the carbon shell of the cobalt nanobeads **10**, a procedure similar to the one applied for the synthesis of catalyst **11** (Pd@Co/C) was employed. The Ni(0) complex $Ni(COD)_2$ was used as a metal source. The optimization of reaction times and temperatures for the synthesis of catalyst **67** is shown in Table 1.

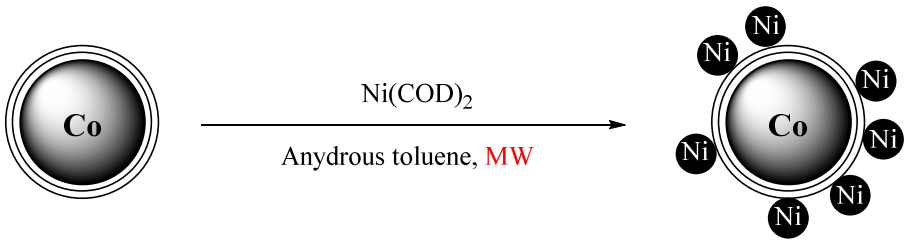

10 **67**

entry	catalyst	Time (min)	T (°C)	loading (mmol/g)	% incorporation
1	**67a**	2	75	0.8	83
2	**67b**	15	75	0.8	80
3	**67c**	2	90	0.1	95
4	**67d**	15	90	0.1	97
5[a]	**67e**	2	100	0.02	91
6[a]	**67f**	2	100	0.1	98
7[a]	**67g**	2	100	1	98

Table 1 Reaction conditions screened for the deposition of Ni NPs on magnetic nanobeads **10**, leading to the synthesis of catalysts Ni@Co/C (**67a-g**). Co/C nanobeads **10** were sonicated under argon in a solution of $Ni(COD)_2$ in anhydrous toluene. Different reaction times and temperatures were evaluated, employing microwave irradiation. [a] After the deposition of the Ni nanoparticles, the catalyst was washed several times with toluene instead of DCM, employed in the other entries.

The highest incorporation percentage was achieved heating up the solution to 100 °C for 2 min (entry 6) by microwave irradiation. Once the reaction conditions were optimized, different metal loadings were evaluated (entries 5 to 7) with the purpose to assess the presence of dissimilarities in the final catalytic activity. Two solvents, DCM and toluene, were tested for the washing step of the synthesised catalysts, also with the aim to examine upcoming differences in the final activity. The ability of nickel to react with chlorinated compounds is in fact known,[21] leading to a loss of catalytic activity if DCM is used. Catalysts **67a** and **67d** (Table 1) were analysed by TEM, images are shown in Figure 2. Nickel nanoparticles tended to agglomerate in big clusters around the carbon shell of the magnetic nanobeads, independently from the metal loading.

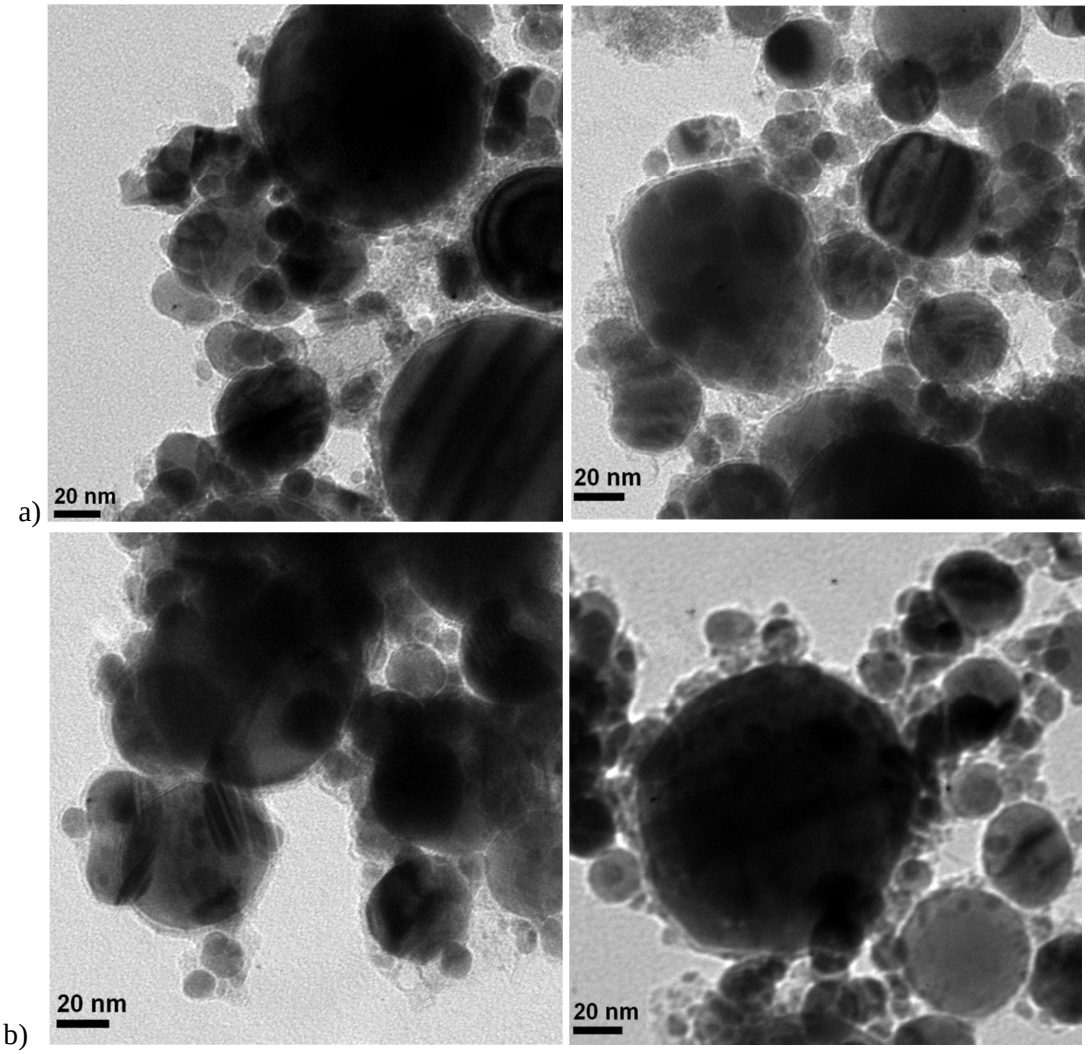

Figure 2 TEM picture of the catalysts **67a** and **67d**. a) Ni loading: 1 mmol/g (**67a**), b) Ni loading: 0.1 mmol/g (**67d**). In both the cases the Ni nanoparticles tended to agglomerate in big clusters around the magnetic nanobeads.

Although the synthesised Ni nanoparticles favoured the formation of big clusters, normally associated to poor catalytic performance,[22] a survey of their activity in a number of model reactions was undertaken. Firstly, the hydrogenation of acetophenone was considered (Figure 3), bearing in mind the work by Alonso *et al*., where in situ synthesised Ni(0) nanoparticles led to the formation of the desired product in high yield.[6]

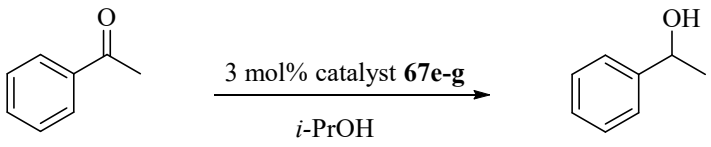

68 **69**

entry	time	T (°C)	yield
1	24 h	78	-
2	6 h	100 (MW)	-

Figure 3 Hydrogenation of acetophenone **68** by catalysts **67e-g**. Acetophenone **68** (0.5 mmol) was stirred with 3 mol% of the selected catalyst **67e-g** in 3 ml *i*-PrOH. In entry 1, conventional heating was applied while in entry 2 the sample was heated using microwave irradiation. No conversion was observed in any case.

Subsequently, the activity of catalysts **67e-g** for the hydrogenation of nitrobenzene **62** was investigated (Figure 4). Once more, none of the synthesised catalysts showed any catalytic activity and no conversion of the starting material was observed.

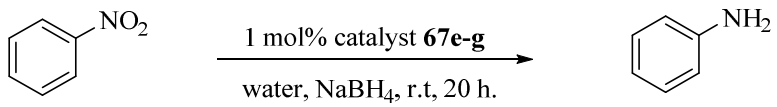

62 **63**

Figure 4 Test reaction of the activity of catalyst **67e-g** for the hydrogenation of nitrobenzene **62**. Nitrobenzene **62** (0.5 mmol) was stirred with 1 mol% of the selected catalyst **67e-g** and $NaBH_4$ (5 mmol) in 3 ml water at room temperature for 20 h. No conversion of the starting material was observed.

Similarly, also the hydrogenation of *para*-nitrophenol **56** (Figure 5) was investigated, considering the promising results obtained with the Au@Co/C nanocatalyst **55** (Chapter 3, Figure 16). Unfortunately, no conversion of the starting material was observed.

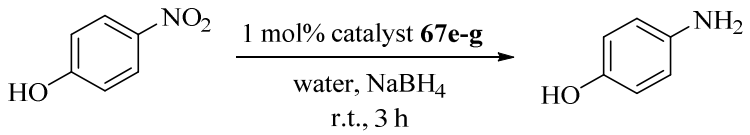

56 **57**

Figure 5 Hydrogenation of *para*-nitro phenol by catalyst **67e-g**. *para*-Nitrophenol **56** (0.5 mmol) was stirred with 1 mol% of the selected catalyst **67e-g** and $NaBH_4$ (5 mmol) in 3 ml water at room temperature for 3 h. No conversion of the starting material was observed.

An additional last attempt was made to evaluate the activity of the synthesised catalysts for the hydrogenation of *trans*-stilbene **64** (Figure 6). No change in the behaviour of the catalysts was observed and no activity was detected. The absence of activity was probably due to the formation of big Ni nanoclusters around the magnetic nanobeads instead of small nanoparticles with a regular distribution.[22] A subsequent XPS analysis of the samples **67a** and **67d**, revealed the presence of Ni(II) species, suggesting that a more strict control over the synthesis and storage conditions is required.

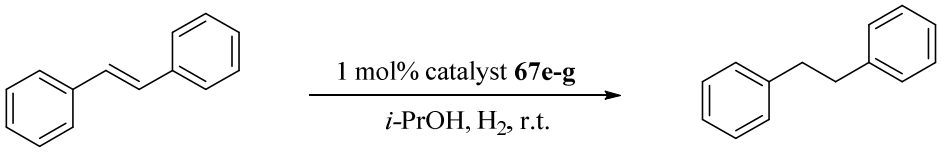

64 **65**

Figure 6 *trans*-Stilbene hydrogenation by catalysts **67e-g**. *trans*-Stilbene **64** (0.5 mmol) was stirred under H_2 with 1 mol% of the selected catalyst **67e-g** in 3 ml *i*-PrOH at room temperature for 6 h. No conversion of the starting material was observed.

In conclusion, deposition of Ni nanoparticles on carbon-coated cobalt nanobeads in high percentage of incorporation was achieved however, the resulting nanocatalysts showed no activity in the reactions examined. This is probably due to the formation of big Ni(II) nanoclusters around the magnetic nanobeads. No differences in the activity were evaluated decreasing the amount of metal deposited on the support.

4.2.2 Nickel nanoparticles on Fe_3O_4 nanobeads (Ni@Fe_3O_4)

In the present section, the deposition of Ni nanoparticles on a different magnetic support is described. Iron oxide (Fe_3O_4) nanobeads **70** were synthesised by thermal decomposition of $Fe(acac)_3$ in the presence of oleylamine and oleic acid as surfactant agents, being in this way characterized by the presence, on the surface, of several C-C double bonds.[23] Because of the high affinity of Ni for these double bonds, their ability to coordinate and stabilize Ni nanoparticles was investigated. Different reaction conditions were screened and are summarised in Table 2. The $Ni(NO_3)_2 \cdot 6H_2O$ salt was employed as metal source, while different types and amounts of reducing agents were tested. The synthesis was achieved stirring the magnetic nanobeads in a solution of the Ni salt in EtOH at room temperature. Table 2 shows that it was necessary to use an excess of $NaBH_4$ (5 or 10 equiv) in order to obtain a high incorporation percentage (entry 6). When a weaker reducing agent was employed, as NH_2NH_2, low percentage incorporations were achieved (entries 4 and 5), while the absence of a reducing agent in the reaction mixture led to no metal incorporation. Catalysts with different metal loadings were synthesised to evaluate possible differences in the catalytic activity. In the TEM pictures (Figure 7) no appreciable difference from the Fe_3O_4 nanobeads **70** could be observed except for a slight tendency to agglomerate.

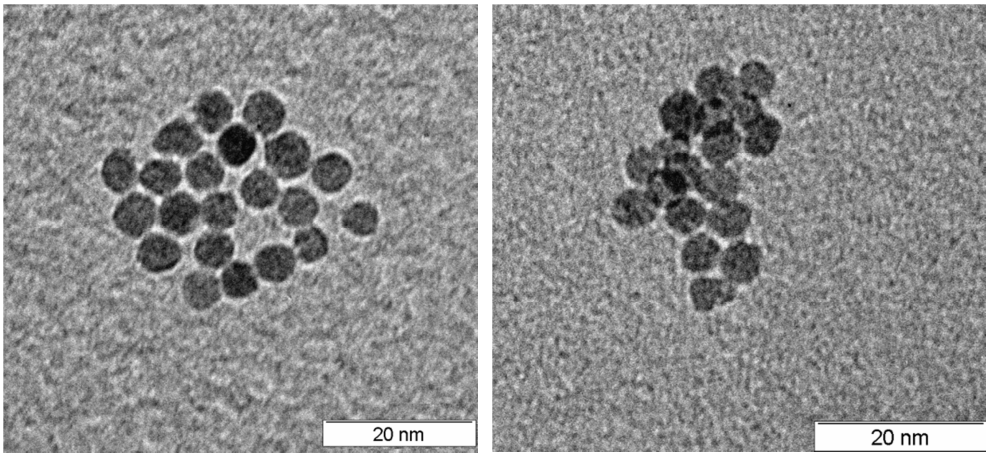

Figure 7 Left: TEM picture of spherical well-dispersed Fe_3O_4 nanobeads **70** with an average size of 5 nm. Right: TEM picture of the catalyst **71f**. The nanobeads show still a uniform size distribution with an average diameter of 5 nm, with a slight tendency to agglomerate.

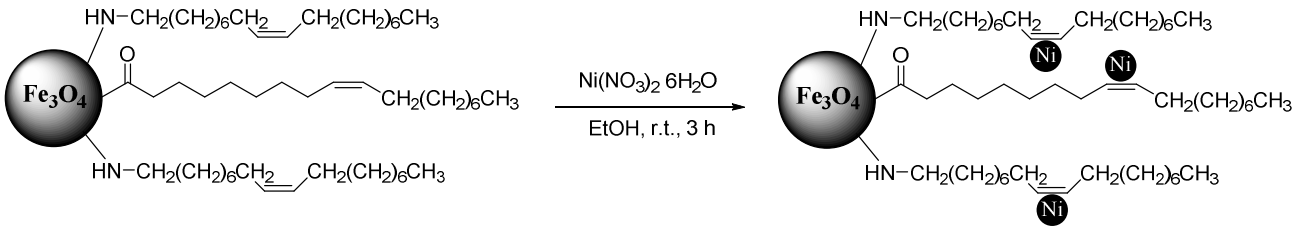

70 **71**

entry	catalyst	reducing agent	equiv	loading (mmol/g)	% incorporation
1[a]	**71a**	$NaBH_4$	1	2.24	55
2	**71b**	$NaBH_4$	1	2.62	63
3	**71c**	$NaBH_4$	0.2	0.12	4
4	**71d**	NH_2NH_2	1	0.08	2
5	**71e**	NH_2NH_2	10	0.16	5
6	**71f**	$NaBH_4$	5	3.06	90
7	**71g**	$NaBH_4$	10	2.76	67
8	**71h**	$NaBH_4$	10	0.32	82
9	**71i**	$NaBH_4$	-	-	-

Table 2 Deposition of Ni nanoparticles on the surface of Fe_3O_4 nanobeads **70**. These were stirred together with the $Ni(NO_3)_2{\cdot}6H_2O$ in EtOH for 2 h before $NaBH_4$ was added and the slurry was stirred for an additional 1 h. [a] Magnetic nanobeads **70** were stirred for only 1 h before addition of $NaBH_4$.

The activity of the thus synthesised catalysts **71b**, **71f**, **71g** and **71h** was firstly tested for the Suzuki-Miyaura cross-coupling of 4-iodotoluene **23** and phenylboronic acid **12**. Different reaction conditions were evaluated and are summarized in Table 3. The reactions were run at room temperature and at 100 °C in THF (entries 1 and 2); considering the work by Tang *et al*., [24] PPh_3 was added in the attempt of reducing any Ni(II) nanoparticles present. Under these conditions no conversion was observed. Then dioxane at reflux was used as solvent (entries 3 to 5), however no reaction took place. An additional attempt was made applying the conditions that led to higher conversion rate working with the Pd@Co/C **11** catalyst. In this case, the indicated amount of catalyst was stirred in a water/EtOH mixture under microwave irradiation. As found in the previous attempts, no conversion of the starting material was observed, independently of the metal loading on the magnetic nanobeads.

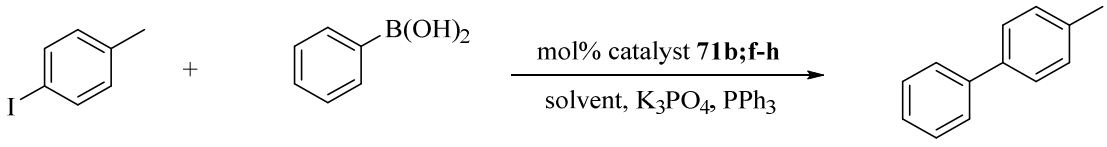

23 **12** **26**

entry	mol% catalyst	solvent	mmol PPh3	mmol K_3PO_4	time	T (°C)	yield
1	3	THF	0.04	1.5	30	r.t.	-
2	2	THF	0.04	1.5	8	100	-
3	2	dioxane	0.1	1.5	15	reflux	-
4[a]	2	dioxane	0.1	1.5	15	reflux	-
5[a,b]	5	dioxane	0.1	1.5	15	reflux	-
6	3	water/EtOH	-	1	1	120	-

Table 3 Suzuki-Miyaura coupling of 4-iodotoluene **23** with phenylboronic acid **12** by catalysts **71b;f-h**. Phenylboronic acid (0.6 mmol) was reacted with 4-iodoanisole (0.5 mmol) in 5 ml of the indicated solvent adding K_3PO_4, PPh_3 if indicated and the indicated amount of the catalyst. [a] The reaction was performed under argon. [b] The reaction was tested only for catalysts **71a;f-g**.

The catalysts were also tested for the hydrogenation of *para*-nitrophenol **56** (Figure 8) but, also in this case, no conversion of the starting material was observed.

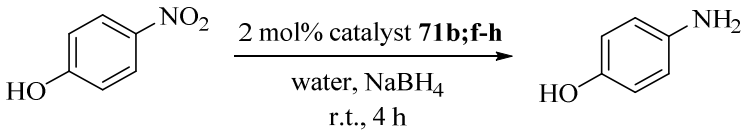

56 **57**

Figure 8 Hydrogenation of *para*-nitro phenol by catalyst **71b;f-h**. *para*-Nitrophenol **56** (0.5 mmol) was stirred with 2 mol% of the selected catalyst **71b;f-h** and $NaBH_4$ (5 mmol) in 3 ml water at room temperature for 4 h. No conversion of the starting material was observed.

A subsequent XPS analysis revealed the presence of NiO species instead of Ni(0) nanoparticles, which is believed to be responsible for the total absence of catalytic activity. It was moreover clarified the inability of the C-C double bonds to coordinate to what was thought to be Ni(0) nanoparticles. Further studies are necessary to achieve the synthesis of an active Ni supported magnetic catalyst, probably being necessary to functionalise the magnetic support. In this direction, a particular coating and functionalisation of the iron oxide nanobeads **70** was studied with the aim of synthesising a catalyst with a further increased surface area on which catalytically active Ni nanoparticles could be incorporated. In 2015, Yue *et al.*[25] developed new magnetic mesoporous silica microspheres combining the characteristics of two different materials: the mesoporous silica with a high surface area, large pore volume and tunable mesostructures and, on the other hand, the magnetic nanoparticles, characterized by easy separation and recyclability. The synthesis has been reproduced and the nanohybrid **74** was synthesised in a 4-step procedure (Figure 9).

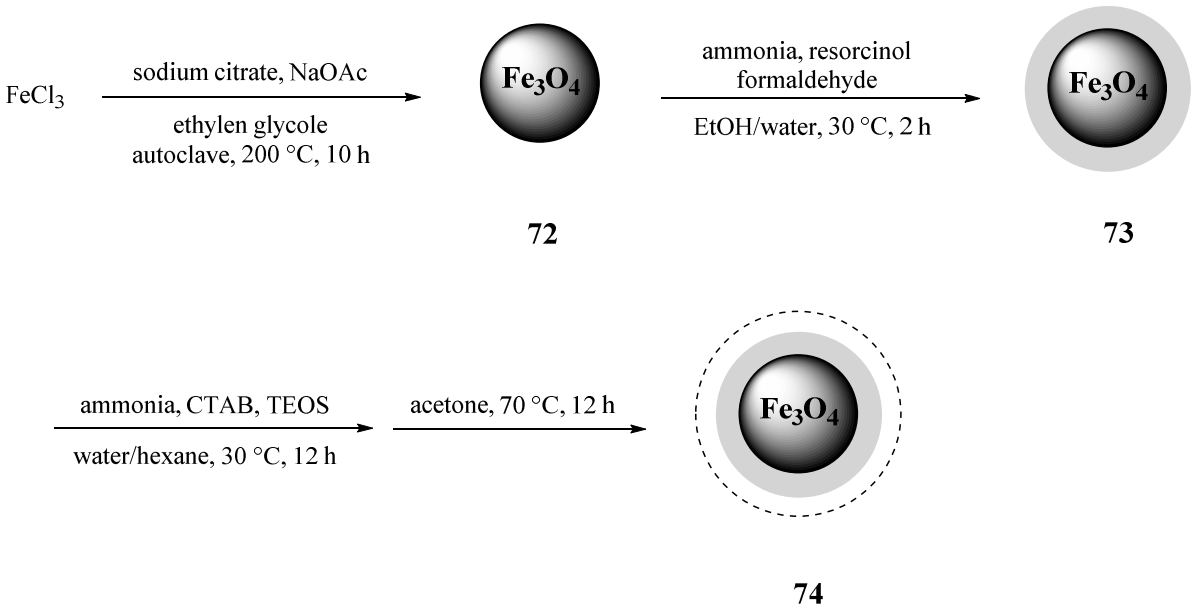

Figure 9 Scheme of the reproduced synthesis of magnetic mesoporous silica microsphere **74**. Firstly, iron oxide nanoparticles **72** were synthesised and coated with a resin, giving the RF@Fe_3O_4 nanobeads **73**. These were afterwards coated with a mesoporous silica shell leading to the formation of the microspheres **74**.

Firstly, new iron oxide nanoparticles with a diameter of 200 nm were synthesised and coated with a resorcinol-formaldehyde resin, leading to the formation of the coated RF@Fe_3O_4 nanobeads **73**. The coating was followed by a biliquid-phase step where the tetraethyl orthosilicate (TEOS) dissolved in hexane was hydrolysed in the oil-water interface and coassambled with the surfactant cetyltrimethylammonium bromide (CTAB) on the surface of the coated microsphere.

After removal of the surfactant, microspheres of 600 nm surrounded by pores of 9 nm, should have been obtained. Figure 10 shows the TEM picture of the RF@Fe_3O_4 nanobeads **73** and the final microspheres **74**. While the resorcinol-formaldehyde coating was successfully achieved, the coating with the silica pores was not accomplished and the microporous texture seemed to connect several magnetic microspheres. To better understand the distribution of this coating, the microspheres were treated by ultrathin microtomming, which consists on coating the substrate with a resin and cut it in slice before being observed at the TEM. In this way it was possible to analyse the material in lateral sections (Figure 10b). Absence of material in the centre of the magnetic nanoparticles is due to the ultrathin microtomming treatment that can cause loss of material.

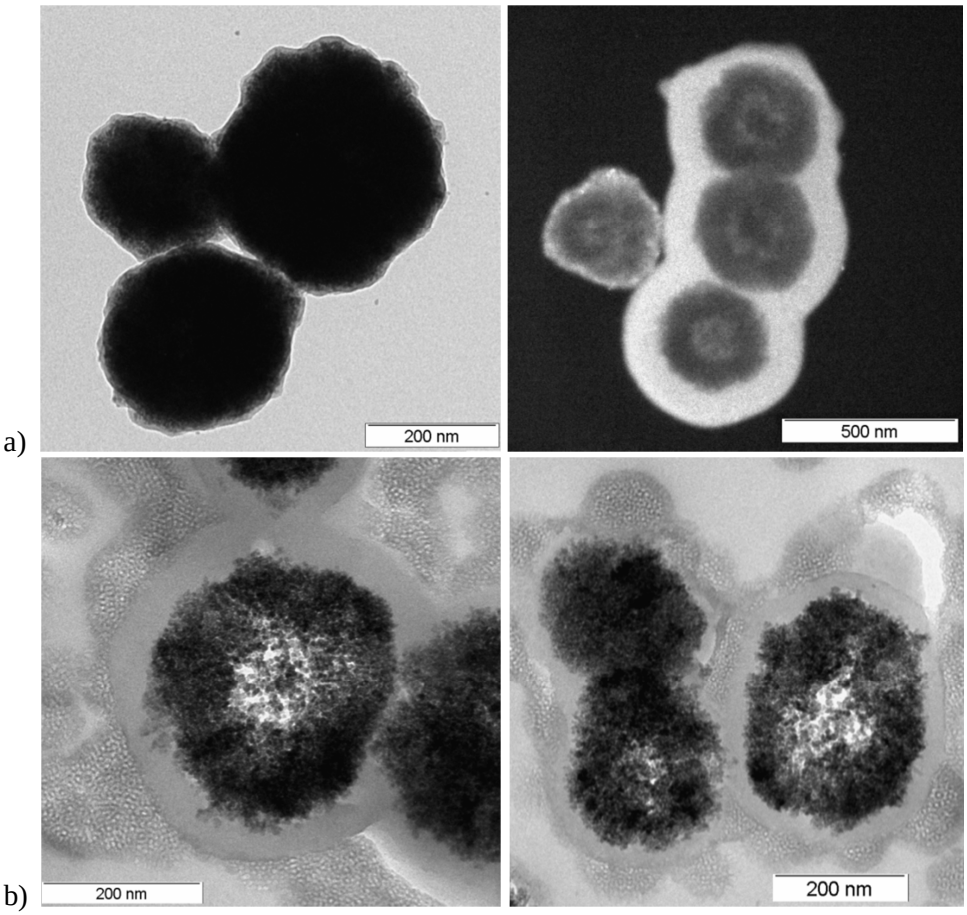

Figure 10 a) TEM picture of RF@Fe_3O_4 **73** under normal (left) and dark field (right), clearly showing the presence of a coating around the magnetic nanobeads **72**. b) TEM picture after ultrathin microtomming of the final microsphere **74**. Microporous silica texture is present between RF@Fe_3O_4 **73**, without creating a real coating.

The procedure was repeated employing as a starting magnetic support the iron oxide nanobeads **70** previously described, however no formation of the resorcinol-formaldehyde resin was achieved. Even though the coating with microporous silica was not achieved, the microspheres **74** were further functionalized by reaction of the hydroxy groups of the silica with 3-aminopropyltriethoxysilane (APTES) (Figure 11), in order to obtain amino groups that can coordinate the Ni nanoparticles.[19]

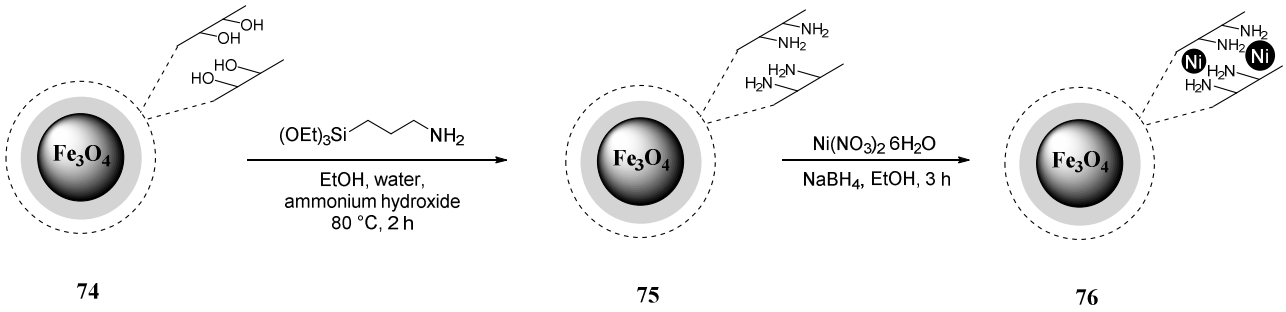

74 **75** **76**

Figure 11 Microspheres **74** were functionalized with amino group by reaction with 3-aminopropyltriethoxysilane. The microspheres **75** were collected and the N loading of 0.76 mmol/g evaluated by elemental microanalysis. Nickel nanoparticles were afterwards deposited on the NH_2-functionalized microspheres **75**, leading to the formation of microspheres **76**, with a Ni loading of 2.37 mmol/g (20% incorporation, evaluated by ICP-OES).

The activity of the nanocatalyst **76** thus obtained was tested in the Suzuki-Miyaura coupling of 4-iodotoluene **23** and phenylboronic acid **12** under the conditions indicated in Figure 12 but no conversion of the starting material was observed.

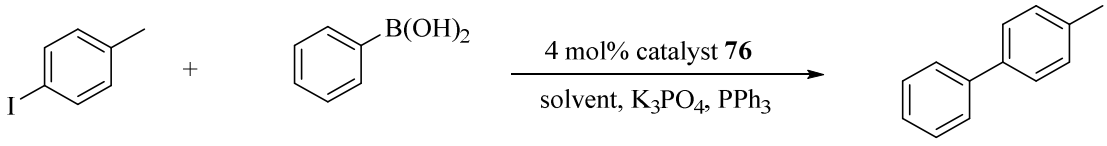

23 **12** **26**

entry	solvent	mmol PPh3	mmol K_3PO_4	Time	T (°C)	yield
1	dioxane	0.1	1.5	8	reflux	-
2	H_2O/EtOH	-	1.5	2	120	-

Figure 12 Suzuki-Miyaura coupling of 4-iodotoluene **23** with phenylboronic acid **12** by catalyst **76**. Phenylboronic acid (0.6 mmol) was reacted with 4-iodoanisole (0.5 mmol) in 5 ml of the indicated solvent adding K_3PO_4, PPh_3 if indicated and 4 mol% of the catalyst.

4.3 Conclusions

In summary, the deposition of Ni nanoparticles on the surface of two different magnetic supports was investigated. In one case, the ability of the graphene-like coating of cobalt nanoparticles to coordinate and stabilise Ni nanoparticles was studied. High incorporation percentages of the metal were accomplished using $Ni(COD)_2$ as metal source. Nevertheless, no catalytic activity for hydrogenation of both nitro derivates and C-C double bonds was exhibited probably because of the formation of big Ni nanoclusters on the surface of the magnetic nanobeads.[22] Moreover, XPS analysis revealed the presence of Ni(II) species. It was known the difficulties to work with this metal, that can so easily oxidize.[20] New synthetic pathways need to be considered in order to obtain an active nanocatalyst. A starting point could be the use of the already mentioned PEI-coated Co/C nanobeads **59**, evaluating the ability of the several amino groups present to coordinate and stabilize the Ni nanoparticles. In the other case, the affinity of Ni for C-C double bonds present on the surface of iron oxide nanobeads was taken in consideration. Also in this case, high metal incorporation percentages were achieved but no catalytic activity was exhibited for both hydrogenation of nitro derivates and Suzuki-Miyaura cross-coupling. TEM pictures of the synthesised nanocatalysts showed no appreciable difference in the average dimensions in comparison with the starting iron oxide nanobeads. Subsequently, XPS analysis revealed the presence of NiO species, probably responsible for the absence of catalytic activity. An additional coating with microporous silica was studied to evaluate the ability of Ni nanoparticles to be coordinated inside the amino-functionalized micropores of the coating. Unfortunately, it was not possible to reproduce the synthesis and the microporous silica coating was not achieved and, once more, no catalytic activity was shown. Further investigations need to be done regarding nickel deposition, the major problem being the persistent oxidation of the metal.

4.4 Experimental section

Material and methods

Carbon coated cobalt nanobeads (Co/C, 20.5 m^2/g, mean particles size ≈ 40 nm) were purchased from Turbobeads Llc, Switzerland. Prior to use, they were washed in a concentrated HCl/water mixture (1:1) 5 times for 24 h. Acid residues were removed by washing with millipore water (x5) and the particles were dried at 50 °C in a vacuum oven. The magnetic nanobeads were dispersed using an ultrasound bath (Sonorex RK 255 H-R, Bandelin) and recovered with the aid of a neodymium-based magnet (15 x 30 mm). All commercially available compounds were used as received. IR-ATR spectroscopy was carried out on a Biorad Excalibur FTS 3000. Elemental microanalysis (LECO CHN-900) was carried out by the micro analytic Department at the University of Regensburg and by the Universidad Complutense de Madrid. Transmission electron microscopy was carried out by Dr. Daniela Paunesco from ETH, Zurich; by Prof. Josef Zweck from the Department of Physic of the University of Regensburg and by the Microscopy Unit of Universitat Rovira i Virgili, Tarragona. Inductively coupled plasma optical emission spectrometry was carried out by University of Regensburg (Spectro Analytical Instruments ICP Modula EOP), by Universidad de Alicante and by MEDAC Ltd, United Kingdom. XPS measurements were performed by Thomas Meier from the Department of Physic at the University of Regensburg and by SuSoS, Switzerland. NMR spectra were recorded with a Bruker AV 300 spectrometer. Gas chromatography was recorded on Fisons Instruments GC8000 equipped with a capillary (30 m x 250 µm x 0.25 µm) and flame ionization detector. TLC were performed on silica gel 60 F254 plates and detection was carried out under UV light.

Iron oxide nanoparticles with an average diameter of 5 nm (70)

1,2-Dodecanediol (5.6 g, 27.7 mmol) and benzyl ether (20 ml) were added to a three-neck round bottom flask and purged with argon. $Fe(acac)_3$ (1.76 g, 5 mmol), oleic acid (4.72 mg, 16.7 mmol) and oleylamine (5.69 g, 21.28 mmol) were added in the described order under argon. The reaction mixture was heated up to 260 °C for 3 h. Once cooled down to room temperature, the nanoparticles were collected by centrifugation, washed several times with EtOH (6 x 20 ml) and acetone (3 x 15 ml) and dried under vacuum for 6 h. The magnetic nanobeads were characterized by elemental microanalysis (C: 16.50; H: 2.74; N: 0.10).

Nickel nanoparticles deposited on the graphene-like shell of cobalt nanobeads (67a-g)

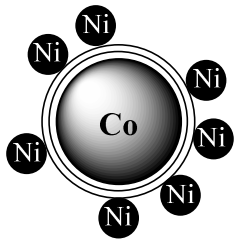

The further indicated amounts of Co/C nanobeads **10** and $Ni(COD)_2$ were introduced in a microwave vial under nitrogen atmosphere. After adding anhydrous toluene (3 ml), the reaction mixture was sonicated in an ultrasonic bath for 10 min and then heated up in a microwave oven at the indicated temperature and time. The catalyst was recovered by an external magnet, the solution decanted and the nanoparticles washed with DCM or toluene (5 x 3 ml). After drying under vacuum, the metal loading was evaluated by ICP-OES.

67a_50 mg Co/C nanobeads; 14 mg, 0.05 mmol $Ni(COD)_2$; 2 min at 75 °C; washing step with DCM. Final Ni loading: 0.8 mmol/g, 83% incorporation.

67b_50 mg Co/C nanobeads; 14 mg, 0.05 mmol $Ni(COD)_2$; 15 min at 75 °C; washing step with DCM. Final Ni loading: 0.8 mmol/g, 80% incorporation.

67c_100 mg Co/C nanobeads; 2.7 mg, 0.01 mmol $Ni(COD)_2$; 2 min at 90 °C; washing step with DCM. Final Ni loading: 0.1 mmol/g, 95% incorporation.

67d_300 mg Co/C nanobeads; 10 mg, 0.03 mmol $Ni(COD)_2$; 15 min at 90 °C; washing step with DCM. Final Ni loading: 0.1 mmol/g, 97% incorporation.

67e_500 mg Co/C nanobeads; 3.2 mg, 0.01 mmol $Ni(COD)_2$; 2 min at 100 °C; washing step with toluene. Final Ni loading: 0.02 mmol/g, 91% incorporation.

67f_300 mg Co/C nanobeads; 10.2 mg, 0.03 mmol $Ni(COD)_2$; 2 min at 100 °C; washing step with toluene. Final Ni loading: 0.1 mmol/g, 98% incorporation.

67g_300 mg Co/C nanobeads; 82 mg, 0.3 mmol $Ni(COD)_2$; 2 min at 100 °C; washing step with toluene. Final Ni loading: 1 mmol/g, 98% incorporation.

Nickel nanoparticles deposited on iron oxide nanobeads (71a-g)

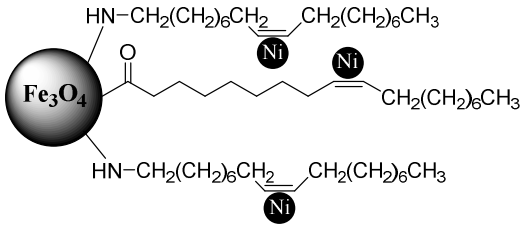

The further indicated amounts of iron oxide nanobeads **70** and $Ni(NO_3)_2 \cdot 6H_2O$ were introduced in a Schlenk tube. After adding EtOH (4 ml), the reaction mixture was stirred at room temperature for 2 h. The indicated amount of $NaBH_4$ or NH_2NH_2 was added and the slurry stirred for an additional 1 h. The catalyst was recovered by an external magnet, the solution decanted and the nanoparticles washed with EtOH (5 x 3 ml). After drying under vacuum, the metal loading was evaluated by ICP-OES.

71a_23.8 mg Fe_3O_4 nanobeads; 27.7 mg, 0.095 mmol $Ni(NO_3)_2 \cdot 6H_2O$; 5 mg, 0.127 mmol $NaBH_4$. Final Ni loading: 2.24 mmol/g, 55% incorporation.

71b_24.7 mg Fe_3O_4 nanobeads; 29.6 mg, 0.102 mmol $Ni(NO_3)_2 \cdot 6H_2O$; 5 mg, 0.127 mmol $NaBH_4$. Final Ni loading: 2.62 mmol/g, 63% incorporation.

71c_32.9 mg Fe_3O_4 nanobeads; 31.2 mg, 0.107 mmol $Ni(NO_3)_2 \cdot 6H_2O$; 1 mg, 0.026 mmol $NaBH_4$. Final Ni loading: 0.12 mmol/g, 4% incorporation.

71d_32.9 mg Fe_3O_4 nanobeads; 31.2 mg, 0.107 mmol $Ni(NO_3)_2 \cdot 6H_2O$; 1 mg, 0.026 mmol NH_2NH_2. Final Ni loading: 0.12 mmol/g, 4% incorporation.

71e_25 mg Fe_3O_4 nanobeads; 39.3 mg, 0.135 mmol $Ni(NO_3)_2 \cdot 6H_2O$; 4.33 mg, 0.135 mmol NH_2NH_2. Final Ni loading: 0.08 mmol/g, 2% incorporation.

71f_76.4 mg Fe_3O_4 nanobeads; 75 mg, 0.258 mmol $Ni(NO_3)_2 \cdot 6H_2O$; 50 mg, 1.272 mmol $NaBH_4$.
Final Ni loading: 3.06 mmol/g, 90% incorporation.

71g_50 mg Fe_3O_4 nanobeads; 60 mg, 0.206 mmol $Ni(NO_3)_2 \cdot 6H_2O$; 78 mg, 1.984 mmol $NaBH_4$.
Final Ni loading: 2.76 mmol/g, 67% incorporation.

71h_100 mg Fe_3O_4 nanobeads; 15 mg, 0.052 mmol $Ni(NO_3)_2 \cdot 6H_2O$; 19 mg, 0.483 mmol $NaBH_4$.
Final Ni loading: 0.32 mmol/g, 82% incorporation.

71i_25.5 mg Fe_3O_4 nanobeads; 40.3 mg, 0.139 mmol $Ni(NO_3)_2 \cdot 6H_2O$.
Final Ni loading: - mmol/g, No incorporation.

Iron oxide nanoparticles with an average diameter of 200 nm (72)

$FeCl_3$ (0.65 g, 4 mmol) and trisodium citrate (0.2 g, 0.77 mmol) were dissolved in ethylene glycol (20 ml). NaOAc (1.20 g, 14.63 mmol) was added under vigorous stirring, continued for additional 30 min. The slurry was transferred to a Teflon-lined stainless-steel autoclave and heated up to 200 °C for 10 h. Once cooled down at room temperature, the magnetic nanobeads were collected by centrifugation, washed several times with EtOH (5 x 20 ml) and water (4 x 15 ml) and dried under vacuum.

Resorcinol-formaldehyde coated iron oxide nanoparticles (73)

Magnetic nanobeads **73** (100 mg) were dispersed by sonication in 30 ml of a mixture of EtOH/water 2:1. Ammonia solution (32%, 0.5 ml), resorcinol (100 mg, 0.9 mmol) and formaldehyde (100 mg, 3.3 mmol) were added in the indicated order and the resulted slurry was stirred for 2 h at 30 °C. The coated magnetic nanobeads **73** were collected with a magnet, washed with EtOH (3 x 10 ml), water (3 x 10 ml) and dried under vacuum.

Magnetic mesoporous silica microspheres (74)

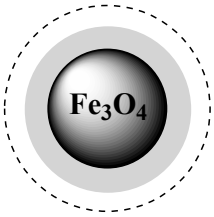

The resorcinol-formaldehyde coated magnetic nanobeads **74** (120 mg) were dispersed by ultrasonication in a mixed solution of water (80 ml), CTAB (500 mg, 1.37 mmol) and ammonia (32%, 0.8 ml). 20 ml of *n*-hexane were added, leading to the formation of a biliquid phase system. To tune the mesoporous size, the slurry was stirred at different rates (170-500 rpm) for 10 min. Subsequently, TEOS (2.5 ml, 11.2 mmol) was added dropwise during 10 min and a gentle stirring (170 rpm), maintaining a biliquid phase solution, was continued for 12 h at 30 °C. The resulting hybrid material was collected by a magnet and washed with EtOH (4 x 15 ml) and water (3 x 15 ml). The microspheres were then dispersed in acetone (30 ml) and refluxed for 12 h. Once at room temperature, they were collected with a magnet, the solution was decanted, new acetone (30 ml) added and, once more, refluxed for 12 h. Finally, the microspheres were collected, washed with EtOH (2 x 10 ml) and dried under vacuum at 40 °C for 12 h.

Amino-functionalized magnetic mesoporous silica microsphere (75)

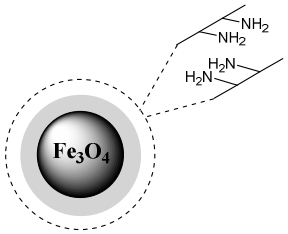

The magnetic mesoporous silica microspheres **74** (20 mg) were dispersed in a water/EtOH 15:1 mixture (32 ml). Ammonium hydroxide (2 ml, 0.166 mmol) and APTES (0.2 ml, 0.166 mmol) were added and the reaction mixture was stirred for 2 h at 80 °C. The functionalized microspheres were collected by a magnet and, after decanting the supernatant, washed with water (4 x 15 ml) and dried under vacuum. The final nitrogen loading of 0.76 mmol/g was evaluated by elemental microanalysis.

Deposition of Ni nanoparticles on amino-functionalized magnetic mesoporous silica microspheres (76)

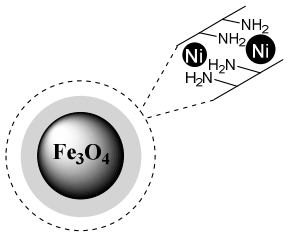

The amino functionalized microspheres **75** (20 mg) and $Ni(NO_3)_2 \cdot 6H_2O$ (33.6 mg, 0.116 mmol) were introduced in a Schlenk tube. After adding EtOH (4 ml), the reaction mixture was stirred at room temperature for 2 h. $NaBH_4$ (24.48 mg, 1,2 mmol) was added and the slurry stirred for an additional 1 h. The catalyst was recovered by an external magnet, the solution decanted and the nanoparticles washed with EtOH (5 x 3 ml). After drying under vacuum, the metal loading was evaluated by ICP-OES (2.37 mmol/g; 20% incorporation).

General procedure for the hydrogenation of acetophenone 68 (GP8)

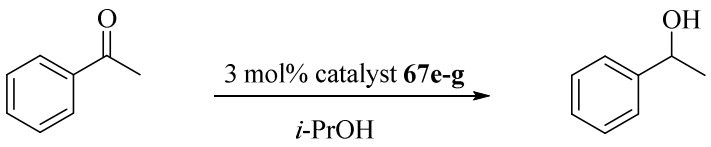

68 **69**

GP8. 3 mol% of supported Ni catalyst (**67e-g**), acetophenone (0.5 mmol) and *i*-PrOH (3 ml) were introduced into a Schlenk tube under the reaction conditions showed in Figure 3. The reaction progress was monitored by TLC. The catalyst was collected with a magnet and the supernatant decanted.

The nanobeads were washed with water (3 x 4 ml) and dried under vacuum. The solvent collected was evaporated under vacuum obtaining a crude material that was analysed by ^{1}H NMR.

General procedure for the hydrogenation of nitrobenzene 62 (GP9)

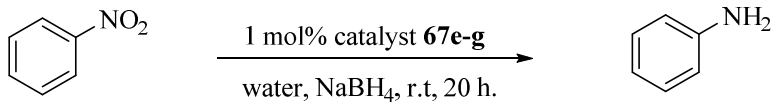

62 **63**

GP9. 1 mol% of supported Ni catalyst (**67e-g**), nitrobenzene (0.5 mmol), $NaBH_4$ (5 mmol) and water (3 ml) were introduced into a Schlenk tube. The reaction mixture was stirred at room temperature for 20 h. The reaction progress was monitored by TLC. The catalyst was collected with a magnet and the supernatant decanted. The nanobeads were washed with water (3 x 4 ml) and dried under vacuum. The solvent collected was evaporated under vacuum obtaining a crude material that was analysed by ^{1}H NMR.

General procedure for the hydrogenation of *para*-nitrophenol 56 (GP10)

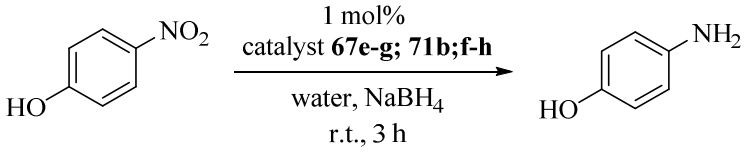

56 **57**

GP10. 1 mol% of supported nickel catalyst **67e-g** and **71b;f-h**, *para*-nitrophenol (0.5 mmol), water (3 ml) and $NaBH_4$ (5 mmol) were introduced into a Schlenk tube. The reaction mixture was stirred vigorously at room temperature for 3 h. The reaction progress was monitored by TLC.

The catalyst was collected with a magnet and the supernatant decanted. The nanobeads were washed with water (3 x 4 ml) and dried under vacuum. The collected solvent was evaporated under vacuum obtaining a crude material that was analysed by ^{1}H NMR.

General procedure for the hydrogenation of *trans*-stilbene 64 (GP11)

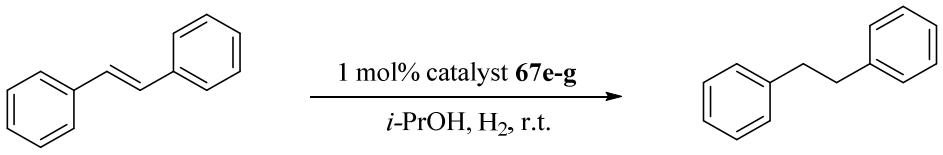

64 **65**

GP11. 1 mol% of supported nickel catalyst (**67e-g**), *trans*-stilbene (0.5 mmol), *i*-PrOH (3 ml) and dodecane (0.5 mmol) as an internal standard were introduced into a Schlenk tube. The reaction mixture was stirred vigorously under 1 atm H_2 (balloon). The reaction progress was monitored by GC. The catalyst was collected with a magnet and the supernatant decanted. The nanobeads were washed with water (3 x 4 ml) and dried under vacuum. The solvent collected was evaporated under vacuum obtaining a crude material that was analysed by ^{1}H NMR.

General procedure for the Suzuki-Miyaura coupling (GP12)

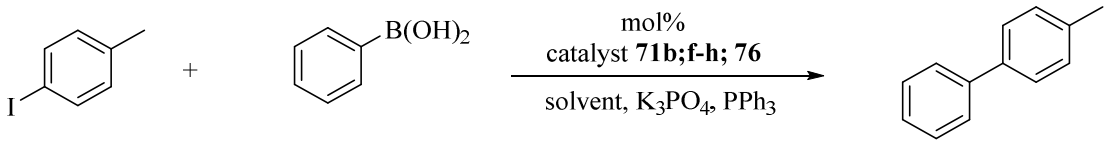

23 **12** **26**

The indicated amount of catalyst **71b;f-h** (Table 3) and **76** (Figure 12), 4-iodotoluene **23** (0.5 mmol), phenylboronic acid **12** (0.6 mmol) and the amount of K_3PO_4 and PPh_3 indicated (Table 3 and Figure 12) were added to a round bottom flask. The reaction mixture was stirred at different reaction temperatures and times, also indicated (Table 3 and Figure 12). The reaction progress was monitored by TLC. The catalyst was collected with a magnet and the supernatant decanted. The nanobeads were washed with water (3 x 4 ml) and dried under vacuum. The solvent collected was evaporated under vacuum obtaining a crude material that was analysed by ^{1}H NMR.

4.5 References

[1] F. Alonso, M. Yus, *Tetrahedron Letters* **1996**, *37*, 6925–6928.

[2] F. Alonso, I. Osante, M. Yus, *Tetrahedron* **2007**, *63*, 93–102.

[3] G. Radivoy, F. Alonso, M. Yus, *Tetrahedron* **1999**, *55*, 14479–14490.

[4] C. Teng, J. He, L. Zhu, L. Ren, J. Chen, M. Hong, Y. Wang, *Nanoscale Research Letters* **2015**, *10*, 1–8.

[5] P. S. Rathore, R. Patidar, S. Rathore, S. Thakore, *Catalysis Letters* **2013**, *144*, 439–446.

[6] F. Alonso, P. Riente, M. Yus, *Tetrahedron* **2008**, *64*, 1847–1852.

[7] F. Alonso, P. Riente, M. Yus, *Tetrahedron Letters* **2008**, *49*, 1939–1942.

[8] F. Alonso, P. Riente, M. Yus, *Accounts of Chemical Research* **2011**, *44*, 379–391.

[9] Y. Moglie, F. Alonso, C. Vitale, M. Yus, G. Radivoy, *Tetrahedron* **2006**, *62*, 2812–2819.

[10] F. Han, *Chemical Society Reviews* **2013**, *42*, 5270–5298.

[11] S. Handa, E. D. Slack, B. H. Lipshutz, *Angewandte Chemie International Edition* **2015**, *54*, 11994–11998.

[12] K. Shimizu, N. Imaiida, K. Kon, S. M. A. H. Siddiki, A. Satsuma, *ACS Catalysis* **2013**, *3*, 998–1005.

[13] C. Ó Dálaigh, S. A. Corr, Y. Gun'ko, S. J. Connon, *Angewandte Chemie International Edition* **2007**, *46*, 4329–4332.

[14] T. Hara, T. Kaneta, K. Mori, T. Mitsudome, T. Mizugaki, K. Ebitani, K. Kaneda, *Green Chemistry* **2007**, *9*, 1246–1251.

[15] A. H. Latham, M. E. Williams, *Accounts of Chemical Research* **2008**, *41*, 411–420.

[16] T. T. Upadhya, S. P. Katdare, P. D. Sabde, V. Ramaswamy, A. Sudalai, *Chemical Communications* **1997**, 1119–1120.

[17] Y. Huang, L. Chunping, J. Bai, Y. Zhu, J. Wang, *Journal of Inorganic and Organometallic Polymers and Materials* **2015**, *25*, 1000–1005.

[18] G. Gunawan, S. Bourdo, A. S. Biris, T. Viswanathan, *Synthesis and Reactivity in Inorganic, Metal-Organic, and Nano-Metal Chemistry* **2013**, *43*, 635–639.

[19] V. Polshettiwar, B. Baruwati, R. S. Varma, *Green Chemistry* **2009**, *11*, 127–131.

[20] R. K. Sharma, M. Yadav, R. Gaur, Y. Monga, A. Adholeya, *Catalysis Science & Technology* **2015**, *5*, 2728–2740.

[21] B. Schrick, J. L. Blough, A. D. Jones, T. E. Mallouk, *Chemistry of Materials* **2002**, *14*, 5140–5147.

[22] S. Sarkar, E. Guibal, F. Quignard, A. K. SenGupta, *Journal of Nanoparticle Research* **2012**, *14*, 1–24.

[23] P. Riente, C. Mendoza, M. A. Pericas, *Journal of Materials Chemistry* **2011**, *21*, 7350–7355.

[24] Q. H. Z. Tang, *The Journal of Organic Chemistry* **2006**, *71*, 2167–2169.

[25] Q. Yue, J. Li, W. Luo, Y. Zhang, A. A. Elzatahry, X. Wang, C. Wang, W. Li, X. Cheng, A. Alghamdi, A. M. Abdullah, Y. Deng, D. Zhao, *Journal of the American Chemical Society* **2015**, *137*, 13282–13289.

NMR Spectra

^{1}H NMR (300 MHz)

^{13}C CNMR (75 MHz)

Solvent: $CDCl_3$

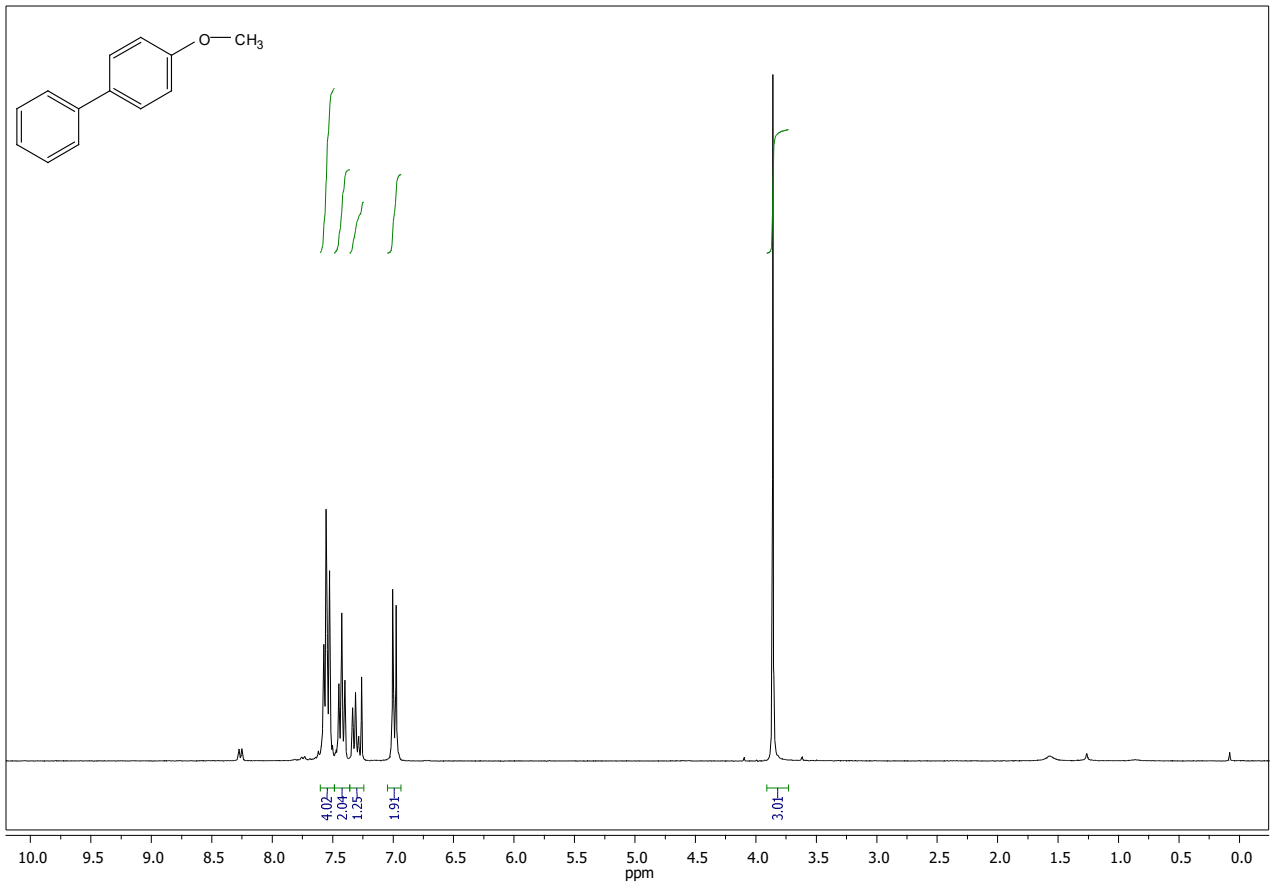
O— CH3
4.02
2.04
1.25
1.91
3.01
10.0 9.5 9.0 8.5 8.0 7.5 7.0 6.5 6.0 5.5 5.0 4.5 4.0 3.5 3.0 2.5 2.0 1.5 1.0 0.5 0.0
ppm

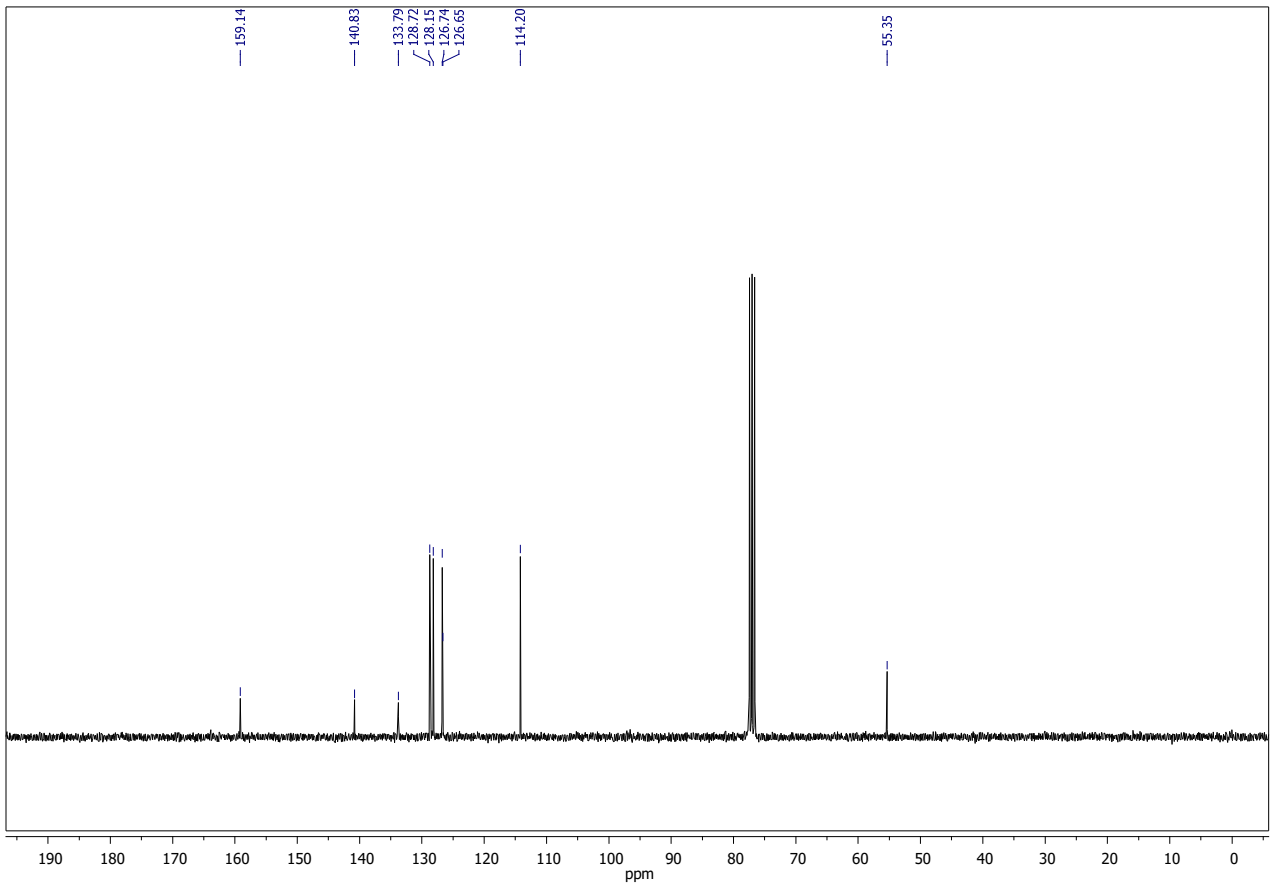
159.14
140.83
133.79
128.72
128.15
126.74
126.65
114.20
55.35
190 180 170 160 150 140 130 120 110 100 90 80 70 60 50 40 30 20 10 0
ppm

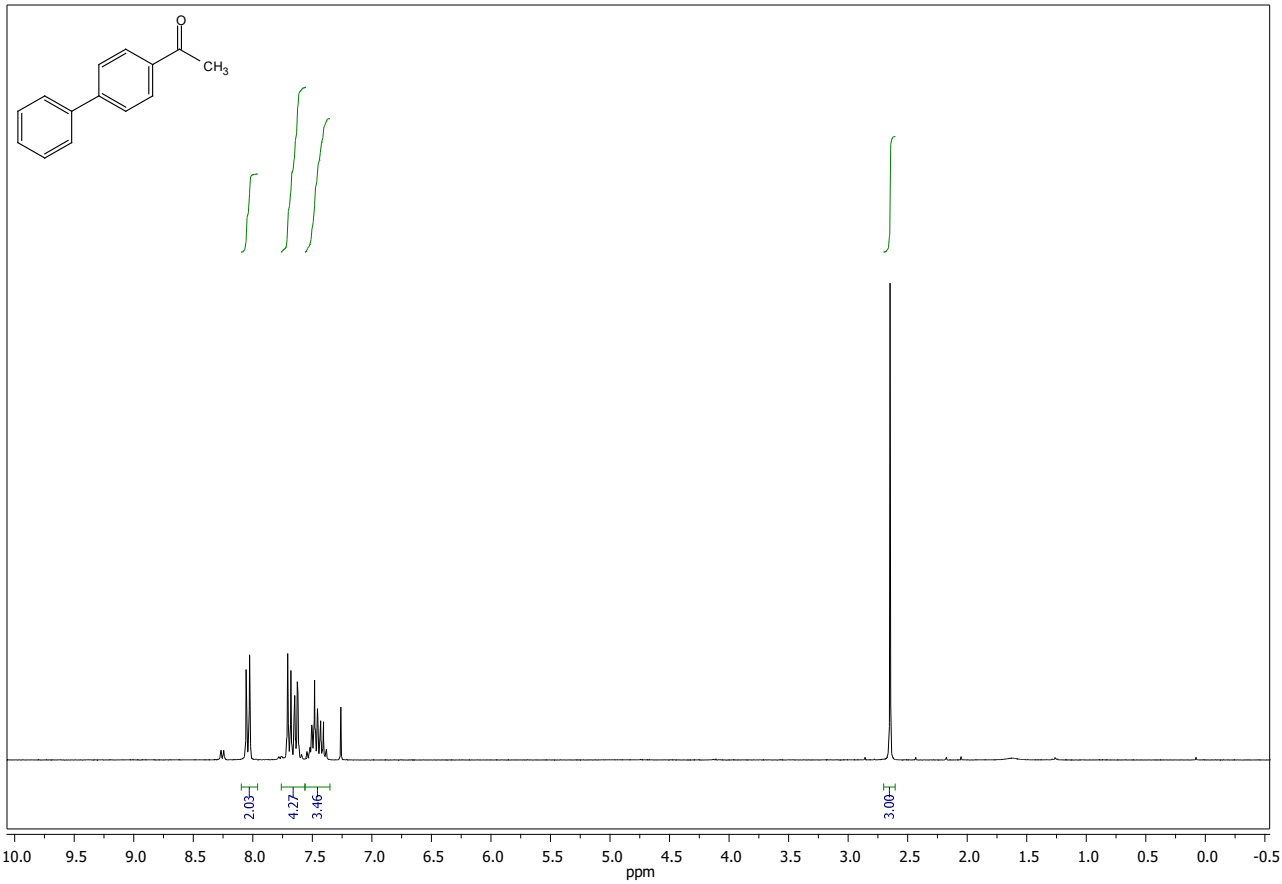
O
CH3
2.03
4.27
3.46
3.00
10.0 9.5 9.0 8.5 8.0 7.5 7.0 6.5 6.0 5.5 5.0 4.5 4.0 3.5 3.0 2.5 2.0 1.5 1.0 0.5 0.0 -0.5
ppm

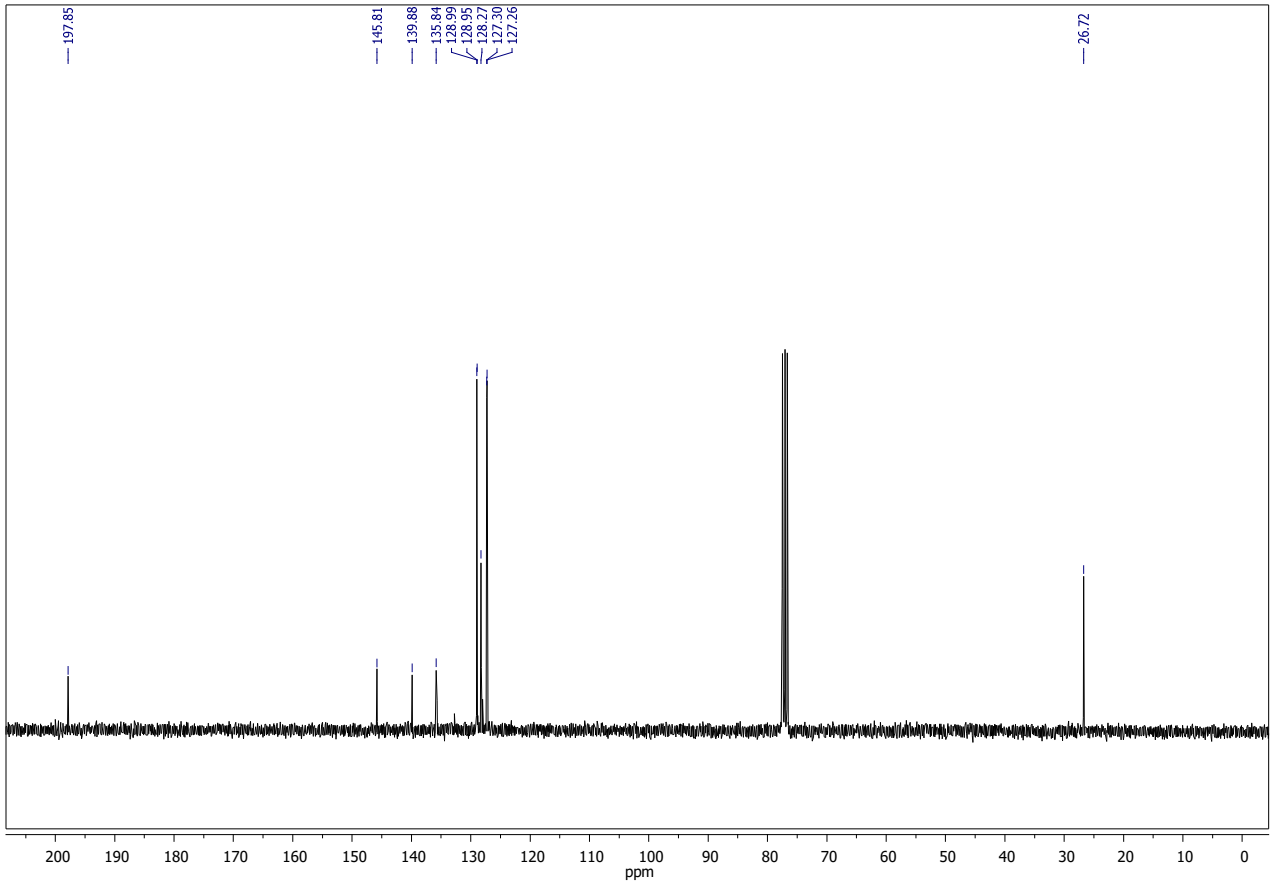
197.85
145.81
139.88
135.84
128.99
128.95
128.27
127.30
127.26
26.72
200 190 180 170 160 150 140 130 120 110 100 90 80 70 60 50 40 30 20 10 0
ppm

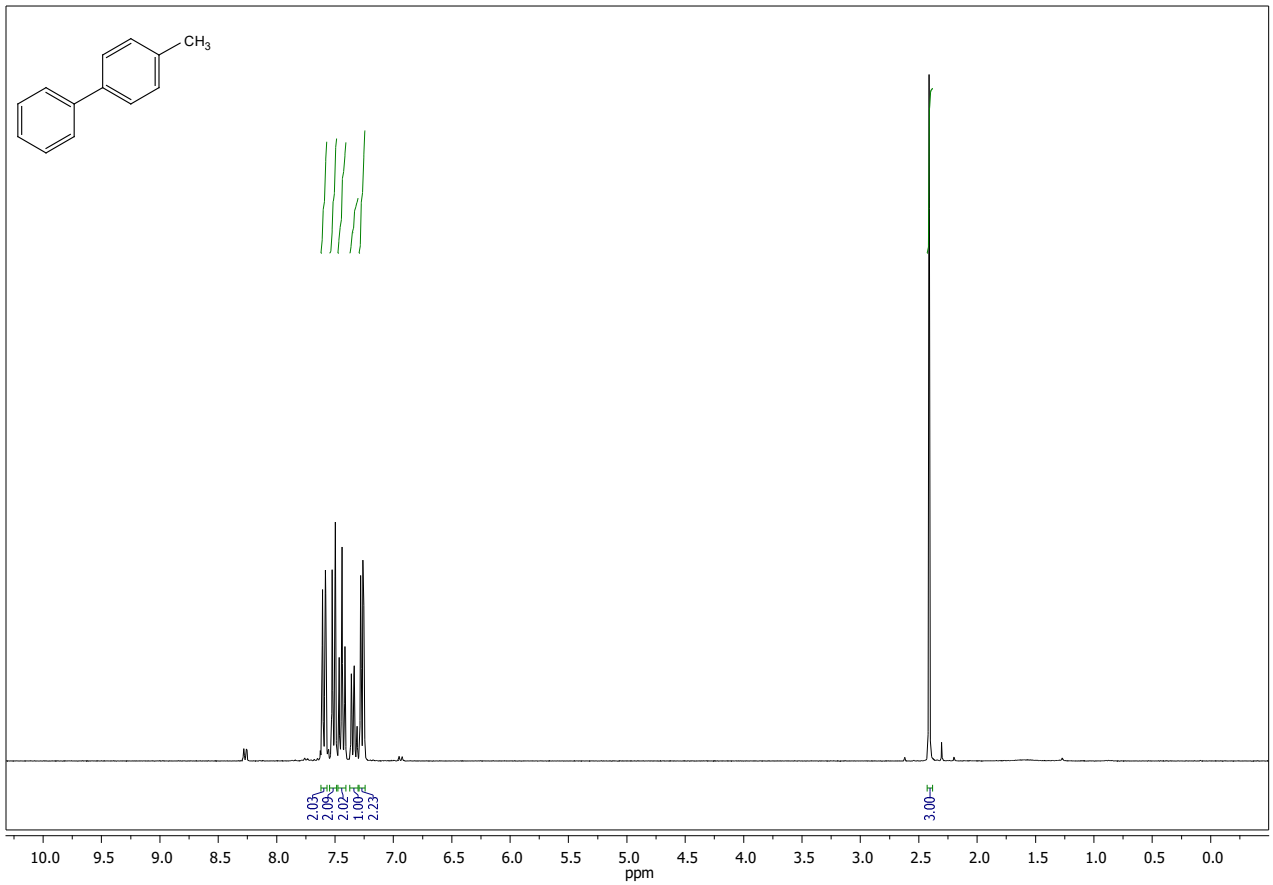
CH3
2.03
2.09
2.02
1.00
2.23
3.00
10.0 9.5 9.0 8.5 8.0 7.5 7.0 6.5 6.0 5.5 5.0 4.5 4.0 3.5 3.0 2.5 2.0 1.5 1.0 0.5 0.0
ppm

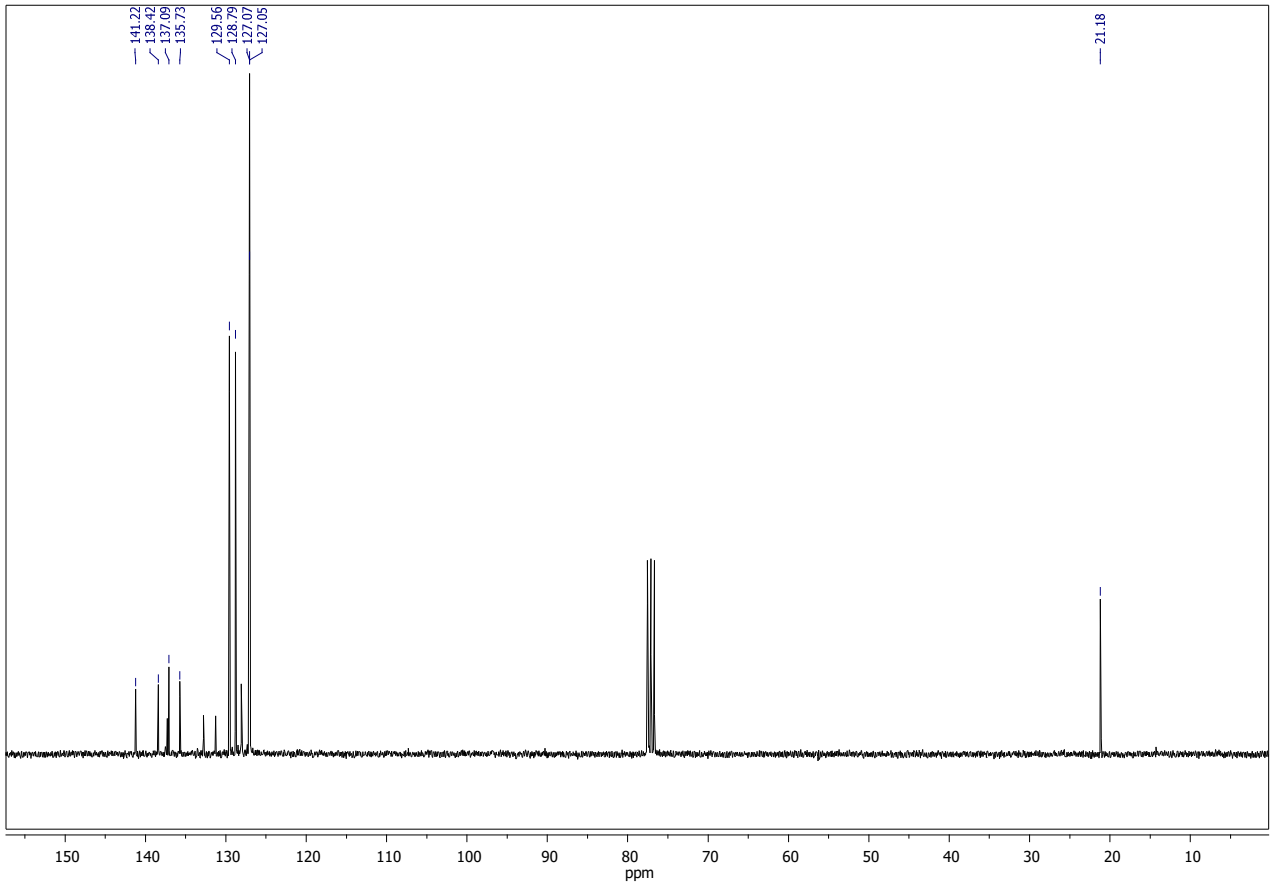
141.22
138.42
137.09
135.73
129.56
128.79
127.07
127.05
21.18
150 140 130 120 110 100 90 80 70 60 50 40 30 20 10
ppm

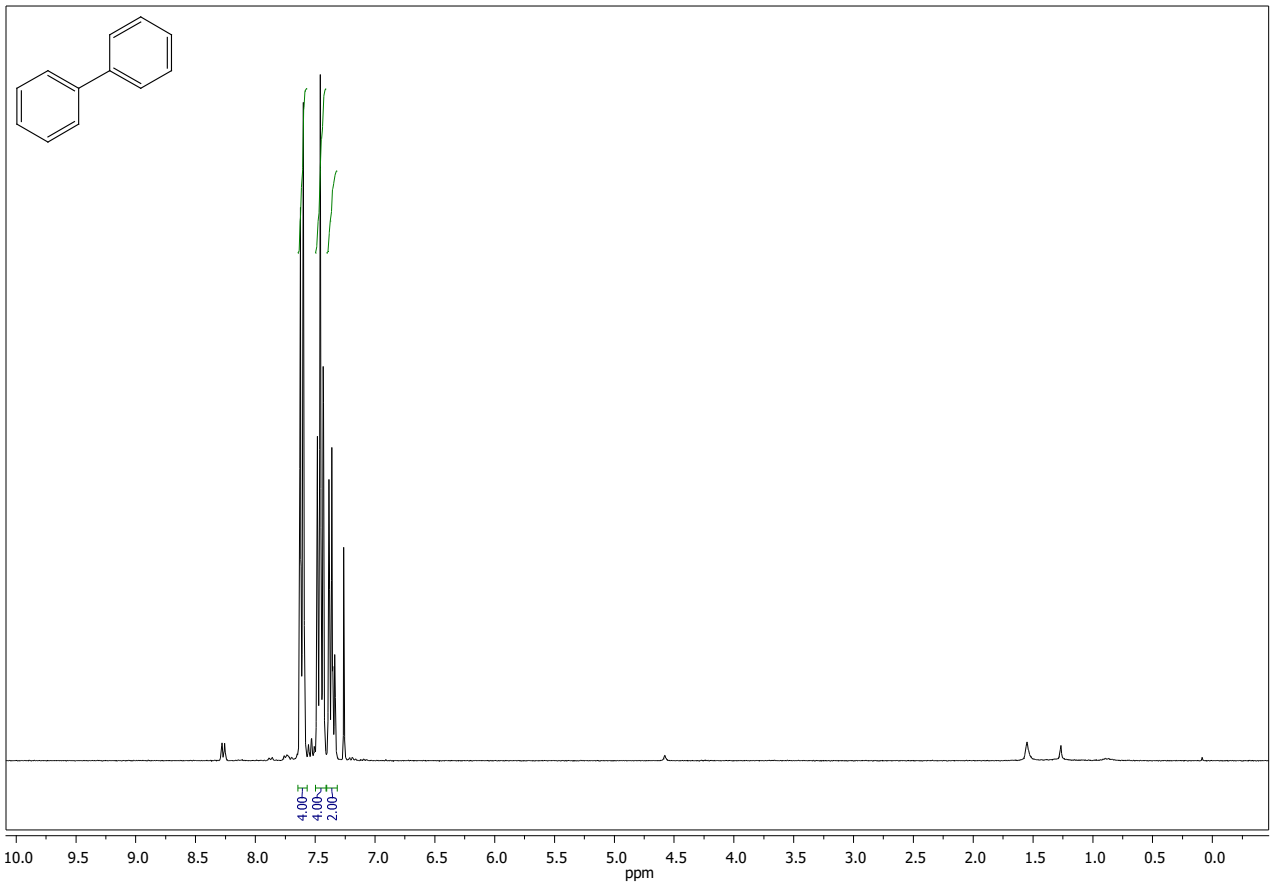
4.00
4.00
2.00
10.0 9.5 9.0 8.5 8.0 7.5 7.0 6.5 6.0 5.5 5.0 4.5 4.0 3.5 3.0 2.5 2.0 1.5 1.0 0.5 0.0
ppm

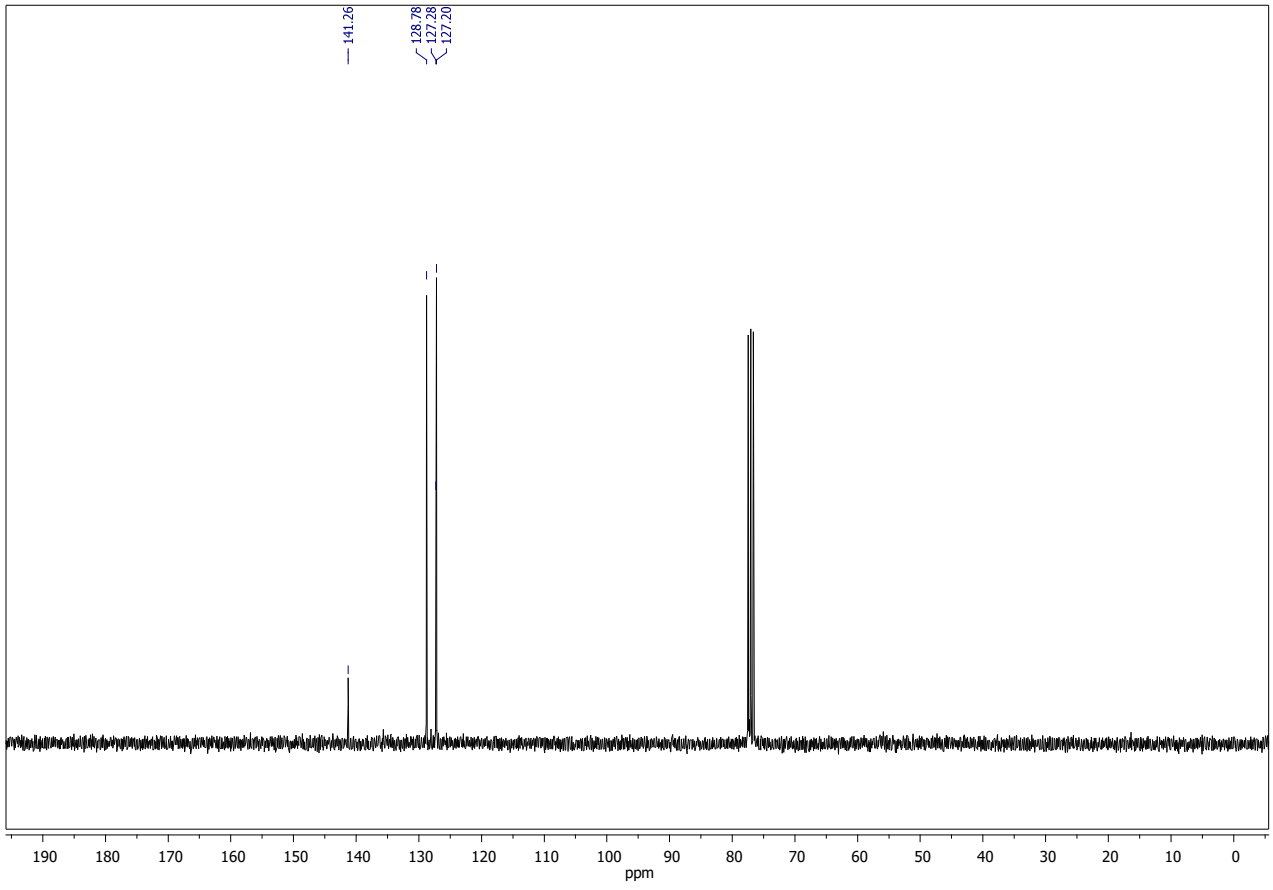
141.26
128.78
127.28
127.20
190 180 170 160 150 140 130 120 110 100 90 80 70 60 50 40 30 20 10 0
ppm

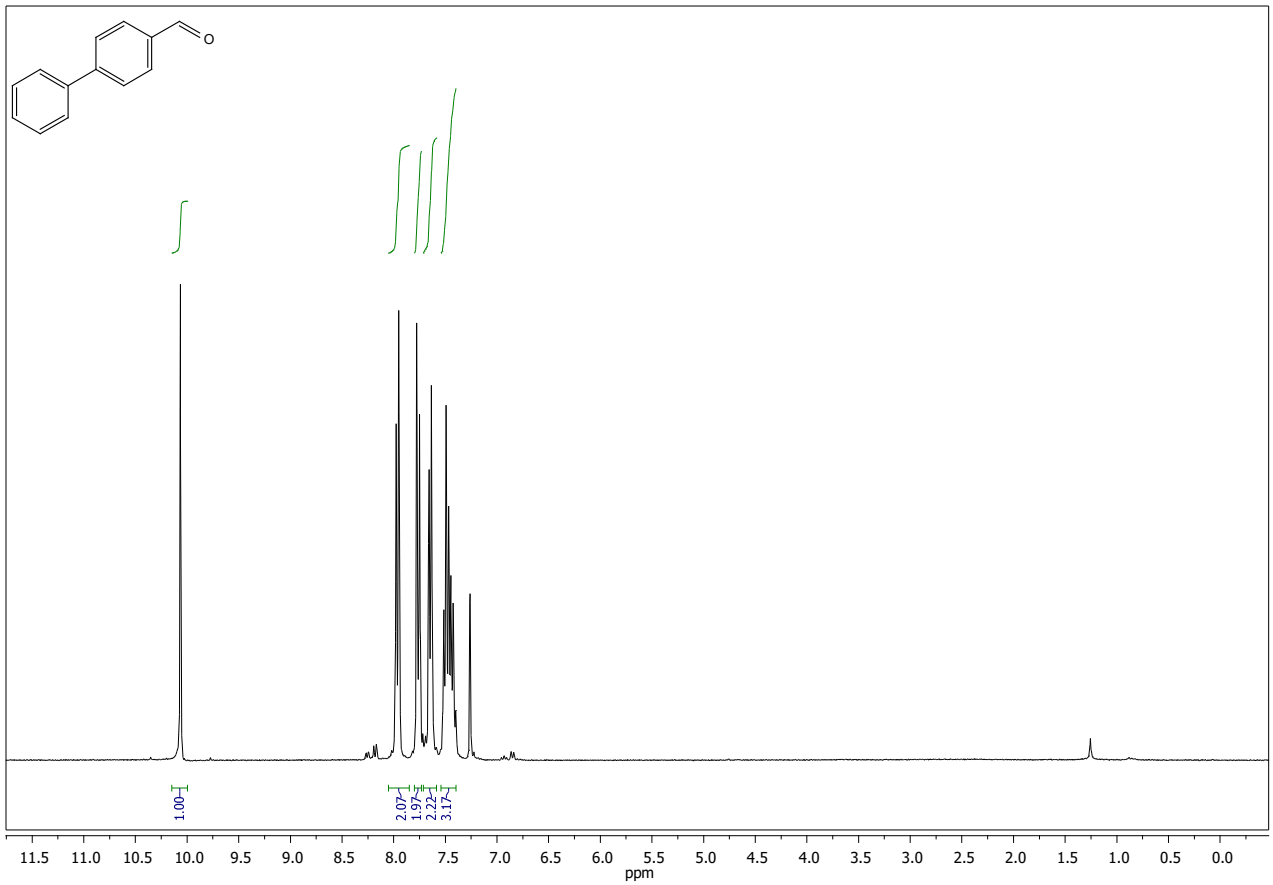
O
1.00
2.07
1.97
2.22
3.17
11.5 11.0 10.5 10.0 9.5 9.0 8.5 8.0 7.5 7.0 6.5 6.0 5.5 5.0 4.5 4.0 3.5 3.0 2.5 2.0 1.5 1.0 0.5 0.0
ppm

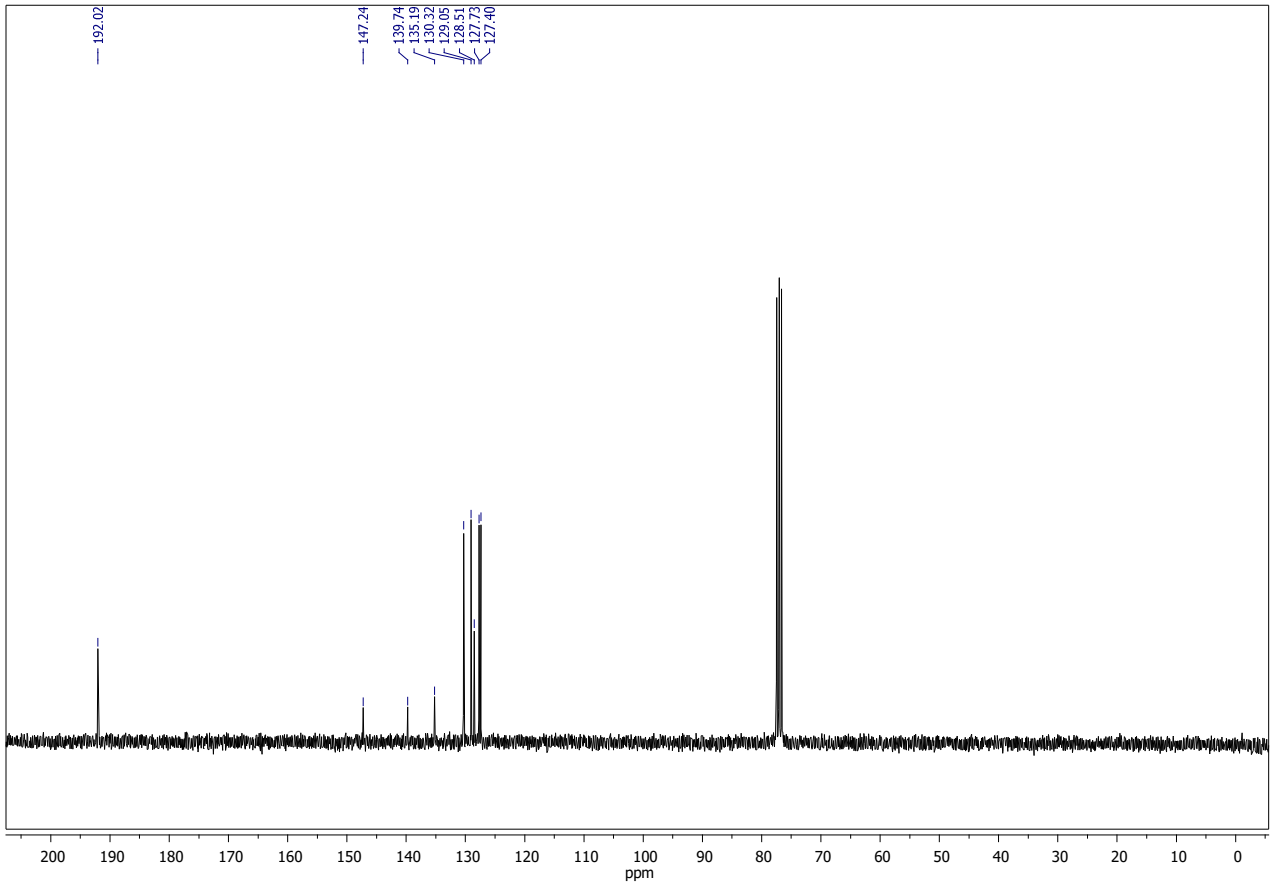
192.02
147.24
139.74
135.19
130.32
129.05
128.51
127.73
127.40
200 190 180 170 160 150 140 130 120 110 100 90 80 70 60 50 40 30 20 10 0
ppm

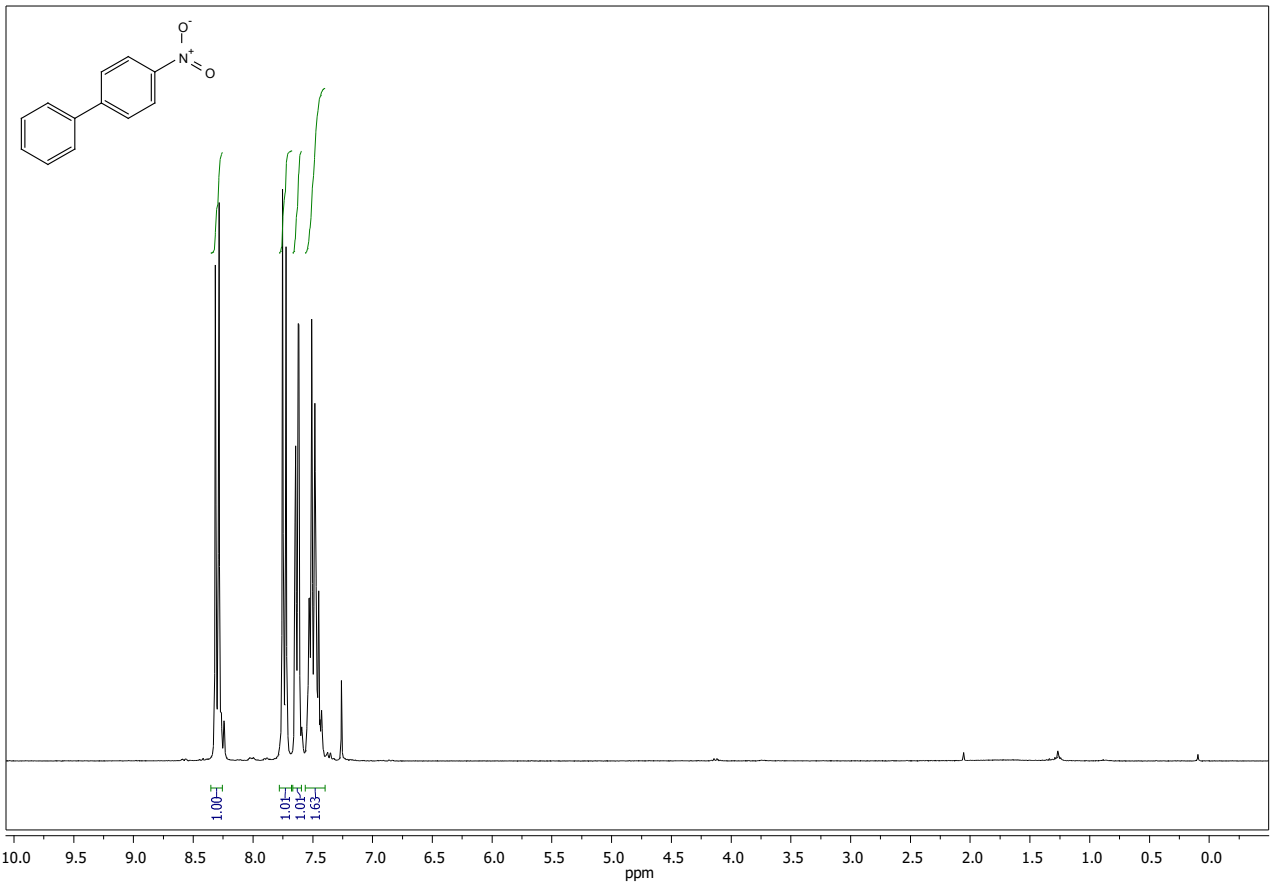
1.00
1.01
1.01
1.63
10.0 9.5 9.0 8.5 8.0 7.5 7.0 6.5 6.0 5.5 5.0 4.5 4.0 3.5 3.0 2.5 2.0 1.5 1.0 0.5 0.0
ppm

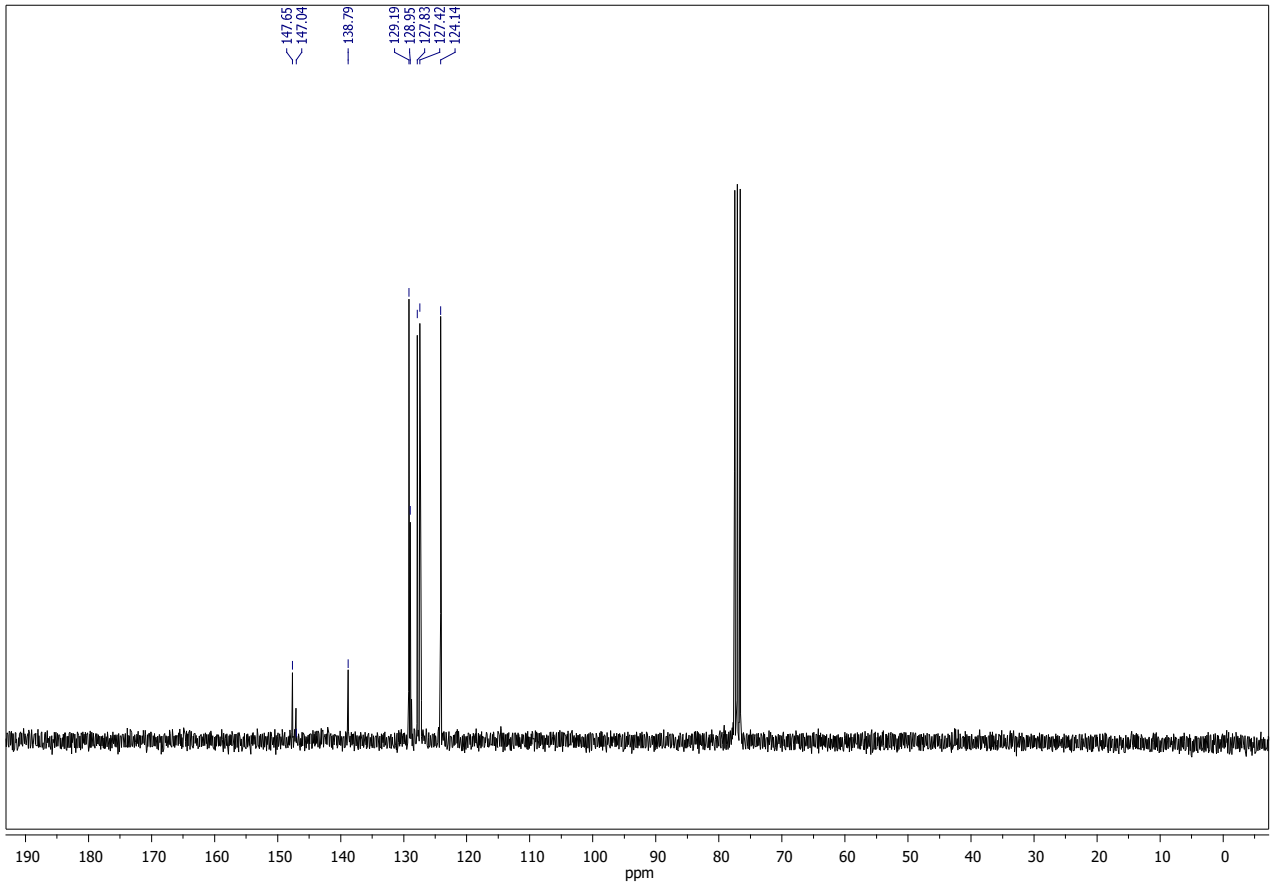
147.65
147.04
138.79
129.19
128.95
127.83
127.42
124.14
190 180 170 160 150 140 130 120 110 100 90 80 70 60 50 40 30 20 10 0
ppm

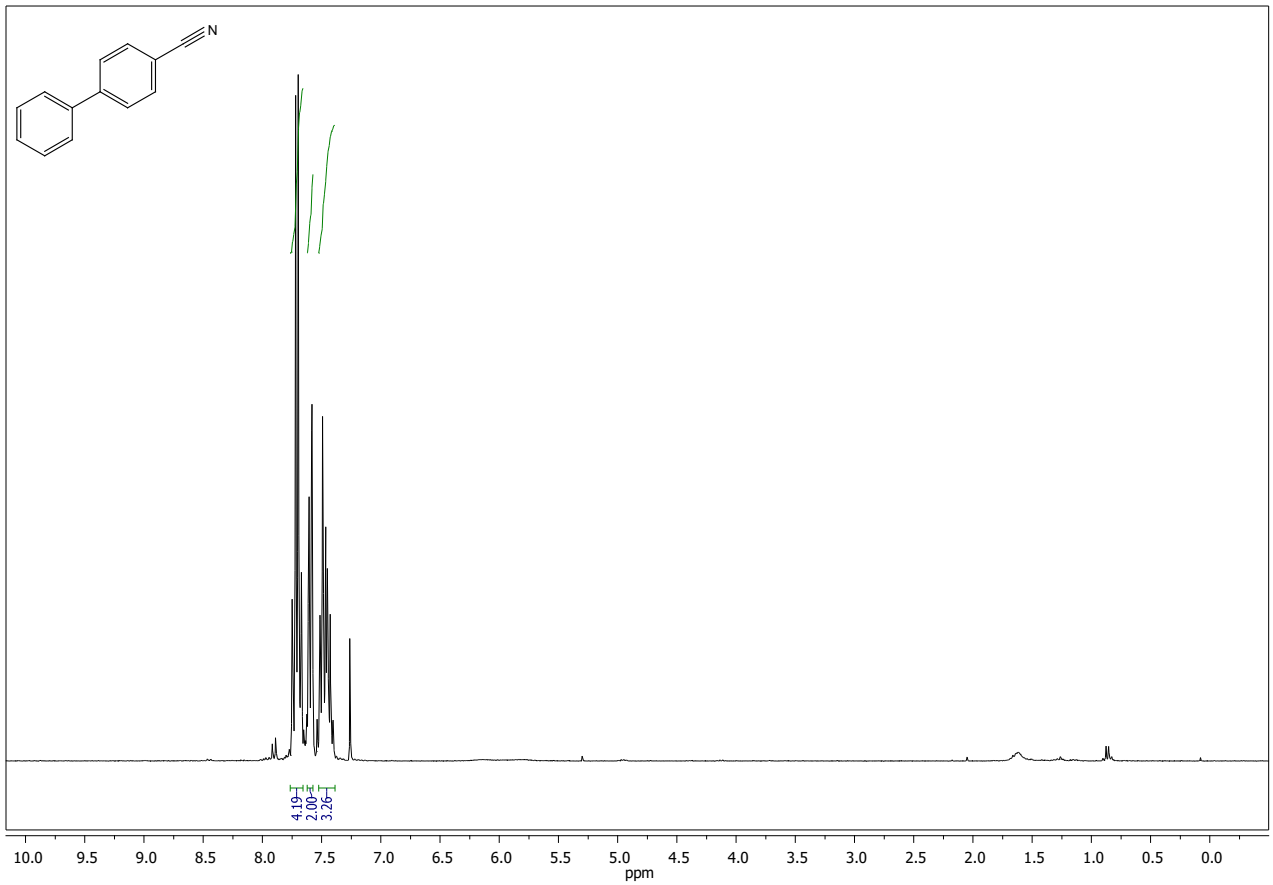
N
4.19
2.00
3.26
10.0 9.5 9.0 8.5 8.0 7.5 7.0 6.5 6.0 5.5 5.0 4.5 4.0 3.5 3.0 2.5 2.0 1.5 1.0 0.5 0.0
ppm

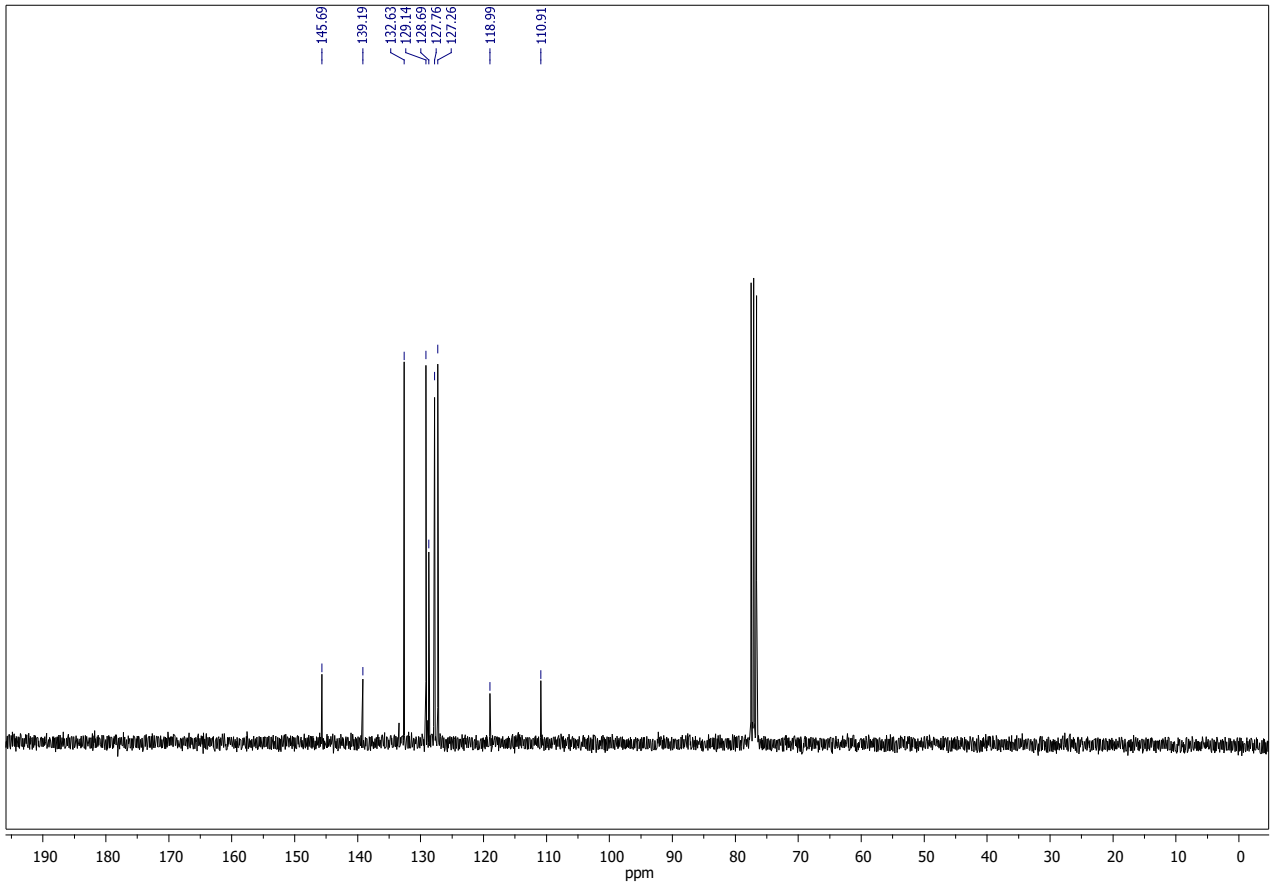
145.69
139.19
132.63
129.14
128.69
127.76
127.26
118.99
110.91
190 180 170 160 150 140 130 120 110 100 90 80 70 60 50 40 30 20 10 0
ppm

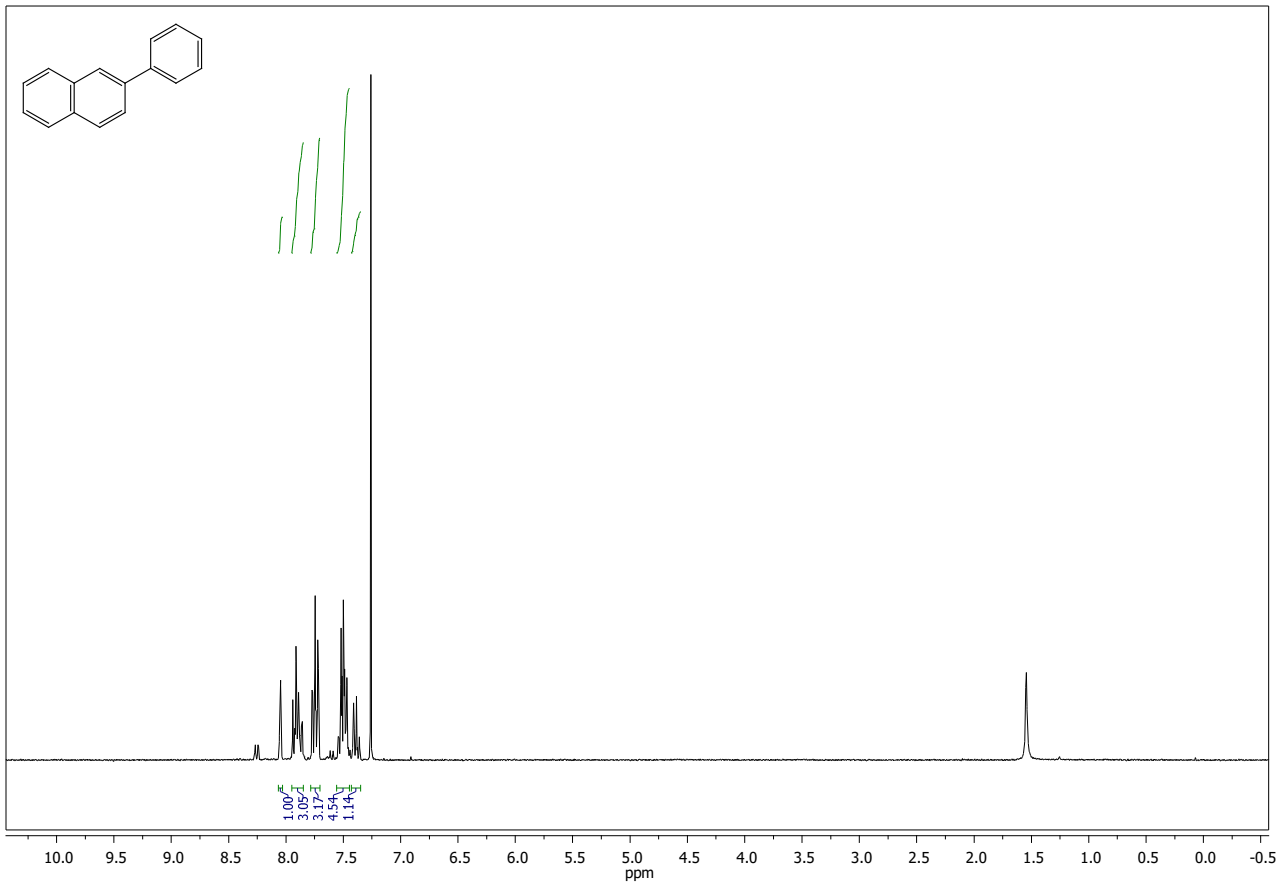
1.00
3.05
3.17
4.54
1.14
10.0 9.5 9.0 8.5 8.0 7.5 7.0 6.5 6.0 5.5 5.0 4.5 4.0 3.5 3.0 2.5 2.0 1.5 1.0 0.5 0.0 -0.5
ppm

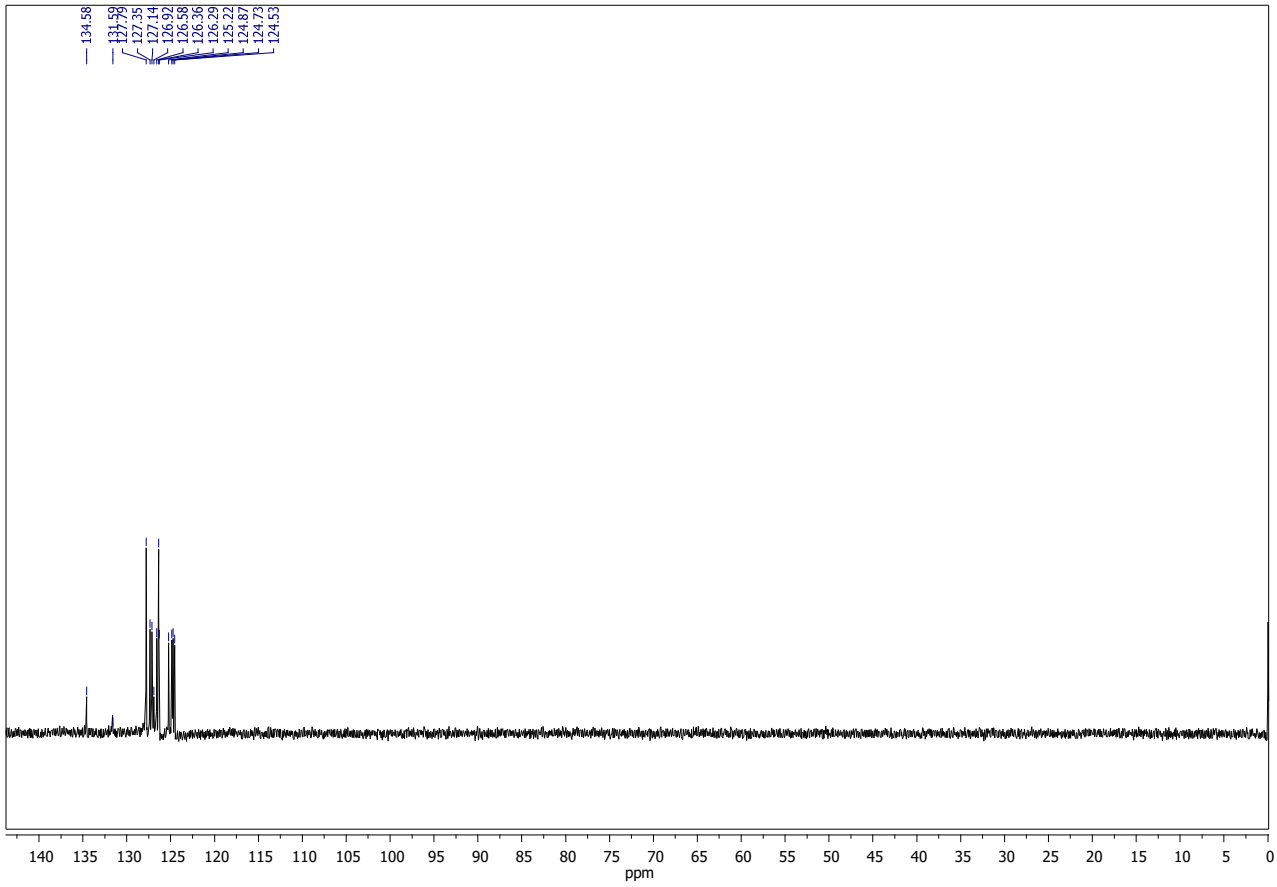
134.58
131.59
127.79
127.35
127.14
126.92
126.58
126.36
126.29
125.22
124.87
124.73
124.53
140 135 130 125 120 115 110 105 100 95 90 85 80 75 70 65 60 55 50 45 40 35 30 25 20 15 10 5 0
ppm

List of abbreviations

acac	acetylacetonate
APTES	3-aminopropyltriethoxysilane
atm	atmosphere
CNTs	carbon nanotubes
Co/C	carbon-coated cobalt nanobeads
COD	cyclo-ocatadiene
CTAB	cetyltrimethylammonium bromide
DCM	dichloromethane
dba	dibenzylidene acetone
DMF	dimethylformamide
DMSO	dimethyl sulfoxide
EtOAc	ethyl acetate
equiv	equivalents
Et_3N	triethylamine
EtOH	ethanol
GC	gas chromatography
GO	graphene oxide
Hz	hertz
ICP	inductively coupled plasma
i-PrOH	*iso*-propanol
IR	infrared
J	coupling constant
m	multiplet
MeCN	acetonitrile
MeOH	methanol
MNPs	metal nanoparticles

MW	microwave
MWCNTs	multi-wall carbon nanotubes
nm	nanometre
NPs	nanoparticles
OES	optical emission spectrometry
p-	*para*-
PEI	polyethylenimine
ppm	part per million
PVP	poly(vinylpyrrolidone)
rGO	reduced graphene oxide
r.t.	room temperature
s	singlet
SWCNTs	single-walled carbon nanotubes
T	temperature
t	triplet
TEM	transmission electron microscopy
TEMPO	2,2,6,6-tetramethyl-piperidine-1-oxyl
TEOS	tetraethyl orthosilicate
THF	tetrahydrofuran
TLC	thin layer chromatography
UV	ultraviolet
Vis	visible
wt%	weight percentage
XPS	x-ray photoelectron spectroscopy
XRD	x-ray diffraction

Curriculum Vitae

Francesca Besostri

Date of birth: 24.01.1985

Nationality: Italian

e-mail: fra.besostri@gmail.com

Education

02.2013 – 01.2016	**Doctoral Studies**
Institution	University of Regensburg-Institute of Organic Chemistry Marie Curie Initial training Network –Mag(net)icFun
Supervisor	Prof. Dr. Oliver Reiser
10.2010 – 09.2012	**Master in Chemistry**
Institution	Università degli Studi di Pavia-Department of Chemistry
Supervisor	Prof. Elisa Fasani, Prof. Dr. Peter Ogilby
Thesis title	Effects of two-photon excitation of Protoporphyrin IX and Fluoroquinolones in cells
10.2007 – 09.2010	**Bachelor in Chemistry**
Institution	Università degli Studi di Pavia-Department of Chemistry
Supervisor	Prof. Elisa Fasani
Thesis title	Fluorescent protein: structure, properties and applications
10.2004 – 09.2007	**Bachelor in Biology**
Institution	Università degli Studi di Pavia
Supervisor	Dr. Solveig Tosi, Prof. Dr. Giovanni Vidari
Thesis title	The apolar fractions of *Siparuna Eggersii*: extraction and antimicrobial activity assays

Professional experience

04.2015-01.2016	**PhD project**
Institution	ICIQ (Institut Català d'Investigatió Quimica), Tarragona Group of Prof. Dr. Miquel A. Pericas
02.2015	**Research Internship**
Institution	Novartis, Basel Group of Dr. Peter Meier
01.2012-07.2012	**Erasmus Project**
Institution	Aarhus University-Department of Chemistry-Centre for Oxygen Microscopy and Imaging Group of Prof. Dr. Peter Ogilby

List of Publications

- *Synthesis of functionalized, dispersible carbon-coated cobalt nanoparticles for potential biomedical applications*
  Kainz, Quirin M.; Fernandes, Soraia; Eichenseer, Corina M.; Besostri, Francesca; Koerner, Helmut; Mueller, Rainer; Reiser, Oliver
  Faraday Discussions, 2014, **175**, 27-40

- *Spatially resolved two-photon irradiation of an intracellular singlet oxygen photosensitizer: Correlating cell response to the site of localized irradiation*
  Gollmer, A.; Besostri, F.; Breitenbach, T.; Ogilby, P. R.
  Free Radical Research, 2013, **47**(9), 718-730

Conferences and workshops

- 20-22 of February, 2013. Magnyfico Workshop, Barcelona. Poster contribution: "Magnetic nanoparticles as recyclable supports for synthesis, purification and biomedical application".

- 22-24 of February, 2013. Mag(net)icFun Kick-off Meeting, Barcelona. Oral presentation: "Carbon-coated metal nanoparticles for catalysis".

- 02-03 of September, 2013. Mag(net)icFun Workshop, ETH Zurich. Oral presentation: "Catalytic activity of Pd nanoparticles on carbon-coated magnetic nanobeads".

- 02-04 of June, 2014. Mag(net)icFun mid-term Meeting, IIT Genoa. Oral presentation: "Catalytic activity of Pd nanoparticles on carbon-coated magnetic nanobeads".

- 19-20 of June, 2014. Marie Sklodowska-Curie Conference, ESOF 2014. Copenhagen. Poster contribution: "Magnetic nanoparticles as recyclable support for catalysis and scavenger for water treatment".

- 27-28 of October, 2014. Mag(net)icFun Workshop, University of Regensburg. Oral presentation: "Deposition of metal nanoparticles on carbon-coated magnetic nanobeads and application in catalysis".

- 23-24 of March, 2015. Mag(net)icFun Workshop, Keel University. Oral presentation: "PEI-coated Co/C nanobeads as support for solid-phase synthesis".

- 16-20 of August, 2015. 250th ACS Meeting, Boston. Oral presentation: "Metal nanoparticles supported on carbon-coated magnetic nanobeads for catalysis"

- 03-04 of March, 2016. Mag(net)icFun Workshop, Trinity College Dublin. Oral presentation: "Metal nanoparticles supported on magnetic nanobeads and their application in catalysis".

Professional References

Prof. Dr. Oliver Reiser
Institut für Organische Chemie
Universität Regensburg, Universitätsstr. 31
93053, Regensburg, Germany
oliver.reiser@ur.de

Prof. Dr. Miquel A. Pericas
ICIQ (Institut Català d'Investigació Química)
Avda. Països Catalans 16
43007 Tarragona
mapericas@iciq.es

Dr. Peter Meier
Novartis International AG
Postfach
CH-4002 Basel
Schweiz
peter.meier@novartis.com

Acknowledgments

I would like to thank all the people that during the last three years give me their time, support and friendship.

University of Regensburg

First of all, I would like to express my gratitude to my advisor Prof. Dr. Oliver Reiser for the continuous support, the interesting discussions and for all the opportunities he offered me during this PhD.
Furthermore, I would like to thank Antje Weigert for all the help and support in handling the bureaucratic practices.
For the technical support I thank Dr. Peter Kreitmeier, Roxane Harteis, Helena Konkel, Brigitte Eichenseher and Klaus Döring. I would also like to thank Joachim Rewitzer for the ICP measurements, Thomas Meier for the XPS analysis and Prof. Josef Zweck for the TEM images.
For the nice laboratory environment and for the several German-English translations, I would like to thank Daniel Dobler.
For the pleasant working environment, I thank all the AK Reiser, in particular Soraia, Dobler, Jimmy, Matze, Benny, Rackl, Andi, Viktor, Okun, Carina, Marina, Saerom, Nanaji, Paul, Roland and Lu for all the nice moments.

I would like to thank also Lamprini and Soraia for all the great moments we had together in Regensburg.

ICIQ Tarragona

For the support given in the 10 months I spent in ICIQ and the interesting and useful discussions, I would like to thank my supervisor Prof. Dr. Miquel A. Pericas.
A special thanks to Dr. Carles Rodriguez for proofreading my thesis, for all the support and help given during my stay in ICIQ and also for organising an amazing volleyball tournament.
For proofreading my thesis, I am also grateful to Dr. Juan Manuel Sarria Toro.
I would like to thank Dr. Paola Riente for all the interesting discussions on nanoparticles and Patricia Llanes for the technical support and for being always available.
A special thanks to Sara Garcia for all the help given regarding paperwork, especially in the final steps of the deposition of the thesis.
For the nice working environment, I would like to show my gratitude to all Pericas group: Carles R., Paola, Laura, Lidia, Patricia, Marta, Pablo, Dina, Carles A., Santiago, Lluis, Tharun, Carmen, Evgeny, Irina.

Novartis, Basel

For giving me the opportunity to do an internship in his group, for the friendly and motivating working environment, I would like to thank Dr. Peter Meier.

For the financial support I would like to thank Marie-Curie Actions, in particular the EU-ITN Network Magn(net)icFun.

A very special thanks go to Soraia. For all the time we spent together, for the great evenings, for rendering the working days less heavy and also for all the support given in these three years! Thanks for your joy, your craziness and mostly for being a really good friend!

I would also like to thank Anna. Lives can take different directions but good friendships stay!

Last but not least, my family. Grazie per avermi supportato e sopportato per tutti questi anni, permettendomi di seguire le mie malsane idee!

Declaration

Herewith I declare that this present thesis is a presentation of my original work prepared single-handed. Wherever contributions from others are involved, all of them are marked clearly, with reference to the literature, licence and acknowledgment of collaborative research.

Regensburg, 17. May 2016

Francesca Besostri